

Distribution Agreement

In presenting this thesis or dissertation as a partial fulfillment of the requirements for an advanced degree from Emory University, I hereby grant to Emory University and its agents the non-exclusive license to archive, make accessible, and display my thesis or dissertation in whole or in part in all forms of media, now or hereafter known, including display on the world wide web. I understand that I may select some access restrictions as part of the online submission of this thesis or dissertation. I retain all ownership rights to the copyright of the thesis or dissertation. I also retain the right to use in future works (such as articles or books) all or parts of this thesis or dissertation.

Signature:

Katherine Marie Hutchinson

Date

MITOCHONDRIAL DEFICIENCIES INFLUENCE VARIABLE PENETRANCE OF
NUCLEAR NAB3 GRANULE ACCUMULATION

By

Katherine Marie Hutchinson
Doctor of Philosophy

Graduate Division of Biological and Biomedical Sciences
Biochemistry, Cell and Developmental Biology

Daniel Reines, Ph.D.
Advisor

Gary Bassell, Ph.D.
Committee Member

Graeme Conn, Ph.D.
Committee Member

Homa Ghalei, Ph.D.
Committee Member

Nicholas Seyfried, Ph.D.
Committee Member

Accepted:

Kimberly Jacob Arriola, Ph.D, MPH
Dean of the James T. Laney School of Graduate Studies

Date

Mitochondrial deficiencies influence variable penetrance of nuclear Nab3 granule accumulation

by

Katherine Marie Hutchinson

B.S., High Point University

Advisor: Daniel Reines, Ph.D.

An abstract of
a dissertation submitted to the Faculty of the
James T. Laney School of Graduate Studies of Emory University
in partial fulfillment of the requirements for the degree of
Doctor of Philosophy
in Graduate Division of Biological and Biomedical Sciences
(GDBBS)
Biochemistry, Cell and Developmental Biology (BCDB)
2022

ABSTRACT

Mitochondrial deficiencies influence variable penetrance of nuclear Nab3 granule accumulation

By Katherine Marie Hutchinson

Yeast regularly withstand changes in their environment and they must adapt their genome in order to survive. From their genome, yeast generate different types of RNA which they use to regulate protein expression. A critical step in generating these RNAs is transcription termination, which is performed through two different mechanisms in yeast depending on the type of RNA transcribed. For protein coding messenger RNA, yeast employ transcription termination through a set of factors brought in by the cleavage/ polyadenylation complex. In the case of non-coding RNAs such as small nuclear RNA, small nucleolar RNA and cryptic unstable transcripts, transcription termination is performed by the Nrd1-Nab3-Sen1 transcription termination complex (NNS), which this thesis focuses on. The choice of transcription termination mechanism is a highly specific and regulated process. RNA polymerase II, which is the enzyme that transcribes the DNA into RNA, contains a C-terminal domain (CTD) on its largest subunit which different termination complex components interact with. Early in transcription, the CTD is heavily phosphorylated at serine 5 of a seven amino acid repeat. This in turn allows Nrd1 to preferentially bind to activate transcription termination. As Pol II progresses down the template, the phosphorylation is removed from serine 5 and serine 2 becomes the predominant form of phosphorylation. This event signals for the binding of cleavage/ polyadenylation factors to deploy polyadenylation-coupled transcription termination.

This thesis focuses primarily on one of the three NNS subunits, nuclear polyadenylated RNA-binding protein 3 (Nab3). Nab3 is a hnRNP-like protein that contains an aspartate/glutamate rich near its N-terminus, an RNA recognition motif and a proline/glutamine rich, prion-like domain at its C-terminus. The C-terminus is essential for viability, for proper transcription termination, for the ability to form amyloid filaments *in vitro* and to assemble a membraneless subcellular compartment *in vivo* known as the Nrd1-Nab3 granule (NNG). The work in this thesis establishes that the assembly and accumulation of the Nrd1-Nab3 granule displays variable penetrance across various yeast strains. Once this variation was discovered and established, this work aimed to explain the cause for variation.

Interestingly, this thesis reports that mitochondrial function and respiratory capacity are key contributors to the variance seen for Nrd1-Nab3 granule accumulation. The data herein demonstrate that NNG accumulation is sensitive to oxidative phosphorylation under carbon restricted conditions and can be reduced by the addition of extracellular ATP, suggesting an ATP-dependent mode of disassembly. Additionally, a serine-arginine protein kinase implicated in the disassembly of other subcellular compartments is shown to be important for Nrd1-Nab3 granule disassembly through mitochondrial function. This work deepens our understanding of the cause for Nrd1-Nab3 granule accumulation variation as well as our understanding of key factors in granule biogenesis.

Mitochondrial deficiencies influence variable penetrance of nuclear Nab3 granule accumulation

By

Katherine Marie Hutchinson

B.S., High Point University

Advisor: Daniel Reines, Ph.D.

A dissertation submitted to the Faculty of the
James T. Laney School of Graduate Studies of Emory University
in partial fulfillment of the requirements for the degree of
Doctor of Philosophy
in Graduate Division of Biological and Biomedical Sciences (GDBBS)
Biochemistry, Cell and Developmental Biology (BCDB)
2022

Acknowledgements

Often, we look back on a chapter of our life and realize it all went by so fast. But we also look back and realize that every moment was building up to this day. Thank you to Mrs. Babic for fostering my first love of science. Thank you to Dr. Srougi for shaping me into the scientist and woman I am today. Thank you to Danny for taking a chance on me and supporting my growth throughout the course of my PhD. Thank you to Jeremy for having the patience and kindness to teach and support me during my PhD. Thank you to my parents for always believing in me and allowing me to chase my dreams. Thank you to my sister who always loves and lifts me up. And thank you to my fiancé/ soon-to-be husband for your endless love, support and dedication to me as your wife. Accomplishments are never achieved alone; the greatest ones always take a village of people. How blessed am I to have the best village around me.

Table of Contents

1.0 Transcription termination and RNA-binding proteins	1
1.1 An introduction to eukaryotic transcription	1
1.1.1 Classes of RNA transcripts	2
1.1.2 Transcription termination in <i>Saccharomyces cerevisiae</i>	3
1.1.3 Messenger RNA transcription termination in <i>Saccharomyces cerevisiae</i>	4
1.1.4 Non-coding transcription termination in <i>Saccharomyces cerevisiae</i>	5
1.2 Components of the Nrd1-Nab3-Sen1 (NNS) transcription termination complex	7
1.2.1 Nrd1: a hnRNP-like protein	7
1.2.2 Nab3: another hnRNP-like protein	8
1.2.3 Sen1: a helicase protein	9
1.3 An introduction to RNA-binding proteins	10
1.3.1 Domains found in RNA-binding proteins	10
1.3.2 Biological roles of RNA-binding proteins	11
1.4 An introduction to prions & prion-like proteins	11
1.4.1 Yeast prions and prion-like proteins	12
1.4.2 Yeast as a model for human neurodegenerative diseases	14
1.5 Nab3: a prion-like protein	15
1.6 Glucose deprivation	16

1.6.1	Transcriptome and proteome changes in response to glucose deprivation.....	17
1.6.2	Nrd1-Nab3 transcript binding changes in response to glucose deprivation.....	19
1.7	Research focus.....	20
1.8	Figures.....	22
2.0	Variable penetrance of Nab3 granule accumulation quantified by a new tool for high-throughput single-cell granule analysis.....	25
2.1	Abstract.....	26
2.2	Introduction.....	27
2.3	Materials and methods.....	30
2.4	Results.....	34
2.4.1	Rationale.....	35
2.4.2	Quantification of the dramatic rearrangement of GFP-Nab3 in yeast nuclei.....	36
2.4.3	The computational tool enables a detailed analysis of fluorescent protein distribution.....	37
2.4.4	Measurement of strain-to-strain differences in GFP-Nab3 granule accumulation.....	39
2.4.5	The granule accumulation phenotype correlates with growth and respiration defects.....	40
2.4.6	Quantification of filament formation by IMP dehydrogenase in cultured human cells.....	41
2.5	Discussion.....	43
2.6	Acknowledgements.....	45

2.7	Figures & tables.....	46
3.0	Nab3 nuclear granule accumulation is driven by respiratory capacity.....	62
3.1	Abstract.....	63
3.2	Introduction.....	64
3.3	Materials and methods.....	67
3.4	Results.....	70
3.4.1	Mitochondrial manipulations in a low granule accumulating yeast strain increase granule accumulation.....	70
3.4.2	Enrichment for a respiratory competent cell population results in a reduction of Nab3 granule accumulation.....	72
3.4.3	Nab3 granule accumulation is lost by the addition of extracellular ATP.....	73
3.4.4	<i>SKY1</i> knockout results in mitochondrial defects and increased Nab3 granule accumulation.....	73
3.5	Discussion.....	74
3.6	Acknowledgements.....	77
3.7	Figures & tables.....	78
4.0	Discussion and future directions.....	89
4.1	Summary.....	89
4.2	The importance of a computational tool to quantify Nab3 granule accumulation in various yeast strains.....	90
4.3	The importance of mitochondrial function on Nab3 granule accumulation.....	90

4.4	Future directions for this research project.....	92
4.4.1	Breaking down the composition of the Nab3 granule.....	92
4.4.2	Identifying key players in assembly and disassembly of the Nab3 granule.....	96
4.4.3	Discovering other factors that influence Nab3 granule accumulation.....	98
4.5	Implications of mitochondrial function in neurodegenerative diseases.....	100
4.6	Final remarks.....	101
4.7	Figures.....	103
5.0	References.....	105

Figure and Tables Table of Contents

Chapter 1

Fig. 1-1 Modes of transcription termination in *S. cerevisiae*

Fig. 1-2 Nrd1-Nab3 mediated transcription termination

Fig. 1-3 Protein domains of Nab3 protein

Chapter 2

Fig. 2-1 Fluorescence microscopy of GFP-Nab3 (green) granule formation in three yeast strains

Fig. 2-2 Workflow

Fig. 2-3 Measurement of the distribution of nuclear GFP-Nab3 in glucose-fed and glucose-starved conditions for a high penetrance granule forming strain

Fig. 2-4 Quantification of granules per cell and distribution of pixel intensities for glucose-fed or glucose-restricted cells

Fig. 2-5 Scoring the distribution of GFP-Nab3 into granules in specific nuclei

Fig. 2-6 Different extents of granule formation in three distinct yeast strains

Fig. 2-7 Growth in the absence of glucose varies with the granule accumulation phenotype.

Fig. 2-8 Granule formation and mitochondrial function.

Fig. 2-9 Quantification of drug-induced “rod and ring” formation by IMP dehydrogenase in human Jurkat cells

Fig. S2-1 The difference between chromosomal and episomal NRD1 does not account for the magnitude of granule formation

Chapter 3

Fig. 3-1 Mitochondrial manipulations in a low granule accumulating yeast strain

Fig. 3-2 Improved respiration capacity results in a decrease in Nab3 granule accumulation

Fig. 3-3 Nab3 granule levels are reduced by the addition of extracellular ATP

Fig. 3-4 Sky1 knockout results in mitochondrial deficiency and increased Nab3 granule accumulation

Fig. 3-5 Equilibrium between pan-nuclear Nab3 and its assembly into a nuclear granule: a working model for Nab3 granule disassembly and accumulation.

Fig. S3-1 A high granule accumulating yeast strain is ρ^-

Fig. S3-2 Confocal microscopy of a glucose starved low granule accumulating strain treated with and without the electron transport uncoupler, FCCP.

Fig. S3-3 Deletions of nuclear encoded genes result in a mitochondrial defect.

Chapter 4

Fig. 4-1 A working model for Nrd1-Nab3 granule function

Tables

Chapter 2

Table 2-1 *S. cerevisiae* strains used in this work

Chapter 3

Table 3-1 *S. cerevisiae* strains used in this work

ABBREVIATIONS

ALS- amyotrophic lateral sclerosis

ALS4- amyotrophic lateral sclerosis type 4

AOA2- ataxia with oculomotor apraxia type 2

bp- base pair

CFIA- cleavage factor IA

CFIB- cleavage factor IB

CID- C-terminal interaction domain

CPA- cleavage polyadenylation complex

CPF- cleavage polyadenylation factor

CTD- C-terminal domain

CUT- cryptic unstable transcripts

DNA- deoxyribonucleic acid

eIF4A- eukaryotic translation initiation factor 4A

hnRNP- heterogenous nuclear ribonucleoprotein

mRNA- messenger RNA

ncRNA- non-coding RNA

NID- Nrd1 interacting domain

NLS- nuclear localization sequence

NNS- Nrd1-Nab3-Sen1 terminaiton complex

NNG- Nrd1-Nab3 granule

OXPHOS- oxidative phosphorylation

PAS- poly(A) site

PFD- prion-forming domain

Pol I- RNA polymerase I

Pol II- RNA polymerase II

Pol III- RNA polymerase III

PrLD- prion-like domain

PrP- single prion-forming protein in mammals

PrP^{Sc}- pathogenic prion protein conformer in mammals

RBD- RNA-binding domain

RBP- RNA-binding protein

RNA- ribonucleic acid

rRNA- ribosomal RNA

RNP- ribonucleoprotein

RRM- RNA recognition motif

Ser(P)5- phosphorylated serine 5

Ser(P)2- phosphorylated serine 2

snRNA- small nuclear RNA

snoRNA- small nucleolar RNA

TRAMP- Trf4/Trf5, Air1/Air2, Mtr4 complex

tRNA- transfer RNA

TSS- transcription start site

UTR- untranslated region

Chapter 1.0: Transcription termination and RNA-binding proteins

1.1 An introduction to eukaryotic transcription

All cells contain a set of instructions known as deoxyribonucleic acid (DNA) that is transcribed into messenger ribonucleic acid (mRNA) and translated into a functional protein product. The processes of transcription and translation are an integral concept in biology and together, form the foundational central dogma¹. Eukaryotic transcription occurs in the nucleus of the cell, separate from the cytoplasmic site of translation, and can be performed by one of three RNA polymerases². RNA polymerase I (Pol I) transcribes ribosomal RNA (rRNA), RNA polymerase II (Pol II) transcribes mRNA and non-coding RNA (ncRNA), and RNA polymerase III (Pol III) transcribes transfer RNA (tRNA) as well as rRNA².

The process of RNA polymerase II transcription is a cycle and involves three stages: initiation, elongation and termination³. Typically, transcription initiation occurs at the transcription start site (TSS), which is a defined position on the 5' end of the gene⁴. Approximately 50 base pairs (bp) upstream and 50bp downstream of the TSS is a region defined as the core promoter of the gene. The core promoter serves as a binding platform for the transcription machinery, which is made up of Pol II and its associated transcription factors⁴. After the transcription machinery is bound, the elongation process begins. During the initial stages of elongation, Pol II is highly regulated through Pol II pausing in which Pol II can accumulate at high levels at a specific template position and particularly near the TSS⁵. Release of Pol II from the paused state is mediated by transcription elongation factors and, upon release, Pol II resumes active elongation⁵. Elongation rates vary between and within genes and are subject to tight regulation⁵. This level of regulation is important in controlling co-transcriptional events such as splicing and termination⁵.

As transcription elongation proceeds, pre-mRNA is generated by Pol II. The pre-mRNA emerges from the exit channel of Pol II where the cleavage-polyadenylation complex (CPA) binds to the poly(A) site (PAS) and processes the 3' end of the pre-mRNA to generate mRNA². Two models currently exist for transcription termination². One model proposes that Pol II senses its movement over a functional PAS and induces a conformational change within the Pol II active site. This conformational change leads to Pol II pausing and then release of Pol II from the DNA². The so-called torpedo model proposes a mechanism in which a nuclear 5'-3' exonuclease is recruited to the 5' end exposed by transcript cleavage at the PAS and begins degrading the transcript by translocating down the RNA. When the nuclease reaches Pol II, this acts as a molecular signal to release Pol II from the DNA². These models are not mutually exclusive.

1.1.1 Classes of RNA transcripts

Different classes of RNA exist in all cells. The focus of this thesis will be on eukaryotic organisms, specifically, the budding yeast *Saccharomyces cerevisiae*. In yeast, RNA can be broken down into protein coding and non-coding types. Coding RNA consists of messenger RNA (mRNA), which ultimately is translated into functional protein³. A wide variety of non-coding RNA is found including ribosomal RNA (rRNA), transfer RNA (tRNA), small nuclear RNA (snRNA), small nucleolar RNA (snoRNA) and cryptic unstable transcripts (CUTs)³. In yeast, Pol II is responsible for transcribing mRNA as well as snRNAs, snoRNAs and CUTs³. Each of these transcripts serve important functions, even those that are non-coding.

Messenger RNA is made by transcribing DNA into pre-mRNA and then pre-mRNA is processed into mature mRNA. mRNA is important to the cell as it is the class of RNA that is

exported from the nucleus to the cytoplasm to be translated by the ribosome into functional protein. Therefore, protein expression is regulated at multiple levels, including the transcriptional level⁶.

Like mRNA, snRNA and snoRNA are transcribed by Pol II⁷. snoRNAs are housed in the nucleolus and are responsible for rRNA processing and modification of rRNA, snRNA and mRNA⁷. Together with proteins, they form ribonucleoprotein complexes that are highly conserved⁷. Like snoRNA, snRNAs are phylogenetically conserved. When pre-mRNA is transcribed, it contains non-coding sequences known as introns and these introns have to be removed in order to create mature mRNA⁸. Introns are removed from mRNA by a ribonucleoprotein complex known as the spliceosome, which contains five essential snRNAs: U1, U2, U3, U4, U5, and U6⁸. These non-coding RNAs are critically important to the cell.

1.1.2 Transcription termination in *Saccharomyces cerevisiae*

In 1988, David Botstein and Gerald Fink speculated that yeast could potentially serve as a model organism for scientific research due to advancements in recombinant DNA technology and biochemical and genetic methodologies^{9, 10}. Today, yeasts are used to study a variety of topics, including transcription termination. Each stage of transcription is highly regulated to control gene expression, including the end stage of termination¹¹. Termination is specifically regulated by transcription termination factors that interact with RNA processing and degradation enzymes to control the fate of the RNA¹¹.

In the budding yeast, *Saccharomyces cerevisiae*, transcription termination can occur via two mechanisms depending on the type of RNA being transcribed³. As previously noted, Pol II transcribes mRNA and non-coding RNA. The termination mechanism deployed by the cell is specific for each type of RNA^{11, 12}. Specifically, when the cell selects the termination mechanism

designed to produce mRNA, a transcript that is further processed and exported to the cytoplasm for translation is produced (**Fig. 1-1**)¹¹. In contrast, when the cell uses the termination mechanism designated for non-coding RNA, a different type of transcript is produced with a different, often nuclear, destination and it can be cleaved in a controlled manner or degraded to completion¹¹.

1.1.3 Messenger RNA transcription termination in *Saccharomyces cerevisiae*

When mRNA is transcribed by Pol II, termination is carried out by protein complexes known as cleavage polyadenylation factor (CPF), cleavage factor IA (CFIA) and cleavage factor IB (CFIB)^{3, 11-13}. While the exact mechanism of termination remains elusive, it is known that the CPA machinery is coupled to the termination process³. Many of the components of the CPA have designated roles in coordinating the transcription termination process. For example, several factors recognize and process signals in the 3'-untranslated region (UTR) of the newly synthesized RNA¹¹.

An important determinant for which type of transcription termination mechanism is deployed by the cell is the phosphorylation status of the C-terminal domain (CTD) of Pol II (**Fig. 1-2**)^{3, 11}. The CTD of the largest subunit of Pol II in *Saccharomyces cerevisiae* consists of a 26 repeat of a heptapeptide (Y₁S₂P₃T₄S₅P₆S₇)^{3, 14, 15}. Within the first few hundred nucleotides of the promoter, serine 5 of the heptapeptide repeats on the CTD of the large subunit of Pol II is phosphorylated (Ser(P)5)^{3, 14, 16}. This phosphorylation event is important as Nrd1 contains a C-terminal interaction domain (CID) that recognizes and binds to the Ser(P)5 CTD of Pol II, thus ensuring that transcription is terminated using the NNS, the non-coding RNA termination machinery³. As transcription progresses, two phosphatases, Ssu72 and Rtr1, dephosphorylate serine 5³. Consequently, further downstream of the promoter, serine 2 of the CTD becomes the

predominant form of CTD phosphorylation (Ser(P)2) which is important for recognition by the CPA machinery to employ coding transcription termination^{3, 14, 16}. The CPA machinery is composed of a distinct set of proteins that terminate the transcription of mRNAs. One is Pcf11, which recognizes and preferentially binds to phosphorylated serine 2^{11, 17}. This recognition and binding event, along with other coordinated events, leads to the cleavage of the nascent RNA at the poly(A) site¹¹. Following cleavage, adenosine nucleotides are added to the 3' end of the RNA, forming the 3' poly(A) tail¹¹. This poly(A) tail is then bound by a poly(A)-binding protein, an event thought to protect the RNA from 3' end degradation as well as promote its nuclear export to the cytoplasm¹¹. Once exported, the mRNA is translated by the ribosome into a functional protein product.

The differential phosphorylation of serine 2 and 5 contained within CTD is important for recognition and binding of RNA processing factors and the selection of a termination mechanism^{14, 16}. Additionally, other amino acids contained within the CTD undergo modifications that are important for transcription termination. These include phosphorylation at serine 7, threonine 4 and tyrosine 1^{3, 16}. Phosphorylation at serine 7 has been shown to be important for proper snRNA gene expression¹⁸ while phosphorylation at threonine 4 has been implicated in histone mRNA 3' end processing¹⁹. Phosphorylation at tyrosine 1 stimulates the binding of an elongation factor and impairs the recruitment of termination factors^{3, 20}. Taken together, modifications of amino acids contained within the CTD of Pol II are important for gene expression and transcription termination.

1.1.4 Non-coding transcription termination in *Saccharomyces cerevisiae*

As previously mentioned, Pol II transcribes both coding and non-coding RNA. Serine 5 of the CTD is phosphorylated within the first few hundred nucleotides of the promoter and this is

a key signal for the non-coding transcription termination mechanism^{3, 14, 16, 21}. Non-coding transcription termination in *Saccharomyces cerevisiae* is carried out by a transcription termination complex known as the Nrd1-Nab3-Sen1 (NNS) complex^{2, 3, 11, 14, 16, 17, 21-26}. Nrd1 contains a C-terminal interaction domain (CID) that binds to the C-terminus of Pol II when Ser(P)5 is present^{3, 14, 21}. This binding event, coupled with Nrd1 and Nab3's abilities to recognize and bind nucleotide sequences in the emerging RNA and function as a heterodimer to recruit Sen1, coordinate transcription termination by NNS^{3, 21}. It is important to note that NNS transcription termination can serve as a fail-safe termination mechanism when coding transcription termination ceases to operate, whereby the NNS machinery rescues polymerases that fail to terminate at the poly(A) signal^{14, 27}.

Non-coding transcription termination is tightly coupled to RNA processing by the Trf4/Trf5, Air1/Air2, and Mtr4 (TRAMP) complex and the nuclear exosome^{3, 14, 21}. The type of processing performed by the TRAMP complex and nuclear exosome is dependent upon the class of non-coding RNA transcribed. In the context of snoRNAs, they are transcribed by Pol II and 3'-end oligoadenylated by the TRAMP complex³. These short oligoadenylate tails which are distinct from longer and more durable polyA tails added to mRNAs, target snoRNA to the exosome where it is matured by trimming the 3' end³. This contrasts with the protective poly(A) tail added to mRNA.³ Pol II is also known to transcribe several CUTs that are terminated by NNS and degraded by the nuclear exosome^{14, 21}. It is important to note that Nrd1 interacts with the nuclear exosome in both scenarios to process nascent ncRNA into protected stable transcripts (snoRNA) or to degrade the nascent RNA completely (CUTs)¹⁴. All these interactions by the NNS, TRAMP and the nuclear exosome are important for the regulation of the production, processing and/ or degradation of ncRNAs.

1.2 Components of the Nrd1-Nab3-Sen1 (NNS) transcription termination complex

Non-coding RNAs transcribed by Pol II are terminated by the Nrd1-Nab3-Sen1 transcription termination complex^{2, 3, 11, 14, 16, 17, 21-26}. This transcription termination complex is comprised of three proteins: Nrd1, Nab3 and Sen1. Nrd1 and Nab3 are both RNA-binding proteins (RBP) and contain an RNA recognition motif (RRM)^{3, 21, 24-26}. These RRM motifs allow Nrd1 and Nab3 to bind the nascent RNA emerging from Pol II to induce transcription termination^{3, 21, 23, 24}. When newly synthesized RNA emerges from Pol II, Nrd1 and Nab3 recognize small consensus sequences in the RNA and initiate termination^{21, 23}. Nrd1 also preferentially interacts with the Ser(P)5 state of the CTD of Pol II to coordinate termination^{3, 14, 16, 21, 23, 24}.

1.2.1 Nrd1: a hnRNP-like protein

Nrd1 was identified in a screen for proteins involved in the function of transcription termination³. This screen identified *trans*-acting factors that were termed nuclear pre-mRNA downregulation (NRD) proteins³. Nrd1 resembles splicing-related mammalian proteins in that it contains a homologous CTD-interacting motif that preferentially binds to the Ser(P)5 version of the CTD of Pol II to engage termination^{3, 14, 16, 21, 23, 24}. Additionally, Nrd1 is considered heterogenous ribonucleoprotein (hnRNP)-like because it binds RNA through an RNA recognition motif homologous to that seen in hnRNPs^{3, 21, 24}. These features make Nrd1 like the mammalian proteins SCAF4 and SCAF8, which bind the CTD of mammalian Pol II and are detected at early, alternative poly(A) sites^{3, 25, 28}.

Nrd1 functions as a heterodimer with Nab3 (described in the next section)^{21, 24}. For efficient NNS termination, the frequent short RNA sequences in the early transcript must be

recognized by Nrd1 and Nab3¹⁴. Nrd1's RRM binds the loose consensus sequence GUAA/G^{3, 14, 21, 24}. Nrd1's binding is enhanced when both Nrd1 and Nab3 are bound to nascent RNA^{3, 21, 24}. Both proteins are important for the termination of non-coding RNAs such as snoRNAs, but have also been shown to bind several coding RNA genes³. Taken together, Nrd1 and Nab3 function in many different aspects of transcription termination and impact the regulation of numerous types of RNA transcripts.

1.2.2 Nab3: another hnRNP-like protein

Nab3 stands for nuclear polyadenylated RNA-binding protein 3 as it was identified in a biochemical screen along with several other RNA-binding proteins isolated from nuclei³. Like Nrd1, Nab3 is an hnRNP-like protein with a recognizable RRM^{21, 24}. Nab3's RRM recognizes the sequence UCUU on nascent RNA but, as seen for Nrd1, it has flexibility in what exact sequence it will bind and binding tightens when bound in the heterodimeric state^{3, 14, 21, 24}. This contributes to the sequence specificity of the two RNA-binding proteins and their ability to tightly regulate and control transcription termination and processing of ncRNA.

In addition to its RRM, Nab3 has a Nrd1 interacting domain (NID) that allows it to dimerize with Nrd1, and a domain that allows it to interact with the helicase, Sen1³. Alongside Nab3's RRM and NID, Nab3 also contains unique sequences on its N- and C-terminus. Nab3's N-terminus is enriched with aspartic acid and glutamic acid residues^{3, 21}. This segment's function is unknown, and it can be removed without impacting viability^{3, 21}. The C-terminus is heavily biased towards the amino acids proline and glutamine (**Fig. 1-3**)^{3, 21}. This domain is important for cell viability, proper transcription termination function, and for Nab3's ability to assemble into amyloid filaments *in vitro* and a granule *in vivo* (to be discussed below)^{3, 24, 26, 29}. Together, these

three proteins work to coordinate transcription termination of non-coding RNAs in *Saccharomyces cerevisiae*.

1.2.3 Sen1: a helicase protein

Sen1 encodes a 240 kDa superfamily I helicase/ATPase, homologous to the human senataxin protein and it is the third part of the yeast nuclear Nrd1-Nab3-Sen1 transcription termination complex^{3, 12, 27, 30}. Sen1 was originally discovered in a screen exploring heat-sensitive mutations that affected tRNA splicing endonuclease activity^{3, 12, 30}. The C-terminal domain of the protein contains the helicase domain, nuclear localization sequence (NLS) and an interaction domain for a phosphatase that is a CPF subunit (Glc7)^{3, 12, 14}. The N-terminal domain interacts with Pol II and endonucleases and is dispensable for viability^{12, 14}. Sen1 is essential for cell viability and is required for the expression, maturation and termination of numerous types of non-coding RNAs²⁷. Sen1 regulates non-coding gene expression by preventing elongation through the activation of premature termination (termination *via* NNS mechanism) and degrading CUTs in coordination with the TRAMP complex and nuclear exosome^{12, 21}. Mutations in the Sen1 helicase domain result in defects in transcript processing and termination, such as transcriptional readthrough, ultimately leading to a genome-wide change in Pol II's profile^{12, 14}.

In addition to acting in non-coding RNA transcription termination, Sen1 has been shown to be involved in the termination of some coding RNAs^{12, 27}. Specifically, Sen1 has been shown to be cross-linked to the ends of mRNA transcripts, suggesting that it is involved in mRNA end formation *via* the cleavage/ polyadenylation process¹². Sen1 is also known to act as a fail-safe termination mechanism for coding RNAs in which it binds newly synthesized mRNA when polyA-coupled termination is read through^{14, 27}. Additionally, Sen1 plays roles in RNA Pol II's

distribution on RNA as well as by resolving R-loops (RNA:DNA hybrid) that naturally form during transcription^{12, 14, 27}.

1.3 An introduction to RNA-binding proteins

RNA-binding proteins (RBP) bind RNA through one or more RNA-binding domains (RBD)³¹. When RBPs bind RNA, the fate of the RNA is changed and this is important for the regulation of gene expression within a cell³¹. RBPs come together and participate in the formation of ribonucleoprotein (RNP) complexes which play multiple roles involved in regulating gene expression³¹.

1.3.1 Domains found in RNA-binding proteins

RNA-binding proteins contain a conserved motif that enables the binding of RNA^{31, 32}. It is important to note that RBPs can bind a specific sequence in the RNA or bind to a structural motif formed by the RNA^{31, 32}. RBPs contain structural domains such as the RNA recognition motif (RRM), heterogeneous nuclear ribonucleoprotein K (hnRNP K) homology domain (KH), and/or DEAD box helicase domain³¹. RRMs are conserved motifs and are important domains in RBPs where they may be present in multiple copies³³. For example, some RBPs, such as Pab1 and Nop4 in yeast, contain multiple RRMs^{34, 35}. Pab1 contains four tandem copies of its RRM, while Nop4 contains four individual RRMs, contributing to these proteins' ability to bind and regulate RNA fate^{34, 35}. hnRNP K domains are evolutionarily conserved domains that modulate binding of short ribonucleotide sequences³⁶. They are also often present in multiple copies per protein³⁶. RNA-binding proteins rely on their structural domains to target, bind and regulate RNA expression, transcription and metabolism.

1.3.2 Biological roles of RNA-binding proteins

RNA-binding proteins have a broad range of functions ranging from RNA biology to cellular metabolism^{32,37}. When an RNA is synthesized by Pol II, RBPs immediately bind the RNA and form RNP complexes that in turn, regulate the fate of the RNA³⁷. In the context of ncRNA, RBPs function to terminate and process ncRNA and assemble ncRNA into RNP complexes³⁷. For mRNA, RBPs are essential in termination and processing of mRNA as well as its export to the cytoplasm for translation into functional protein³⁷. RBPs also assist in the production and degradation of RNA, thus playing critical roles in regulating RNA expression³⁷.

Widely studied functions of RBPs include transcription termination, RNA transport, degradation of RNA, and post-transcriptional gene regulation^{32, 37}. However, only 60% of RBPs found in yeast have functions related to RNA biology or contain structural motifs predicted to enable RNA binding³². Other proteins studied have emerged as RBPs but have other classifications such as glycolytic enzymes^{32, 37}. One study found that over half of the RBPs identified in a microarray analysis were previously identified enzymes, many of them functioning in metabolism³⁷. This exemplifies how diverse RBP function can be and suggests a more complex network of RBP functions ranging from gene regulation to metabolism^{32, 37}. In order to perform these diverse roles, RBPs vary their RNA-binding modes and their RNA-binding specificities³².

1.4 An introduction to prions and prion-like proteins

A prion is a type of infectious protein particle that arises from a modified isoform of a protein and lacks nucleic acid³⁸⁻⁴². Prion proteins often assemble into organized amyloid filaments with a cross β -sheet structure and become self-propagating infectious agents^{38-41, 43}. For example,

in mammals there is a single prion-forming protein (PrP) that is responsible for causing prionopathies^{38, 39, 41, 42, 44}. Prionopathies are infectious neurodegenerative diseases, that are able to spontaneously transmit from one individual to another⁴⁴. Human prionopathies include Creutzfeldt–Jakob disease (CJD), fatal familial insomnia (FFI), Gerstmann–Sträussler–Scheinker syndrome (GSS), and kuru^{38, 39, 41}. PrP becomes a prion protein in mammals when a portion of its α -helical and coil structure is turned into a β -sheet (PrP^{Sc})^{38, 41, 44}. When these modified isoforms arise, the physiochemical properties of the protein are altered and this leads to changes in the protein's biological function³⁸. For example, PrP is soluble in non-denaturing detergents and digested by proteases, whereas the prion protein is insoluble and partially resistant to proteases³⁸. Prions are classified as such not solely based on their misfolded state, but on their transmissibility as well^{38, 39, 41}. This is an important distinguishing feature of prions because many diseases involve misfolded proteins³⁹. The diseases caused by the prion-forming protein are currently incurable and deadly³⁹.

In contrast to the single mammalian prion, there are several human proteins that are considered prion-like^{39, 44}. They are classified as prion-like due to their compositional similarity (Q/N-rich domains) to prion proteins as well as their ability to aggregate and propagate pathology^{40, 44}. However, they are prion-like due the non-infectious disease state they induce compared to the infectious disease state induced by prion proteins⁴⁴. These diseases are neurodegenerative in nature and include Alzheimer disease, Parkinson disease, frontotemporal dementia, and amyotrophic lateral sclerosis (ALS) to name a few^{39-41, 44}. For example, the human RNA-binding protein FUS contains a Q-rich domain and has been found in cytoplasmic aggregates which have been implicated in ALS⁴⁰. Thus, both prion and prion-like proteins exist in mammals.

1.4.1 Yeast prions and prion-like proteins

Numerous naturally occurring prion proteins have been found in *Saccharomyces cerevisiae* and have helped inform our understanding of mammalian prion proteins^{39, 40, 43, 44}. The majority of these prion proteins contain prion-forming domains that are enriched in the amino acids glutamine and asparagine (Q/N)^{39, 40, 45}. It is important to note there are numerous other amyloid- and prion-forming proteins in yeast that are not enriched in Q/N, and thus Q/N enrichment is not a requirement for amyloid formation or prion activity³⁹. Several proteins in both mammals and yeast contain domains with high compositional similarity to a prion and these protein domains are termed prion-like domains (PrLD)^{39, 42}. A yeast prion is defined by its cytoplasmic/nuclear inheritance to progeny whereas a prion-like protein in yeast does not necessarily display inheritability⁴². A handful of mammalian PrLD proteins, which have similarities to yeast PrLD proteins, are implicated in various neurodegenerative diseases in humans such as Alzheimer disease and Parkinson disease³⁹⁻⁴¹, thus making yeast PrLD proteins an insightful tool for better understanding human neurodegenerative diseases.

At least 10 known prions have been identified in *S. cerevisiae*⁴⁰. The prion form of the Sup35 [*PSI*⁺] and Ure2 [*URE3*] proteins were the first prions discovered in yeast through a genetic screen to uncover non-chromosomal genetic elements with non-Mendelian genetic inheritance^{39, 40, 42-44}. These two yeast prion proteins share common sequence characteristics that have enabled identification of additional prions in yeast^{39, 43}. These characteristics include an N-terminal prion-forming domain (PFD) and a C-terminal functional domain^{39, 43}. The PFDs of both proteins are Q/N-rich and intrinsically disordered^{39, 40, 43}, meaning the domain does not take on a stable secondary structure. Additionally, charged and highly hydrophobic residues relative to the yeast proteome are underrepresented in PFDs^{39, 43}. Interestingly, the PFD can be appended to other

proteins and support prion formation in this non-native context^{39, 40}. Additionally, the primary sequence of the PFD can be scrambled and still support prion formation^{39, 40}. This indicates that the amino acid composition and not the primary sequence is responsible for prion activity^{39, 40}. In order to be considered a prion, a protein must be able to form prion aggregates, recruit additional soluble protein and convert it to the prion form and be fragmented to generate new independently segregating aggregates during cell division^{39, 45}.

Prions often alter the protein's normal cellular function, thus leading to downstream effects and cellular changes overall⁴⁰. For example, Sup35 is part of the translation termination complex⁴⁰. When [*PSI*⁺] forms, there is a reduction in translation termination efficiency and an increase in nonsense-codon read-through as well as programmed frameshifting^{40, 43, 44}. This results in changes in RNA stability as well as altered functionality of the encoded polypeptides⁴³. The [*URE3*] prion results in upregulation of poor nitrogen source usage, even when rich sources are present^{40, 43}. Thus, formation of prions results in cellular changes overall⁴³.

1.4.2 Yeast as a model for human neurodegenerative diseases

While there is only one known prion in humans, yeast contain several^{39, 40}. Thus, yeast prions have been leveraged to design and develop algorithms that aim to predict prion and prion-like proteins³⁹. Numerous algorithms have been developed and each has a distinctive set of parameters used to predict prions³⁹. Alberti *et al.* developed a robust prediction algorithm³⁹ which employed modeling as well as prion-like activity assays^{39, 43}. Alberti *et al.* bioinformatically scanned the yeast genome for proteins with prion-like features and identified 100 yeast proteins that contained the greatest compositional similarity to known yeast PFDs^{39, 43}. They then subjected

these candidates to genetic, cell biological, and biochemical assays to determine their prion-forming capacity^{39, 43}. Their conclusion was that at least 24 yeast proteins contain PFD⁴³.

S. cerevisiae is a useful model organism for studying human neurodegenerative diseases because, like mammals, *S. cerevisiae* contains prions and prion-like proteins⁴⁰. Furthermore, human diseases have successfully been modeled in *S. cerevisiae*. For example, the human prion-like, RNA-binding protein, FUS, forms cytoplasmic aggregates in human cells and these aggregates are implicated in ALS⁴⁰. FUS's cytoplasmic aggregation has been recapitulated in *S. cerevisiae* in an induced proteinopathy⁴⁰. Additionally, the use of *S. cerevisiae* to predict PrLDs in human proteins has proved useful for studying human neurodegenerative diseases. For example, the human proteins hnRNPA_{2B1} and hnRNPA₁ are two proteins that contain PrLDs⁴⁰. Familial mutations in these domains are associated with neurodegeneration through amyloid formation⁴⁰. Furthermore, the ability to predict PrLD in human proteins has helped identify human proteins involved in neurodegenerative diseases⁴⁰. For example, HNRPDL is a human protein that contains a PrLD and is linked to the development of limb-girdle muscular dystrophy⁴⁰. Additionally, at least nine other neurodegenerative diseases have pathogenic proteins with disease-linked poly-Q expansions⁴⁰. Thus, *S. cerevisiae* is useful for numerous reasons when studying human disease.

1.5 Nab3: a prion-like protein

As previously stated, Nab3 is part of the essential NNS transcription termination complex found in *S. cerevisiae*³. Its protein structure contains a non-essential, aspartate/glutamate rich N-terminus, an RNA recognition motif (RRM) and an essential, proline/glutamine rich prion-like domain (**Fig. 1-3**) as determined by Alberti *et al.*^{21, 24, 29, 43}. Nab3 also contains a Nrd1 interaction domain (NID) that allows it to heterodimerize with Nrd1 to perform transcription termination

functions³. Nab3's RRM is important for cell growth and enables Nab3 to bind RNA that contains the sequence UCUU²¹. The C-terminus of Nab3 scores highly as a prion-like domain *via* the Alberti *et al.* algorithm partly due to its polyglutamine repeats and was shown to be important for proper transcription termination^{21, 24, 43}. Additionally, the C-terminus of Nab3 is sufficient to induce the assembly of recombinant fusion proteins into higher order multimers, suggesting that multimers of Nab3 are important for proper transcription termination and transcript processing/degradation²⁵. The recombinant domain can form amyloid filaments *in vitro*, similar to those seen for human prion-like proteins that form filaments in certain neurodegenerative diseases^{26, 43}. The biochemical and biophysical characteristics of these filaments are typical of low complexity regions of other RNA-binding proteins that are resistant to dissociation by anionic detergent and form β -sheet rich structures²⁶. Additionally, the prion-like domains from other yeast prions, such as Sup35, can be exchanged with Nab3's and still support viability and transcription termination⁴⁶. In addition to *in vitro* polymerization, Nab3 also displays *in vivo* prion-like characteristics. Upon glucose starvation (discussed below), Nab3 re-localizes from pan-nuclear to a condensed nuclear granule²⁹. Furthermore, Nab3's PrLD is required for its recruitment to the nuclear granule structure²⁹.

1.6 Glucose deprivation

Glucose is a key nutrient and signaling molecule in yeast⁴⁷. Depletion of glucose is known to regulate gene expression through pathways that lead to repression and de-repression of specific genes at the transcriptional level as well as at the translational level⁴⁷. Glucose starvation also results in the induction of subcellular compartments, such as P-bodies and stress granules, known to regulate protein expression in *S. cerevisiae*^{47, 48}. P-bodies and stress granules are

ribonucleoprotein (RNP) structures formed in both mammalian and yeast cells from RNA-binding proteins and RNA⁴⁸⁻⁵⁰. These structures form in the cytoplasm in response to a variety of cues including exposure to stress, such as glucose deprivation, or specific developmental transitions and can be thought of as a mechanism aimed to regulate mRNA translation and degradation in response to changing cellular environments^{48, 49}. Stress granules are viewed as “storage depots” and hold proteins and translationally repressed mRNA until conditions are suitable to resume translation of said mRNA⁴⁸⁻⁵⁰. In contrast, P-bodies house machinery used to degrade mRNA^{48, 50}. These structures are dynamic and change with the cellular environment⁴⁸.

Stress granules form by a self-assembly process that involves RNA-binding proteins with prion-like domains⁴⁸. Intriguingly, ~30% of prion-forming domains reside in RNA-binding proteins, suggesting an importance of prion-like mechanisms in the transport, translation and metabolism of mRNA⁴⁵. The PrLD of these RNA-binding proteins enable the protein to adopt various physical states such as a liquid droplet, a hydrogel or amyloid filament⁴⁵. These varying states contribute to the overall function or dysfunction of the protein within the cell. For example, the structures formed by prion-like proteins in neurodegenerative diseases are not readily reversible and result in a disease state of the cell. In contrast, structures like P-bodies or stress granules are dynamic and allow for normal biological function and regulation of mRNA and protein expression. It is important to note that while prion-like proteins are often implicated in neurodegenerative disease states, they also serve normal biological functions within the cell⁴⁵.

1.6.1 Transcriptome and proteome changes in response to glucose deprivation

Microorganisms, such as yeast, experience nutrient limitations in their natural environments⁵¹. One type of nutrient limitation they can experience is glucose deprivation⁵¹. As

previously mentioned, glucose is a key signaling molecule for mammalian and yeast cells⁴⁷. Thus, it is not surprising that the transcriptome and proteome change in response to glucose levels. A genome-wide study performed in yeast demonstrated that the change from glucose-replete to glucose-deplete conditions involves the integration of numerous major signaling and regulatory pathways^{51,52}. These specific experiments showed that glucose depletion leads to the transcription of cytochrome genes, TCA/glyoxylate cycle genes and carbohydrate storage genes^{51, 52}. Furthermore, this work demonstrated that glucose depletion also leads to the repression of genes involved in protein synthesis which includes ribosomal proteins, tRNA synthetases as well as translation initiation, elongation and translation factors^{51, 52}.

Since then, many other studies have been performed and revealed that there is an increase in the transcription of genes related to high-affinity glucose uptake, the tricarboxylic acid cycle, and oxidative phosphorylation compared to glucose-replete conditions^{53, 54}. Additionally, the location of histone acetylation on genes shows a shift from growth-promoting genes to gluconeogenic and fat metabolism genes⁵⁵. Gene analysis identified specific gene motifs in upstream sequences that may be recognized by transcription factors, such as Nab3 and Nrd1, which are involved in controlling gene expression during glucose starvation⁵³. It is important to note that other nutritional situations, such as ethanol as the sole carbon source or amino acid starvation, cause distinct changes to the transcriptome⁵³.

Studies have also looked at the transcriptome in response to the re-addition of glucose to glucose-depleted cells. These studies reveal that the cellular response to the re-addition of glucose is fast, with metabolic changes occurring within seconds followed by transcriptome changes within minutes of glucose re-addition^{51, 56}. Approximately one-third of genes were significantly and differentially expressed upon the re-addition of glucose^{51, 57}. These included genes involved in

growth, carbon catabolite repression, and ribosomal biogenesis^{51, 57}. These findings demonstrate the important and significant transcriptional reprogramming in response to the re-addition of glucose and the cellular changes moving the cell towards a state of active growth⁵¹.

1.6.2 Nrd1-Nab3 transcript binding changes in response to glucose deprivation

Under glucose replete conditions, Nrd1 and Nab3 are known to bind to specific sequences in nascent non-coding RNA (snoRNAs, snRNAs and CUTs) during transcription termination by Pol II^{2, 3, 11, 14, 16, 17, 21-26}. These transcripts are then processed or degraded by the TRAMP and nuclear exosome complexes respectively^{2, 3, 11, 14, 16, 17, 21-26}. While Nrd1 and Nab3 bind to the expected terminator sequences downstream of the snoRNA, Nrd1 also binds to the upstream region of some snoRNAs and plays a role in mRNA 3' end formation for some protein-coding genes²³. Nrd1 and Nab3 are also shown to bind to transcripts transcribed by RNA Pol III²³. Thus, under glucose-replete conditions, Nrd1 and Nab3 are involved in the termination of numerous types of RNA transcripts.

Studies performed by Jamonnak *et al.* revealed that Nrd1 and Nab3 binding to transcripts changes during glucose depletion²³. Specifically, there is a substantial upstream shift in the binding of Nrd1 to snoRNA, approximately 100 nucleotides upstream relative to the position Nrd1 binds in glucose-replete conditions²³. Interestingly, all these Nrd1 binding sites are within the mature snoRNA²³. Jamonnak *et al.* proposed that this change in Nrd1, which correlates with Nrd1 and Nab3's condensation into a nuclear granule, indicates a change in function for NNS during glucose starvation^{23, 29, 58}. They further proposed that this change could be indicative of earlier termination directed by an altered Nrd1-Nab3 binding specificity or could be attributed to Nrd1-Nab3 mediated degradation of mature snoRNA in the absence of glucose²³. However, studies have

yet to elucidate the function of the Nrd1-Nab3 granule or the precise mechanisms which govern its assembly and dissolution.

1.7 Research focus

It is well established that proteins reorganize in response to physiological stimuli to form subcellular compartments. For example, RNA-binding proteins, such as Pub1 and Nab3, reorganize to form cytoplasmic stress granules and nuclear granules in yeast respectively^{29, 59}. While much is known about the function and the mechanisms which govern stress granule assembly and dissolution, little is known about the Nab3 nuclear granule. Prior to this thesis, foundational work was done that provided insight into Nab3's ability to reorganize in response to glucose deprivation and the features of Nab3 that are required for its reorganization.

First, it was discovered that a stretch of glutamines and the final 18 amino acids found in the C-terminus of Nab3 could assemble into a tetrameric form like the human hnRNP-C protein²⁵. Subsequent experiments demonstrated that purified, prion-like last 134 amino acids of Nab3's C-terminus can assemble into amyloid filaments and a hydrogel *in vitro*.^{24,26} Additionally, Nab3 and its binding partner, Nrd1, condense into a nuclear speckle in response to glucose deprivation *in vivo* and the Nab3 prion-like domain is required for its assembly into a nuclear granule^{29, 58}. These findings supported other work at the time that showed RNA binding proteins with low complexity domains could form subcellular compartments in which RNA metabolism takes place²⁶.

These findings led to the questions of: 1) what functional purpose this rearrangement serves for the cell, as well as 2) what mechanism(s) underlies granule assembly and dissolution persist. This thesis addresses the latter question. I document an inability of cells to use non-fermentable carbon sources which leads to a glucose starvation-dependent growth deficit that

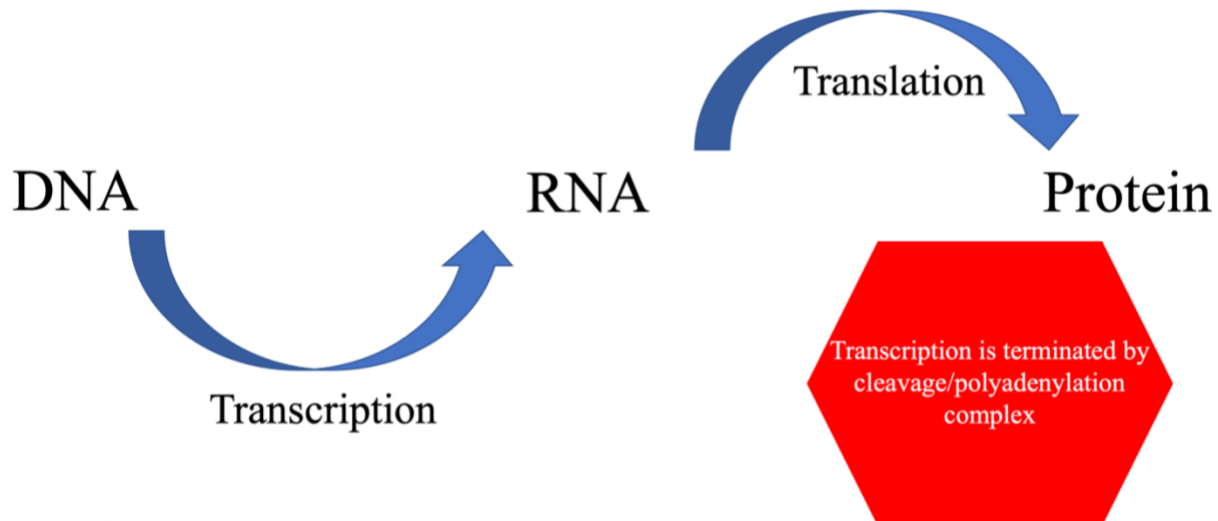
correlates with a high granule forming phenotype. This suggested that Nab3 granule accumulation is related to mitochondrial function and respiration. I expand upon this hypothesis by demonstrating that defects in mitochondrial function result in higher levels of Nab3 granule accumulation. Furthermore, I show that a yeast strain known to be heterogeneous for mitochondrial function can be placed under selective pressure to enrich for a homogenous population that shows improved mitochondrial function and a reduction in Nab3 granule accumulation. I further support the respiration hypothesis by demonstrating that addition of extracellular ATP is sufficient to reduce Nab3 granule accumulation in a high accumulating yeast strain. Lastly, I explore the effects of a serine-arginine protein kinase implicated in yeast stress granule disassembly. I document that the deletion of this kinase results in an inability to use non-fermentable carbon sources and leads to an increase in Nab3 granule accumulation. This work provides the first foundational documentation of cellular drivers of Nab3 granule accumulation and supports a model in which there is a dynamic equilibrium between granule accumulation and disassembly that is driven by intracellular ATP levels.

An additional piece of work found in this thesis is the development a new computational tool developed to rapidly quantify the distribution of fluorescent proteins in large numbers of cells. Specifically, I used this tool to analyze and quantify Nab3 granule formation upon the removal of glucose in confocal images of live yeast cells. Use of this algorithm allowed us to characterize granule accumulation across strains of *S. cerevisiae* and established that granule accumulation is a phenotype with variable penetrance.

1.8 Figures

Fig. 1-1

A



B

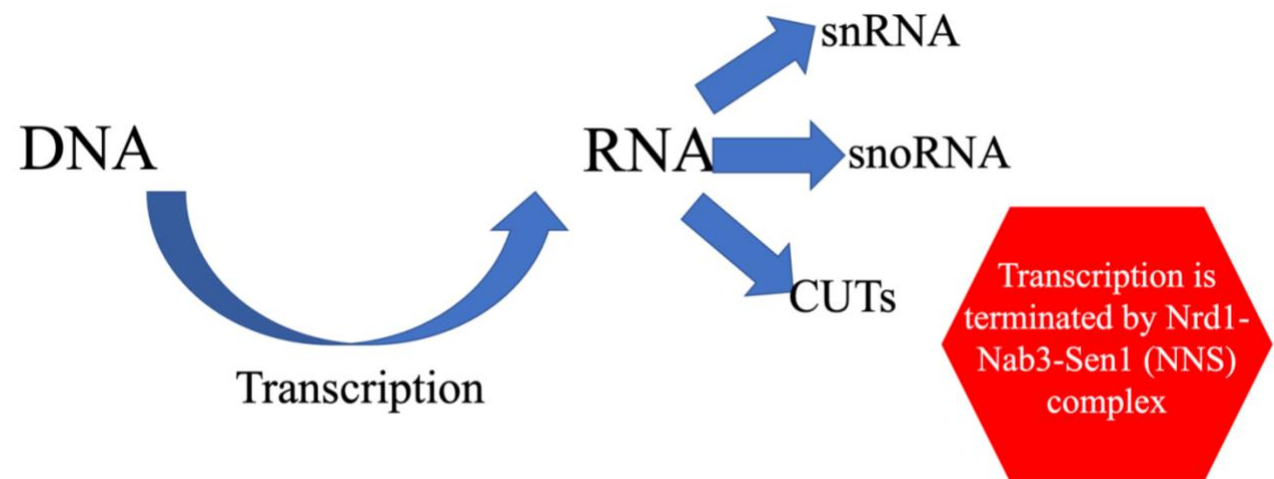


Fig. 1-1 Modes of transcription termination in *S. cerevisiae*

(A) When messenger RNA (mRNA) is transcribed by the cell, transcription is terminated by proteins brought in the by cleavage/ polyadenylation complex.

(B) When noncoding RNA (ncRNA) is transcribed by the cell, transcription is terminated by the Nrd1-Nab3-Sen1 (NNS) transcription termination complex.

Fig.1-2

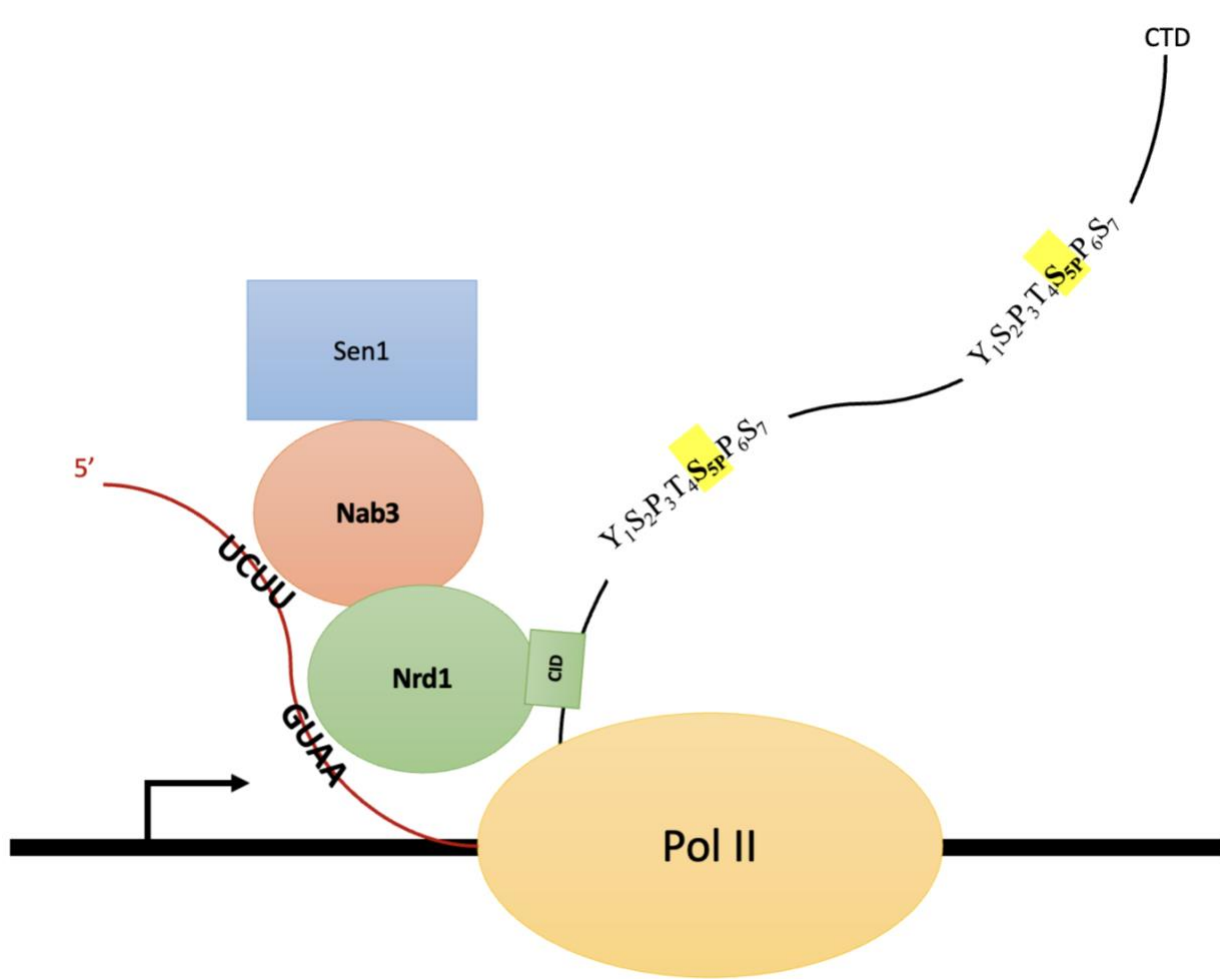
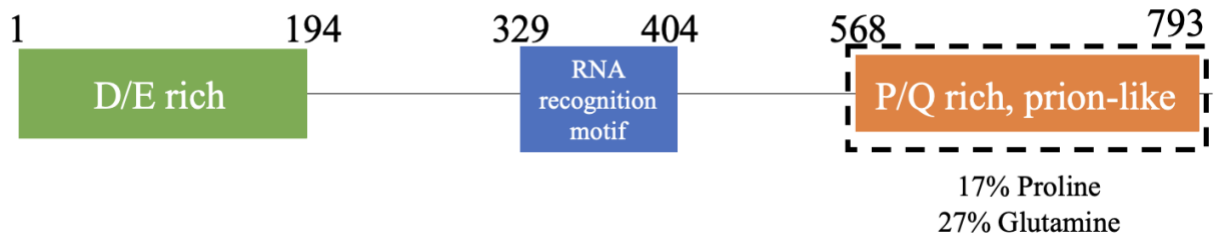


Fig. 1-2 Nrd1-Nab3 mediated transcription termination

Pol II binds DNA and begins to transcribe RNA. Serine 5 of Pol II's CTD is phosphorylated (Ser(P)5) within the first few hundred nucleotides of the promoter (yellow highlighted region on CTD). Ser(P)5 is important for coordinating non-coding transcription termination, which is carried out by a complex known as Nrd1-Nab3-Sen1 (NNS), as Nrd1 contains a C-terminal interaction domain (CID, gray box) that allows Nrd1 to bind to the C-terminus of Pol II when Ser(P)5 is present. Nrd1 and Nab3 function as a heterodimer during transcription termination and each contain a RRM that recognizes and binds the nascent RNA (dark blue boxes). These binding events are all important to the coordination of non-coding transcription termination.

Fig. 1-3

**Fig. 1-3 Protein domains of Nab3 protein**

Nab3 contains a non-essential, aspartate/ glutamate rich N-terminus (green), an RNA recognition motif (blue) and an essential, proline/ glutamine rich prion-like domain (orange).

**CHAPTER 2.0: Variable penetrance of Nab3 granule accumulation quantified by a
new tool for high-throughput single-cell granule analysis**

K. Hutchinson was responsible for Fig. 2-1, 2-6, 2-7, S2-1 and contributed to Fig. 2-8. Additionally, all microscopy that contributed to the generation of the computational tool was completed by K. Hutchinson.

Hunn, Jeremy C et al. “Variable penetrance of Nab3 granule accumulation quantified by a new tool for high-throughput single-cell granule analysis.” *Current genetics*, 10.1007/s00294-022-01234-2. 17 Mar. 2022, doi:10.1007/s00294-022-01234-2

*These findings were published in *Current Genetics* on March 17, 2022. Supplemental information can be found online at: <https://pubmed.ncbi.nlm.nih.gov/35301575/>

2.1 Abstract

Reorganization of cellular proteins into subcellular compartments, such as the concentration of RNA-binding proteins into cytoplasmic stress granules and P-bodies, is a well-recognized, widely studied physiological process currently under intense investigation. One example of this is the induction of the yeast Nab3 transcription termination factor to rearrange from its pan-nucleoplasmic distribution to a granule at the nuclear periphery in response to nutrient limitation. Recent work in many cell types has shown that protein condensation in the nucleus is functionally important for transcription initiation, RNA processing, and termination. However, little is known about how subnuclear compartments form. Here we have quantitatively analyzed this dynamic process in living yeast using a high-throughput computational tool and fluorescence microscopy. This analysis revealed that Nab3 granule accumulation varies in penetrance across yeast strains. A concentrated single granule is formed from at least a quarter of the nuclear Nab3 drawn from the rest of the nucleus. Levels of granule accumulation were inversely correlated with a growth defect in the absence of glucose. Importantly, the basis for some of the variation in penetrance was attributable to a defect in mitochondrial function. This publicly available computational tool provides a rigorous, reproducible, and unbiased examination of Nab3 granule accumulation that should be widely applicable to a variety of fluorescent images. Thousands of live cells can be readily examined enabling rigorous statistical verification of significance. With it, we describe a new feature of inducible subnuclear compartment formation for RNA-binding transcription factors and an important determinant of granule biogenesis.

Keywords: Nab3, granule, penetrance, low complexity domain

2.2 Introduction

The reorganization of proteins to form subcellular compartments in response to physiological stimuli has provided novel insight into cellular structure and the mechanisms by which cells compartmentalize their biochemical and molecular events. RNA-binding proteins, such as Pub1, which is found in yeast stress granules⁵⁹, have been examined for their ability to dramatically reorganize in cells. Proteins in this class often harbor a low complexity domain (LCD) important for self-assembly and localization to subcellular granules^{60, 61}. LCDs typically lack stable secondary structural elements due to their intrinsic disorder; however, the domain can become structured and highly organized by assembling *via* phase separation. This process has been studied by a variety of methods, fluorescence microscopy being one well-established approach⁶².

The essential *Saccharomyces cerevisiae* RNA-binding transcription factors, Nab3 and Nrd1, together with Sen1, serve a critical function in terminating transcription by RNA polymerase II³. This so-called NNS complex is involved in biogenesis of snRNAs, snoRNAs, and other small non-coding RNAs, as well as in regulating gene expression through mechanisms of attenuation⁶³⁻⁶⁷. NNS functions through a set of interactions with RNA and RNA polymerase II culminating with the displacement of the nascent transcript from the elongation complex by the Sen1 helicase subunit³. Nab3 and Nrd1 harbor conserved, hnRNP-like, RNA recognition motifs^{68, 69}. During glucose restriction, the abundance and identity of cellular RNA undergoes a dramatic change in concert with Nab3 and Nrd1's association with a new set of RNAs and a change in their positions on previously bound transcripts^{23, 70, 71}. Intriguingly, this transcriptomic reprogramming is accompanied by Nab3 and Nrd1's migration from a distribution that is broadly nucleoplasmic, to one that is a tightly focused nuclear punctum or granule^{29, 58}. The functional consequence of this rearrangement is unclear, although the inducible accumulation of the Nab3 granule resembles the

formation of cytoplasmic ribonucleoprotein structures such as the stress granule, which also aggregates in response to glucose restriction.

The cellular signaling pathway involved in the formation of the Nab3-Nrd1 granule is unknown, however, Nab3 and Nrd1 each possess the potential to spontaneously self-assemble^{25, 26, 29} due to their glutamine-rich LCDs⁴³. These two, and other yeast proteins with low complexity domains, can self-assemble and form aggregates in living cells. Nab3's LCD (27% glutamine, 20% proline over 225 residues) is required for its ability to polymerize and has been extensively characterized both *in vitro* and *in vivo*. The purified recombinant domain and full length Nab3 protein assemble into amyloid filaments and gels with a characteristic cross- β structure, as assessed by negative stain electron microscopy, thioflavin dye-binding, circular dichroism, fiber diffraction, and semi-denaturing gel electrophoresis^{21, 25, 26, 29, 46}. Hence, the Nab3 LCD has several features of the many RNA-binding proteins that form subcellular compartments by phase separation. Through genetic analysis, it is evident that Nab3 also multimerizes *in vivo*⁷². The incorporation of Nab3 into a granule in response to glucose restriction is dependent on its LCD, as well as the domain's high glutamine content. Nab3's RNA recognition motif is also necessary for this re-localization²⁹. Some, but not all, heterologous LCDs from other proteins can substitute for the Nab3 domain in terms of sustaining viability. The resulting chimeric proteins assemble into granules, suggesting that the main function of the domain is to support self-assembly⁴⁶. The Nab3-granule in live cells is sensitive to treatment with the aliphatic alcohol 1,6 hexanediol, which is consistent with, although does not alone prove, a phase separation basis for granule accumulation²⁹. Granule formation is reversible and Nab3 rapidly redistributes to the nucleoplasm following glucose refeeding²⁹. Cytoplasmic compartments similar to the Nab3 granule, such as stress granules, are disassembled by chaperone ATPases such as Hsp104 in yeast⁷³. Thus,

respiration and the efficient generation of ATP plays an important part in the steady state accumulation of stress granules. The machineries that assemble or dissociate the Nab3 granule are not known.

Analysis of Nab3 granule formation and disassembly would benefit from a quantitative understanding of the specifics of the protein's distribution between the nucleoplasm and granule compartments, as well as how widespread the phenomenon is. To this end, we have developed a computational tool that enables the rapid quantification of the distribution of fluorescent proteins in cells. We characterize the granule accumulation process and show for the first time that the granule accumulation phenotype displays variable penetrance across *S. cerevisiae* strains. Furthermore, we document a glucose starvation-dependent growth deficit, and the inability to use non-fermentable carbon sources, both of which correlate with the granule forming phenotype, strongly suggesting that Nab3 granule accumulation is related to mitochondrial function and respiration. This computational tool enabled us to measure several features of protein re-localization in a large numbers of organisms. The approach is versatile in that parameters can be set for a diversity of applications which allows the tracking of varied fluorescent proteins through subcellular compartments in a variety of cell types. Indeed, we have used it here to score the well-known capacity of IMP dehydrogenase to polymerize into structures known as rods and rings in immunofluorescent images of fixed human cells.

2.3 Materials and methods

Plasmid Construction

The plasmid pRS315-NRD1 was generated by PCR amplification of *NRD1* from genomic DNA targeting the region 600 bp upstream and 500 bp downstream of the *NRD1* open reading frame using oligonucleotides 5'-ATATAAGCTTCTACTGCGCACGTATAGCGC-3' and 5'-ATATCTCGAGAATATGCCGGAAACGTCCAC-3'. The PCR product and pRS315 plasmid were cut with *HindIII* and *XhoI* restriction enzymes and ligated. The pRS315-HA-NRD1 plasmid was generated by inserting two tandem HA tags after the start codon of the NRD1 ORF in pRS315-NRD1 by PCR mutagenesis using the oligonucleotides 5'-TATCCGTATGATGTTCCGGATTATGCATATCCGTATGATGTTCCGGATTATGCACAGCAGGACGACGATTTTCA-3' and 5'-CATTATGGGATGTTTAGTATGTTTGTTC-3'.

Yeast Strain Construction

Yeast strains used in this paper are presented in Table 1. DY4580 was generated using high efficiency lithium acetate transformation⁷⁴ to transform DY4543 with a PCR product encoding *HTB2* tagged with mCherry and marked with *HIS3* that was amplified from genomic DNA of yeast strain YOL890 (gift from Dr. S Wentz) using 5'-GCAGCTGAACCAGCTTTACC-3' and 5'-GCTTTCAGTCGAAAACAGC-3'. Transformants were isolated by growth on SC his⁻ media and verified by PCR.

DY4724 was generated by transforming DY1620 with pRS315-HA-NRD1. Transformants were selected on SC leu⁻ ura⁻ media. A single transformant was then struck onto 5-fluoroorotic acid to cure DY4724 of pAC3314-NRD1, resulting in DY4736. DY4736 was used to generate DY4746 using the pop-in/pop-out method of allele replacement⁷⁵ to integrate GFP onto *NAB3* as an N-

terminal tag in its native chromosomal location. DY4756 resulted from transformation of DY4746 with a yomCherry-tagged *HTB2* PCR product generated from pFA6a-link-yomCherry-kan⁷⁶ using 5'-GGTGACGGTGCTGGTTTA-3' and 5'-TCGATGAATTCGAGCTCG-3'.

DY4771 was generated from YSC1059 (Horizon Discovery LLC) by allele replacement using pop-in/pop-out to integrate GFP in frame with *NAB3* in its native chromosomal location. DY4772 resulted from homologous recombination using a PCR product of mCherry-tagged *HTB2* into DY4771, as described above for the generation of DY4580.

To replace chromosomal *NRD1* in a strain that had only plasmid-borne *NRD1*, a Cas9 guide sequence was designed to target the *NATI* cassette disrupting the chromosomal *NRD1* locus of DY4826. A Cas9-expressing plasmid that also generates the needed guide RNA, was made by inserting the guide DNA oligonucleotides into pCAS⁷⁷ by PCR using 5'-CGGATGGGGTTCACCCTCTGGTTTTAGAGCTAGAAATAGC-3' and 5'-AAAGTCCCATTCGCCA-3'. Donor *NRD1* DNA was generated by PCR from pRS316-*NRD1* using 5'-CTACTGCGCACGTATAGCGC-3' and 5'-AATATGCCGGAAACGTCCAC-3'. The pCAS plasmid and donor DNA were transformed into DY4826 and selected with G418. Candidates for the reinsertion of *NRD1* in place of *NATI* were screened for the loss of nourseothricin sensitivity, and the correct strain was chosen after sequence-confirmation of a PCR product from genomic DNA. The isolate was screened for the loss of both pCAS and pRS315-HA-*NRD1* yielding strain DY4834. DY4826, was constructed from DY4746 by C-terminal tagging of *HTB2* with mCherry using *Schizosaccharomyces pombe* *HIS5* as a downstream auxotrophic marker in the recombination cassette, as described previously²⁹.

DY4772 was grown in YPD containing 20 µg/mL ethidium bromide for 24 h at 30°C as described⁷⁸. Cells were plated on YPD and colonies were replica plated onto YPEG to test for loss

of respiratory function. Two independent colonies were selected for further analysis (DY4849 and DY4850). The *COX3* sequence in mitochondrial DNA was analyzed by PCR using 5'-GGTAATATGAATATGGTATATTTAGC-3' and 5'-GTTACAGTAGCACCAGAAGATAATAAG-3'. Control primers for *NAB3* were 5'-GTGTAACCCTGAATTGTTGAAGAG-3' and 5'-CAGAGGAAACAAATGAAGAGGTGCG-3'.

Yeast Growth Assays

Yeast strains were grown to saturation at 30°C in the appropriate selection media. For solid medium growth assays, saturated cultures were diluted with sterile water to a concentration of 10^7 cells/ml, serially diluted 10-fold, and five spots of 10 µl of each dilution were applied to the appropriate solid media and grown at 30°C.

For liquid growth assays, cultures were inoculated and grown to saturation at 30°C. Cultures were reseeded and grown to mid-log phase in glucose-containing media. Cells were washed three times into media without glucose (starvation media) and incubated at 30°C for 2 hours. At the conclusion of the 2hr starvation period, an aliquot of cells (“refed”) were resuspended in glucose-containing medium, optical densities (600 nm) were measured, and cultures diluted to a final OD_{600} of 0.05. The remainder of the cells were maintained in starvation media and diluted to OD_{600} of 0.05. Three 100µl biological replicates were plated in triplicate in a 96-well plate and placed onto a BioTek Epoch 2 plate reader at 30°C. Optical densities were measured every 20 minutes until growth plateaued.

Confocal Microscopy and Image Analysis

Cells containing GFP-tagged Nab3 and fluorescently tagged histone H2B, were grown to log phase in the appropriate, glucose-containing, selection media. Cells were split and washed three times into the appropriate media without glucose (starvation media) or with glucose, incubated at 30°C for 2 hours and placed onto single cavity microscope slides containing 1.5% agar pads in the appropriate media. Z-stacks of both bright field and fluorescence were obtained at room temperature on a Leica SP8 point scanning confocal microscope using the HyD (GaAsp) and PMT-transmitted light detectors, an HC PL APO 63X, 1.40 numerical aperture oil immersion lens at a working distance 0.14mm. The microscope settings used are as follows: 488nm line from an argon laser and 594 helium neon laser, pinhole 1 AU, image capture format 1024x1024, scan speed 400 Hz, pixel dwell time 1.2 μ s. Eight-bit images were acquired using the Leica Application Suite X 3.0.2.16120 (Leica) and converted to .png files. Images presented in figures are displayed as maximum intensity projections. Color channels were split using FIJI⁷⁹ and quantified using the MATLAB software⁸⁰. Nuclear mask intensity thresholds were set at 17 relative fluorescence units (rfu) and had to be 40 pixels in size. The fluorescence intensity of pixels with GFP-Nab3 were averaged individually for each mask after excluding the 10 highest value pixels. Preliminary manual measurements showed that the granules were often 10 pixels or less and this exclusion was done to prevent skewing of the average with bright pixels that would be present in potential granules. The standard deviation (σ) of pixels in the mask were calculated and pixels with intensities $>3\sigma$ (“3 σ ” pixels) over the mean were identified. (The threshold of $\mu+3\sigma$ worked well for both Nab3 and IMPDH2, but this value may need to be adjusted for accurate detection of granules in other systems where the relationship between the concentrations of the soluble and condensed species differ.) The size of clusters, in terms of the number of adjacent 3 σ pixels, was scored for each nuclear mask. The full MATLAB script is freely available through GitHub.

Jurkat cell culture

Jurkat E6-1 cells were obtained from ATCC and grown in RPMI (Gibco) supplemented with 10% fetal bovine serum, penicillin, and streptomycin in the presence of 5% CO₂. Cells were maintained in T-75 flasks, passaged when $\leq 70\%$ confluent, and routinely tested for mycoplasma contamination (Lonza). Cells were plated in 12-well plates at a concentration of 10,000 cells/mL. Mycophenolic Acid (MPA; Sigma) dissolved in 0.1M NaOH was administered to cells at a final concentration of 10 μ M. Cells not destined for MPA treatment received an equal volume of the drug vehicle. Cells were treated for two hours, washed twice with phosphate buffered saline (PBS) supplemented with 10 μ M MPA (treated cells) or an equal volume of vehicle (0.1M NaOH) and resuspended in 167 μ L PBS with appropriate supplement before dispensing to glass coverslips pre-treated with poly-L-lysine (Sigma; P4707) for 1 hr at 22 °C. Cells were fixed with 4% (v/v) paraformaldehyde (Electron Microscopy Sciences; 15710) in PBS for 15 min followed by washing with PBS twice for 5 min. Cells were permeabilized with 0.1% Triton X-100 in PBS and incubated for one hour with 1% BSA (USBiological) in PBS and incubated overnight with rabbit anti-IMPDH2 antiserum⁸¹ diluted 1:10,000. After 16 hrs, coverslips were washed with PBS four times for 5 min each and incubated for one hour with goat anti-rabbit AlexaFluor 488 (Invitrogen) secondary antibody diluted 500-fold. Coverslips were washed with PBS twice for 5 min each followed by staining with Hoechst 33342 (Invitrogen) for four minutes before mounting on glass slides with a mounting mixture of 1, 4-phenylenediamine (Sigma) and Mowiol 4-88 (Sigma). Cured slides were imaged on a Biotek Lionheart FX using the “DAPI” and “GFP” filter cubes in addition to its brightfield capability. The three channels were merged in FIJI to generate a composite image.

2.4 Results

2.4.1 Rationale

The scope of this report is twofold: It provides new information regarding the accumulation of a nuclear granule composed of RNA-binding proteins as well as presenting a computational tool that quantifies this phenomenon which should prove widely applicable.

In the absence of glucose, there is a dramatic movement of the transcription termination factors Nab3 and Nrd1 from a pan-nuclear distribution to tight nuclear granules^{29, 58}. During our investigation of this process, we noted that the extent to which cells displayed Nab3 granules in the population varied (“high”, “medium”, and “low”) with distinct strains having different, but consistent, levels of granule accumulation in the absence of glucose (**Fig. 2-1**). To rigorously quantify this, we sought to develop an automated and unbiased method to score Nab3-containing granules in thousands of cells from multiple biological replicates.

Three yeast strains were each engineered to contain two fluorescent fusion proteins: a red fluorescent protein fused to histone H2B to mark the nucleus, and Nab3 tagged with green fluorescent protein (GFP) (**Table 2-1**). Both fusion genes reside at their natural chromosomal loci with expression driven by their native promoters. We used two common strains of *S. cerevisiae*. One is a standard laboratory strain, BY4741, that is a derivative of S288C⁸². Another is W303 (Horizon Discovery, LLC). A third is a variant of W303 engineered to contain *NRD1* on a plasmid covering a chromosomal deletion of the gene. Cells in exponential growth were washed and incubated for 2 hr at 30°C in media lacking glucose, applied to an agarose pad, and examined using a Leica SP8 confocal microscope. The microscope-native .lif file format was converted to a MATLAB readable file (in this case, a .png file) and analyzed by a script written for MATLAB (available through GitHub at <https://github.com/Kelley-Lab-Computational-Biology/Granule>) that scores the fluorescence intensity of the pixels in the digitized image.

Detection and selection of granules in fluorescent images pose several challenges. Heterogeneity of protein levels from one cell to another can make a simple threshold approach for selection fail to select granules in low-expression cells or incorrectly select regions of high-expression in cells that are not actually granules. Additionally, noise in the fluorescence intensity within a cell can lead to individual pixels being bright enough to be considered a granule while being considerably smaller than verified granules. We developed a computational tool in MATLAB to address these issues using two primary strategies. First, threshold levels were determined on a cell-by-cell basis to account for heterogeneity of expression by using histogram analysis of individual cells. The cutoff value for the cell is then set to the mean value of the fluorescence in the nucleus plus 3 times the standard deviation. Second, we incorporated a step that allows the user to select a minimum size that a bright object must reach to be considered a granule.

The workflow for image processing is shown in Fig. 2-2. Nuclei were identified using both fluorescent-histone H2B intensity and size criteria. These values identified nuclei without falsely identifying non-nuclei. The objects that met these criteria were considered nuclear masks within which the distribution of GFP-Nab3 was studied. The average fluorescent intensity of GFP-Nab3 was calculated for the pixels defined by this nuclear mask. Pixels with intensities >3 standard deviations over the mean (3σ pixels) were identified. The features of granules as defined by clusters of adjacent 3σ pixels were analyzed for each nuclear mask.

2.4.2 Quantification of the dramatic rearrangement of GFP-Nab3 in yeast nuclei

A primary consideration in the quantification of these granules is the size of objects that can be considered a granule. Allowing any single pixel of sufficient intensity to be counted may

identify noise as a granule. However, requiring an object to be particularly large to be scored as a granule may miss actual granules. To address this, we examined granule accumulation across a range of size cutoffs. As a first step, we examined a strain whose population displayed a very high level of cells with granules under starvation conditions (**Fig. 2-1, “high”**). To choose how large an object would be considered a granule, we plotted the percent of nuclei containing pixel clusters *versus* minimum granule size (**Fig. 2-3A**). In other words, the graph displays the fraction of cells defined as containing a granule for each minimum size of a potential granule. Glucose-fed cells do not contain granules and rarely, if ever, contain more than three contiguous 3σ pixels. In contrast, the vast majority of glucose-starved cells contained clusters of three or more such intense pixels. Almost half of the starved cells contained very large clusters (≥ 8 pixels) of GFP-Nab3 fluorescence.

From this analysis, we chose to define a Nab3 granule as a cluster of ≥ 4 adjacent 3σ pixels, guided by the finding that the maximal difference between glucose-depleted and glucose-fed cultures, in terms of the percent of cells harboring clusters of 3σ pixels, was observed at ≥ 3 pixels (**Fig. 2-3B**).

2.4.3 The computational tool enables a detailed analysis of fluorescent protein distribution

Most cells appeared to display a single peripherally located granule in the nucleus, however, some cells with multiple granules were occasionally observed. To quantify the distribution of granules in an individual cell, a mid-logarithmic culture of cells from the high granule accumulating strain was washed free of glucose. One half was reseeded into glucose-free medium and the other half was inoculated into glucose-containing medium. This was repeated for six separate cultures each of which was started from a single independent colony. Granule

accumulation was scored from confocal micrographs for an average of ~1200 cells per culture. The number of cells that contained 1, 2, or 3 granules per nucleus was averaged for each culture and plotted (**Fig. 2-4A**). This analysis showed conclusively that nuclei typically contained only a single granule and rarely ($5.8 \pm 5.3\%$) contained a second granule. Thus, the granule most often appears as a solo subcellular compartment as opposed to multiple compartments within the nucleus such as seen for nuclear speckles which characterize sites of mammalian SR proteins⁸³.

To gain a better understanding of the distribution of GFP-Nab3 across a population, we plotted the fluorescence intensity of 100,000 randomly chosen nuclear pixels from a single field of cells from glucose-replete and glucose-depleted cultures. As seen in the violin plot of Fig. 2-4B, the median fluorescence intensity was 76 rfu for glucose-fed cells with a very broad spread of intensities. Glucose-depletion dropped the median substantially (36 rfu), as most nuclear pixels had relatively low fluorescent values, while a small number of pixels that represent the granules, concentrated GFP-Nab3. The data is a quantitative reflection of the dramatic rearrangement that GFP-Nab3 undergoes in which it condenses to a small nuclear volume during glucose starvation at the expense of the broad, nucleus-wide distribution, seen under vegetative growth conditions.

We also analyzed GFP-Nab3 distribution in specific glucose-fed and glucose-starved cells to emphasize the changing distribution of the protein in individual nuclei as a consequence of glucose restriction (**Fig. 2-5**). Six randomly chosen nuclei of equal size were analyzed and plotted for both glucose-fed and glucose-depleted cells. This analysis again showed that starvation induces the Nab3 protein to leave the majority of the volume of the nucleus and become a compact locus represented by a cluster of high intensity pixels (**Fig. 2-5, orange**). It also emphasizes that the distribution of pan-nuclear GFP-Nab3 in vegetatively growing cells is evenly distributed, and rarely appears greater than the cutoff of three standard deviations, confirming the stringency of

this threshold. In contrast, the fraction of GFP-Nab3 that migrates to a granule upon starvation varied from 25-44%. When a similar analysis was carried out for all nuclei in an entire field, an average of 26% ($\pm 14\%$ standard deviation, $n=1121$ cells) of GFP-Nab3 ends up in the granule after glucose restriction, while only 1% ($\pm 2\%$, $n=1264$ cells) of the protein finds itself in the brightest pixels in glucose fed cells.

2.4.4 Measurement of strain-to-strain differences in GFP-Nab3 granule accumulation

Having characterized this quantification tool, we used it to revisit the variation in granule accumulation between strains (**Fig. 2-1**). Defining the granule as four or more contiguous 3σ pixels, we scored the penetrance of granule accumulation in the strains displayed in Fig. 2-1. Cultures of logarithmically growing cells from each strain were washed and incubated in glucose-free medium for 2 hrs at 30°C. The “high” granule forming strain showed a penetrance of 79.2% ($\pm 13.4\%$) of the cells with a GFP-Nab3 granule (**Fig. 2-6**). The strain designated as “medium” possessed granules in 52.4% ($\pm 17.7\%$) of its cells. The “low” strain had 3.1% ($\pm 1.6\%$) of its cells accumulating granules. These granule accumulation levels were all statistically significantly different from each other when strains were compared pairwise ($p < 0.0001$ each). The latter two were engineered identically to contain the two fluorescently tagged proteins (GFP-Nab3 and mCherry-histone H2B) in the strains BY4741 (medium) or W303 (low), respectively. The high granule accumulating strain, which was under study for other purposes, was derived from W303, and contained the sole *NRD1* gene on a plasmid covering its deleted chromosomal copy. (A similar granule-accumulating phenotype was observed when the sole *NRD1* gene was situated in the chromosome (**Supplemental Figure S2-1**)). Note that the starved low granule-accumulating strain still contained significantly more granules than even the high granule strain when the latter had

access to glucose (**Fig. 2-6**, $p < 0.0003$). Thus, it appears that granules are seen widely but the abundance level can vary.

The distinct extents of granule accumulation for each strain was a reproducible property of individual colonies isolated from each (a biological replicate was a liquid culture derived from an independent colony for a given strain) and was observed when cultures were restarted from glycerol stocks. Knowing Nab3 granule accumulation is glucose starvation-dependent, we tested the growth of each under prolonged starvation conditions to begin to understand the molecular basis for strain differences.

2.4.5 The granule accumulation phenotype correlates with growth and respiration defects

Prior work showed that when glucose-starved cells were refed, the granules rapidly dissolve and cell division resumes²⁹. The different extent of granule accumulation between strains led us to consider if they might display distinct phenotypes. Cells were glucose-starved and tested for how rapidly they restart growing after seeding them into fresh glucose-containing medium. All three types of granule-accumulating strains were able to resume growth when resupplied with glucose (**Fig. 2-7**, “+ glucose”). Interestingly, yeast are known to be able to grow after prolonged glucose starvation by using internal reserves through micro-lipophagy and autophagy⁸⁴. When the three strains were tested for growth during prolonged starvation, it was clear that the low granule-accumulating strain was the most robust and entered logarithmic growth after almost 20 hrs (**Fig. 2-7**). The medium granule-accumulating strain emerged into logarithmic growth after ~35hrs and the high granule-accumulating strain could not grow in the absence of added glucose. Hence, there is an inverse correlation between growth in the absence of glucose and granule accumulation.

Survival in the absence of glucose has been reported to require respiration⁸⁴. Based on this, we tested the strains' respiratory function using glycerol/ethanol as a carbon source (**Fig. 2-8A**). Consistent with the growth patterns in the absence of glucose (**Fig 2-7**), the high granule-accumulating strain was unable to grow compared to the low strain, while the medium strain showed an intermediate growth capability (**Fig. 2-8A**, upper right panel).

If mitochondrial oxidative phosphorylation is related to granule accumulation, then compromising respiration in the low granule-accumulating strain should lead to a higher level of granule accumulation. To test this, the low strain was treated with ethidium bromide, an agent known to efficiently deplete mitochondria of their circular genome rendering the strain oxidative phosphorylation-defective, a phenotype referred to as “petite”⁸⁵⁻⁸⁷. Two independent isolates were obtained and neither could grow using glycerol/ethanol as a carbon source (**Fig. 2-8A**, lower right panel). The strains were put through the glucose starvation regimen and granules were quantified. Both were able to accumulate granules to a level statistically significantly above the untreated parent (low) strain (**Fig. 2-8B**). The loss of mitochondrial DNA was confirmed for *COX3* sequences for the two ethidium bromide-generated strains. This was also seen for the high granule-accumulating strain discussed above. We conclude that ethidium bromide treatment indeed generated respiration defective petite cells and that the high granule-accumulating strain was a spontaneous petite variant that was isolated serendipitously. Interestingly, the medium granule-accumulating strain which appears respiration defective based on its growth patterns, contained this particular mitochondrial DNA (**Fig. 2-8C**, *COX3*), suggesting its respiratory defect is distinct (and milder, **Figs. 2-7 and 2-8A**) from that seen for the high strain.

2.4.6 Quantification of filament formation by IMP dehydrogenase in cultured human cells

It seemed likely that the computational tool used here to score nuclear granules could be more generally applied to tracking protein rearrangements. We turned to a very different protein assembly process in an unrelated cell type. IMP dehydrogenase (IMPDH) is an enzyme involved in GTP metabolism that is highly conserved⁸⁸. The protein detects substrate and product levels in cells and when nucleotide synthesis is needed, it redistributes from its normal pan-cytoplasmic location to structures called rods and rings which are filaments of octamers of the enzyme^{81, 89}. Most, if not all cells, can be induced to assemble IMPDH after treatment with the drug mycophenolic acid, which inhibits the enzyme, leaving cells depleted for guanine nucleotides⁸⁹.

Micrographs of human cells cultured from a T-cell leukemia (Jurkat) treated with mycophenolic acid or vehicle and stained by indirect immunofluorescence with an anti-IMPDH2 polyclonal antibody were examined with a BioTek Lionheart widefield microscope (**Fig. 2-9A**). Nuclear DNA was counterstained with Hoechst 33342. Micrographs were examined with the computational tool as described above for yeast GFP-Nab3 fluorescence using the parameters described above. Here, the Hoechst-fluorescence channel was used to define a nuclear mask. Clusters of contiguous 3σ pixels in images labeled with anti-IMPDH2 fluorescence were scored in cells that were mycophenolic acid treated or untreated. As has been observed for a variety of cell types⁸⁹, some rods pre-exist in the undrugged state (**Fig. 2-9A**, left) and mycophenolic acid treatment strongly induces the extensive assembly of additional rods, noted here for Jurkat cells for the first time (**Fig. 2-9A**, right).

In examining a new protein in a different context, we again evaluated the appropriate size cutoff to score a granule. An application of the MATLAB script to these images showed that approximately half of the control cells display polymers of IMPDH2 that are ≥ 5 adjacent 3σ pixels in size (**Fig. 2-9B**, left, no drug). In contrast, just over half of the drug-treated cells showed 3σ

pixel collections of 28 or more, consistent with the very large, micron-length filaments of IMPDH2 found in mycophenolate-treated cells (Fig. 9B, left, +drug)⁸⁹. The maximal difference between the percent of treated cells with rods and the percent of untreated cells with rods was seen at 19 pixels (**Fig. 2-9B**, arrow, ~80% vs ~20%, **Fig. 2-9B**, inset). The clear difference between the size of GFP-Nab3 granules (above) and the large rods formed from IMPDH2, emphasize the versatility of this tool in its ability to set the extent of the area that defines a target compartment.

2.5 Discussion

Here we establish the first documentation of significant differences in yeast strains' abilities to assemble a well-defined nuclear granule composed of an essential RNA-binding protein, while concurrently presenting a widely applicable computational tool that quantifies this phenomenon.

We observed significant differences in yeast strains' abilities to assemble a well-defined nuclear granule composed of the essential RNA-binding protein, Nab3. The observed variation is a stable feature of each strain, revealing differences in penetrance. The poor ability of the higher granule accumulating strains to grow in the absence of glucose suggested they had compromised mitochondria. Deliberately damaging oxidative phosphorylation by depleting low granule accumulating cells of their mitochondrial DNA by treating them with ethidium bromide, was consistent with this hypothesis. The resulting strains lacked at least one region of mitochondrial DNA, failed to grow using glycerol/ethanol as a carbon source, and accumulated a significant number of granules over the untreated parental strain. These features paralleled those of the naturally occurring high granule accumulating strain we initially found. This led us to conclude that the high granule accumulating strain was a spontaneously arising petite that was serendipitously isolated. Its parental strain possessed *COX3* mitochondrial DNA sequences, could

use glycerol/ethanol as a carbon source, and showed a low level of Nab3 granules. The medium granule-accumulating strain, did not lose *COX3* sequences, was partially competent to grow in the absence of glucose and in the use of glycerol/ethanol, and displayed an intermediate level of granules, leading us to conclude it had a distinct basis for its level of granule accumulation which could still be mitochondrially based. Indeed, the S288C lineage from which it is derived is known to have a Ty1 insertion in *HAPI*, a mitochondrial biogenesis regulator, that renders the Hap1 protein hypomorphic and alters mitochondrial function^{90, 91}. In any case, the detailed quantification made possible using this computational tool allowed us to dissect these aspects of granule formation. A complete understanding of its molecular basis will require further analysis.

Aside from quantifying the fraction of cells with a granule, the program allowed us to quantify a number of other attributes of granules, including the fraction of nuclear protein destined for the granule, the distribution of the number of granules per nucleus, the size of the granule, and the magnitude of the striking nuclear reorganization of the protein. It enables rapid, rigorous statistical analysis and is unbiased, thus it is preferable to manual scoring methods. Additionally, the process is largely automated and high-throughput, yielding information from a large number of cells; in essence, allowing statistically rigorous determinations from large data sets. The tool is most useful in analyzing a change in distribution of a protein from a homogeneous soluble state to a specific structure and *vice versa*, thus the approach is applicable to other structures that form by any mechanism (*e.g.*, phase-separation or subunit polymerization). We demonstrated the tool's versatility by effectively identifying the aggregation of IMPDH2 into the prominent rod structures seen in many cell types. This vastly different application demonstrates how easily the settings can be recalibrated to score a variety of fluorescent compartments, thus widening the future utility of our tool.

In sum, by exploiting a computational tool capable of analyzing large populations of cells or organisms, we revealed variation in a phenotype that is currently under intense investigation, namely the aggregation of RNA-binding proteins into subcellular compartments in response to physiological challenges. This led us to discover the involvement of mitochondria and oxidative phosphorylation in granule biology.

2.6 Acknowledgements

This work was funded by National Institutes of Health (R01 GM120271 to D.R. and R15 GM128026 to J.K.), the Emory University School of Medicine and the Emory Integrated Cellular Imaging Core. The content is solely the responsibility of the authors and does not necessarily reflect the official views of the National Institute of Health. The authors acknowledge Drs. Judy Fridovich-Keil, Saman Najmi, Sohail Khoshnevis, and Homa Ghalei for helpful discussions and a critical reading of the manuscript. The technical expertise of Laura Fox-Goharioon is also appreciated.

2.7 Figures & Tables

Table 2-1 *S. cerevisiae* strains used in this paper

Strain	Genotype	Reference
BY4741	<i>MATa his3Δ1 leu2Δ0 met15Δ0 ura3Δ0</i>	Research Genetics
DY1620	<i>MATα can1-100 his3-11,15 leu2-3,112 trp1-1 ura3-1 NRD1::natMX4 [pAC3314-Nrd1]</i>	Corbett Lab (Emory U.)
DY4543	<i>MATa his3Δ1 leu2Δ0 met15Δ0 ura3Δ0 GFP-NAB3</i>	Loya & Reines, 2018
DY4580	<i>MATa his3Δ1 leu2Δ0 met15Δ0 ura3Δ0 GFP-NAB3 HTB2-mCherry::HIS5</i>	This Study
DY4724	<i>MATα his3-11,15 leu2-3,112 trp1-1 ura3-1 NRD1::natMX4 [pAC3314-Nrd1] [pRS315-HA-Nrd1]</i>	This Study
DY4736	<i>MATα can1-100 his3-11,15 leu2-3,112 trp1-1 ura3-1 NRD1::natMX4 [pRS315-HA-Nrd1]</i>	This Study
DY4746	<i>MATα can1-100 his3-11,15 leu2-3,112 trp1-1 ura3-1 NRD1::natMX4 GFP-NAB3 [pRS315-HA-Nrd1]</i>	This Study
DY4756	<i>MATα can1-100 his3-11,15 leu2-3,112 trp1-1 ura3-1 NRD1::natMX4 GFP-NAB3 HTB2-yomCherry::kanMX [pRS315-HA-Nrd1]</i>	This Study
DY4771	<i>MATα ade2-1 can1-100 his3-11,15 leu2-3,112 trp1-1 ura3-1 GFP-NAB3</i>	This Study
DY4772	<i>MATα ade2-1 can1-100 his3-11,15 leu2-3,112 trp1-1 ura3-1 GFP-NAB3 HTB2-mCherry::HIS5</i>	This Study
DY4789	<i>MATa/ MATα ADE2/ade2-1 CAN1/can1-100 his3Δ1/ his3-11,15 leu2Δ0/ leu2-3,112 met15Δ0/MET15 TRP1/trp1-1 ura3Δ0/ura3-1 GFP-NAB3/GFP-NAB3 HTB2-mCherry::HIS3/ HTB2-mCherry::HIS5</i>	This Study
DY4826	<i>MATα can1-100 his3-11,15 leu2-3,112 trp1-1 ura3-1 NRD1::natMX4 GFP-NAB3 HTB2-mCherry::HIS5 [pRS315-HA-Nrd1]</i>	This Study
DY4829	<i>MATα/ MATa ADE2/ade2-1 can1-100/can1-100 his3-11,15/his3-11,15 leu2-3,112/leu2-3,112 trp1-1/trp1-1 ura3-1/ura3-1 NRD1::natMX4/NRD1 GFP-NAB3/GFP-NAB3 HTB2-yomCherry::kanMX/HTB2-mCherry::HIS5 [pRS315-HA-NRD1]</i>	This Study
DY4834	<i>MATα can1-100 his3-11,15 leu2-3,112 trp1-1 ura3-1 NRD1::natMX4 GFP-NAB3 HTB2-mCherry::HIS5</i>	This Study
YOL890	<i>ura3-1 his3-11,15 leu2-3,112 lys2 htb2-mCherry::HIS5</i>	S. Wente (Vanderbilt U.)
YSC1059	<i>MATα ade2-1 can1-100 his3-11,15 leu2-3,112 trp1-1 ura3-1</i>	Horizon Discovery LLC

Figure 2-1

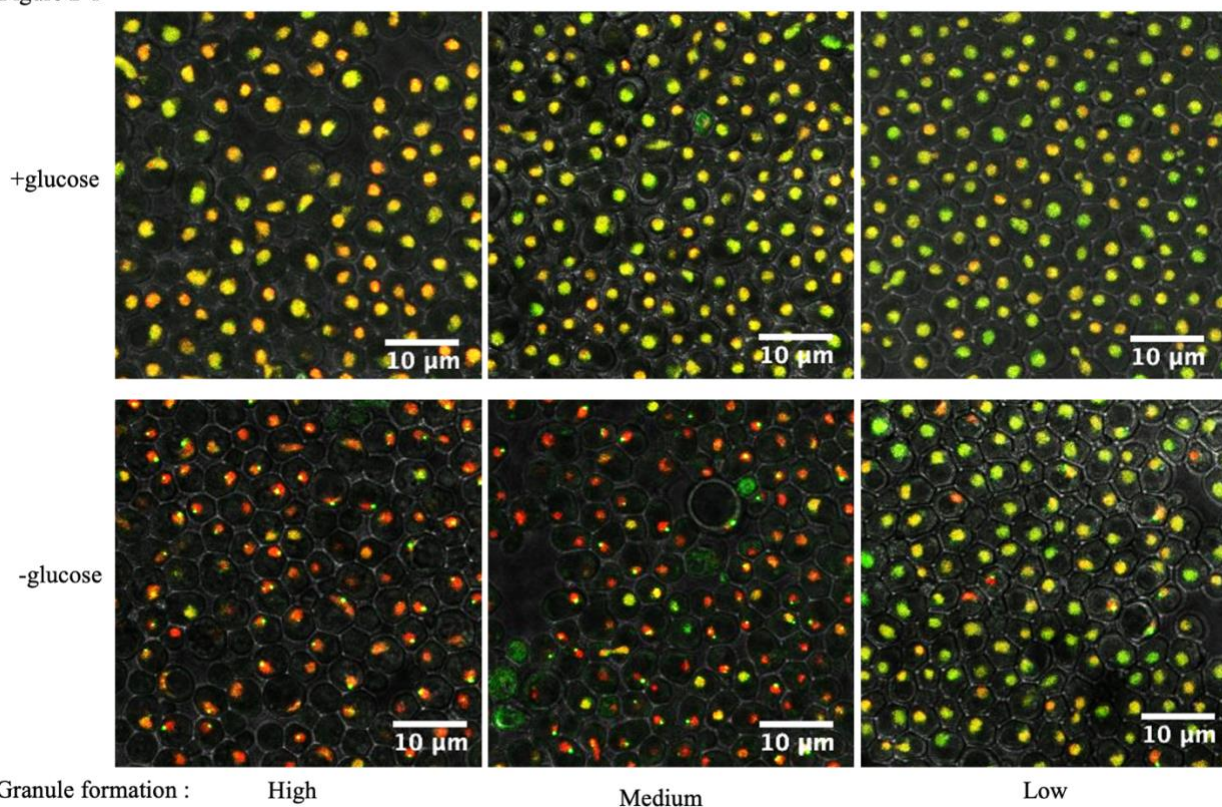
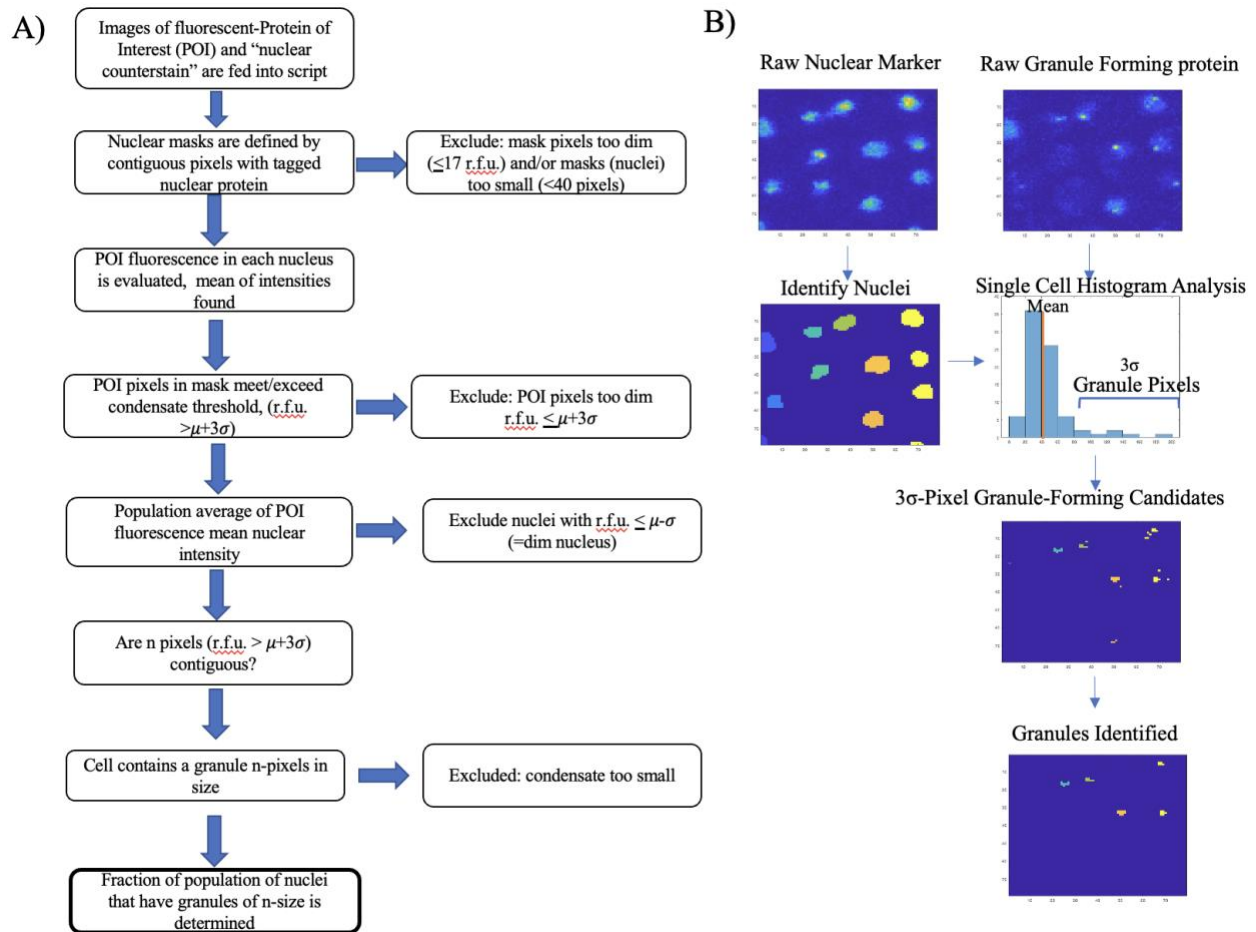


Fig. 2-1 Fluorescence microscopy of GFP-Nab3 (green) granule formation in three yeast strains

Three different strains of yeast cells (DY4756, 'high'; DY4580, 'medium'; DY4772 'low') were grown to mid-log phase, washed free of growth media, and resuspended in fresh media with or without glucose as described in Materials and Methods. Nuclei were labeled with histone H2B tagged with mCherry. Nab3 was tagged with GFP.

Figure 2-2

**Fig. 2-2 Workflow**

(A) The steps employed to process digital micrographs are shown in flow chart form. The individual steps are described in the text.

(B) Images from the workflow for the MATLAB script showing steps in image processing.

Figure 2-3

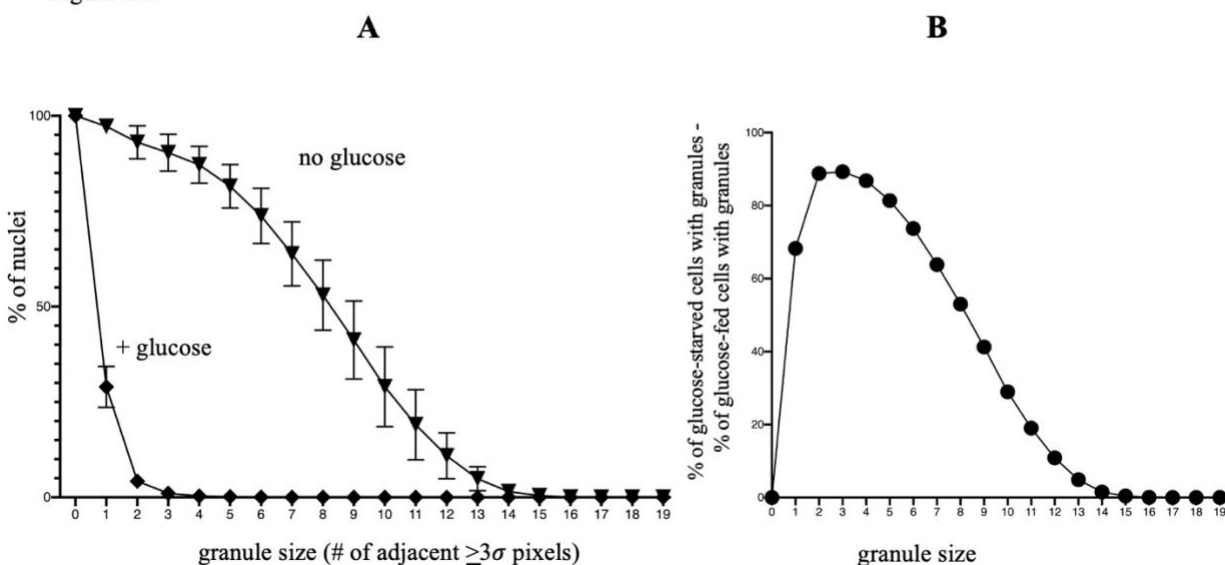


Fig. 2-3 Measurement of the distribution of nuclear GFP-Nab3 in glucose-fed and glucose-starved conditions for a high penetrance granule forming strain

(A) *Clustering of 3s pixels in yeast nuclei before and after glucose starvation.* Fluorescent images of glucose-starved DY4756 were analyzed by a MATLAB script to score pixel intensity of GFP-Nab3 in a nuclear mask defined by H2B-mCherry. The number of adjacent pixels whose intensities were greater than or equal to three standard deviations ($3s$) above the mean pixel intensity in that mask, were quantified. The percent of cells (Y-axis) bearing a given number of $3s$ pixel clusters (X-axis) was analyzed for six biological repeats ($n=6$; different cultures on different days) and the mean and standard deviations were calculated. The Y-axis value for zero adjacent $\geq 3s$ pixels was set at 100%.

(B) *Difference between glucose-fed and glucose-starved cells in terms of their GFP-Nab3 distribution as a function of granule size.* The “% of cells” values (Y-axis in part A) at each pixel cluster size (X-axis in part A) in glucose-fed cells from part A were subtracted from their Y-axis

value at that pixel cluster size for the cognate glucose-starved cells. This difference was then plotted for each pixel cluster size.

Figure 2-4

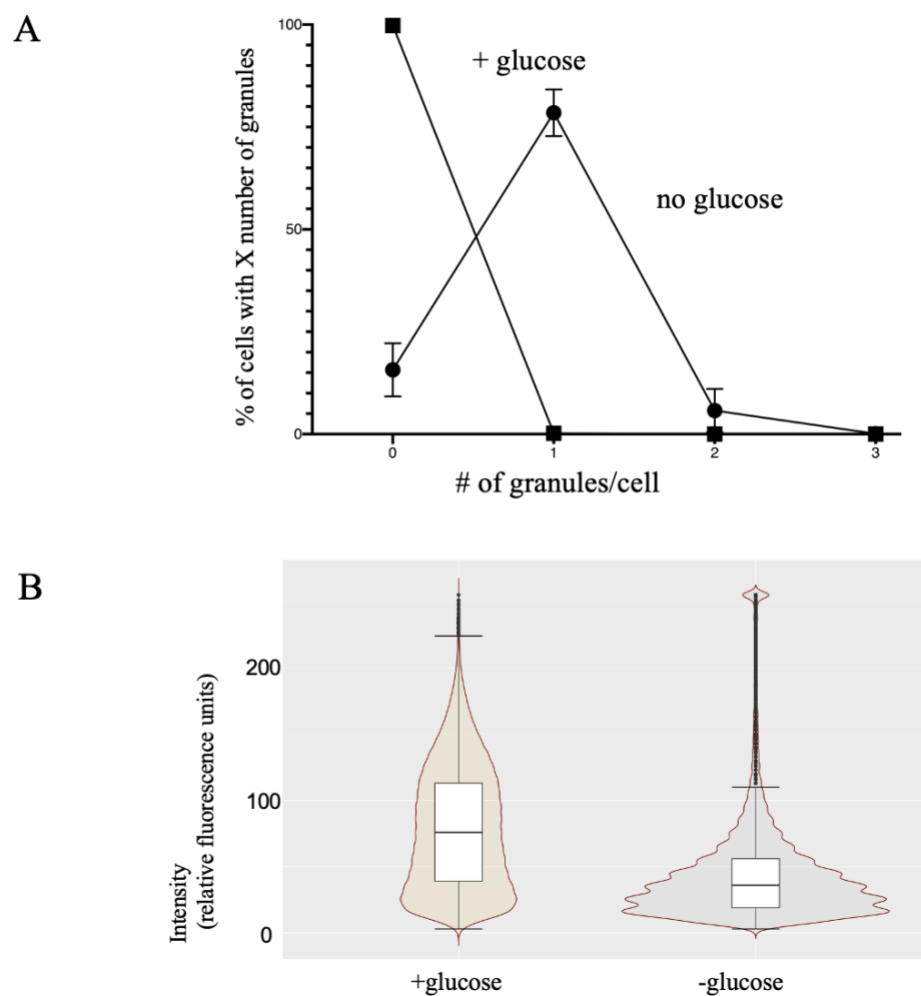


Fig. 2-4 Quantification of granules per cell and distribution of pixel intensities for glucose-fed or glucose-restricted cells

(A) *Granules per cell*. Yeast strain DY4756 was grown in the presence or absence of glucose as described in Materials and Methods. The number of granules of ≥ 4 pixels with $\geq 3s$ intensities above the mean was calculated for each nucleus in cells from each of six biological replicates ($n=6$). Averages and standard deviations were plotted.

(B)*Distribution of pixel intensities for populations of fed or starved cells.* All values for GFP-Nab3 pixel intensities from a single field each of strain DY4756 grown in the presence or absence of glucose were collected. From these datasets, 100,000 pixels were randomly selected from each sample in MATLAB using the *datasample* function (without replacement). The datasets were then imported into RStudio and violin plots were created using the *ggplot2* package, scaled by area.

Figure 2-5

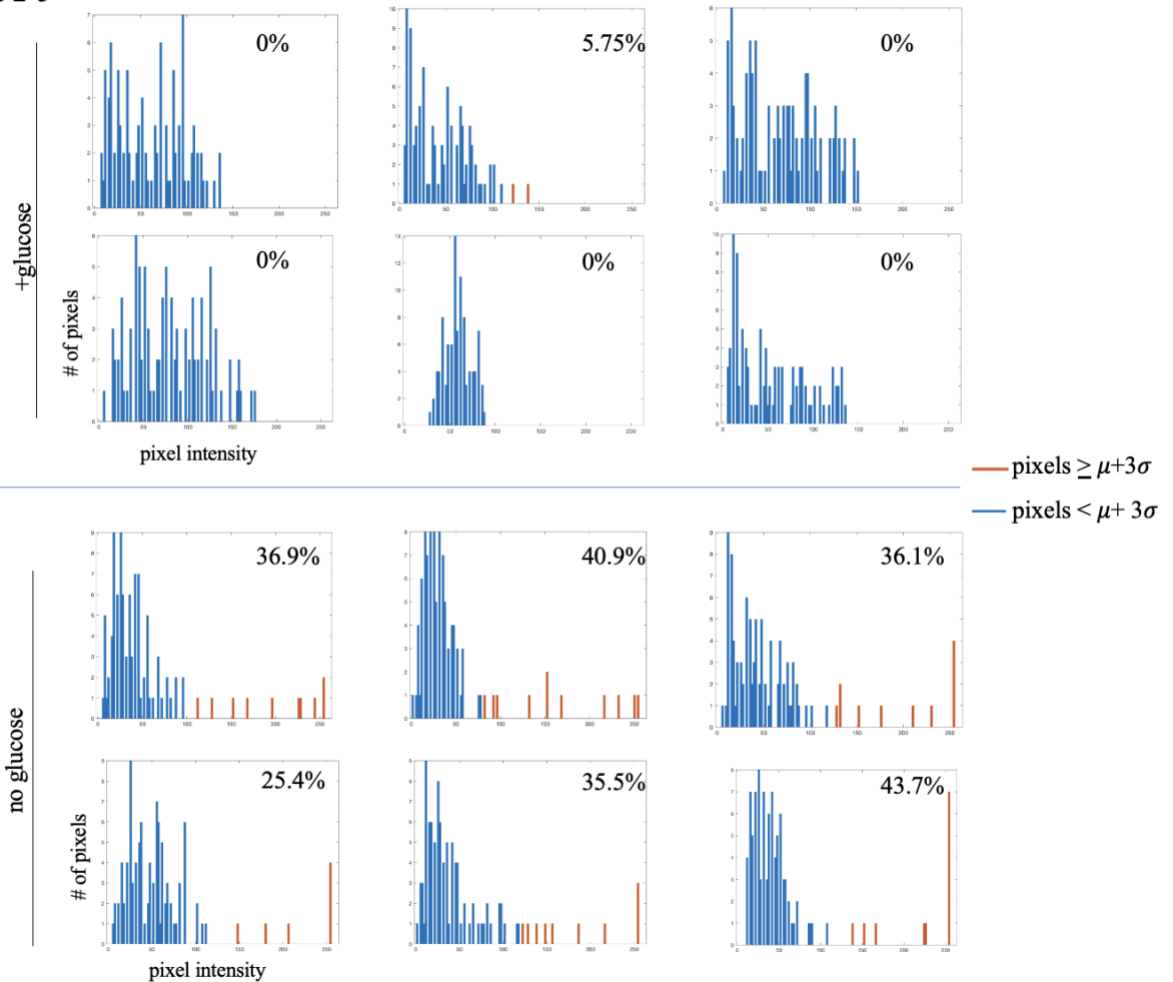


Fig. 2-5 Scoring the distribution of GFP-Nab3 into granules in specific nuclei

Six nuclear masks consisting of 100 pixels were arbitrarily selected from images of strain DY4756 grown in the presence and absence of glucose. GFP-Nab3 pixel intensities for each mask were plotted in separate histograms. The pixels that exceed the $\mu + 3\sigma$ threshold are highlighted in orange. The percentage shown in each histogram is calculated by:

$$100 \times \frac{\sum(\text{Pixel intensities exceeding granule threshold})}{\sum(\text{Pixel intensities in nuclear mask})}$$

Figure 2-6

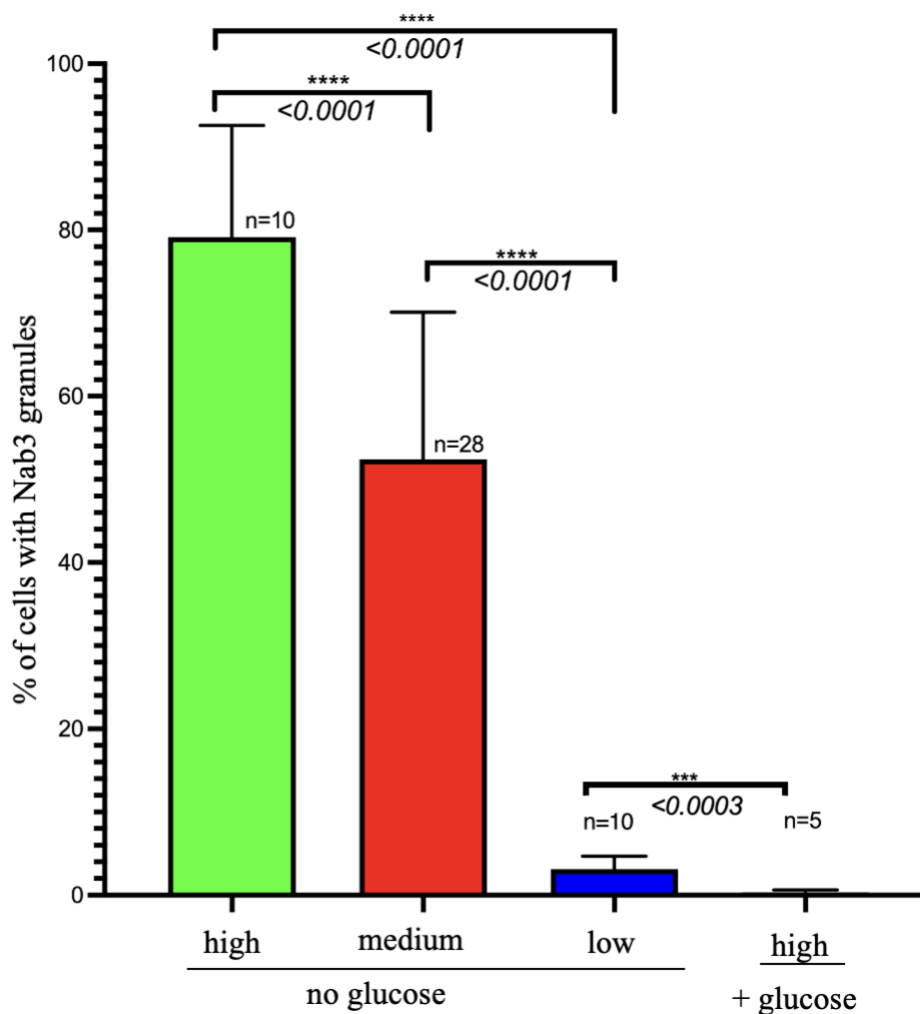


Fig. 2-6 Different extents of granule formation in three distinct yeast strains

The three yeast strains shown in Fig. 2-1 (DY4756, DY4580, DY4772; high, medium, and low, respectively) were glucose-starved and analyzed by fluorescent microscopy. DY4756 was also grown in the presence of glucose as a positive control. Fields of cells from biological replicates (the indicated n values) were grown on different days. The average and standard deviation of the percent of cells containing GFP-Nab3 granules (≥ 4 adjacent 3s pixels) were calculated for each strain and plotted on a bar graph. Fields contained an average of 895 cells each.

Figure 2-7

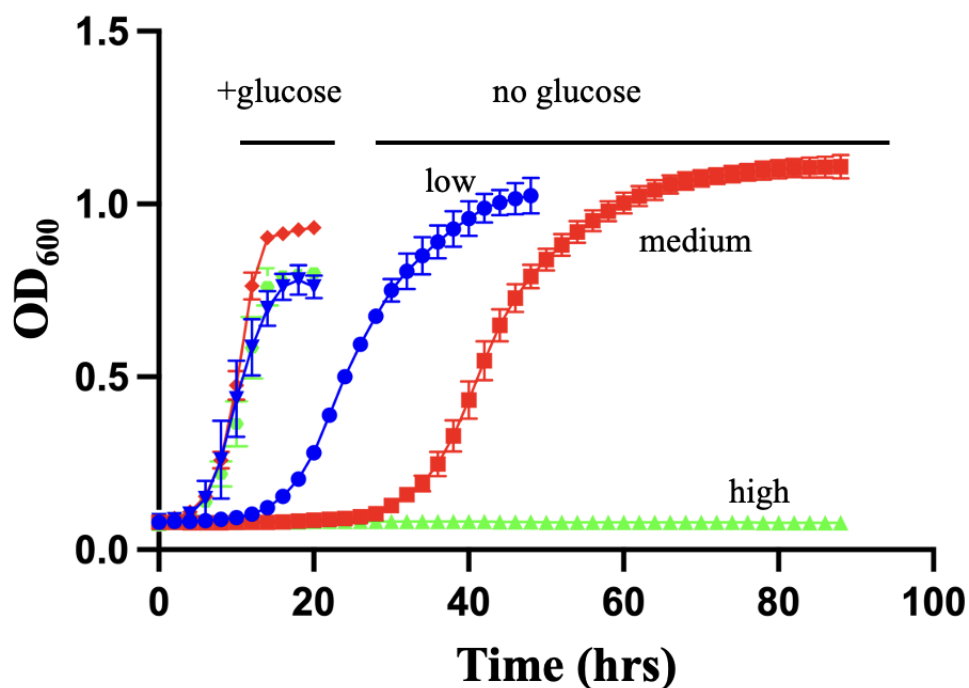
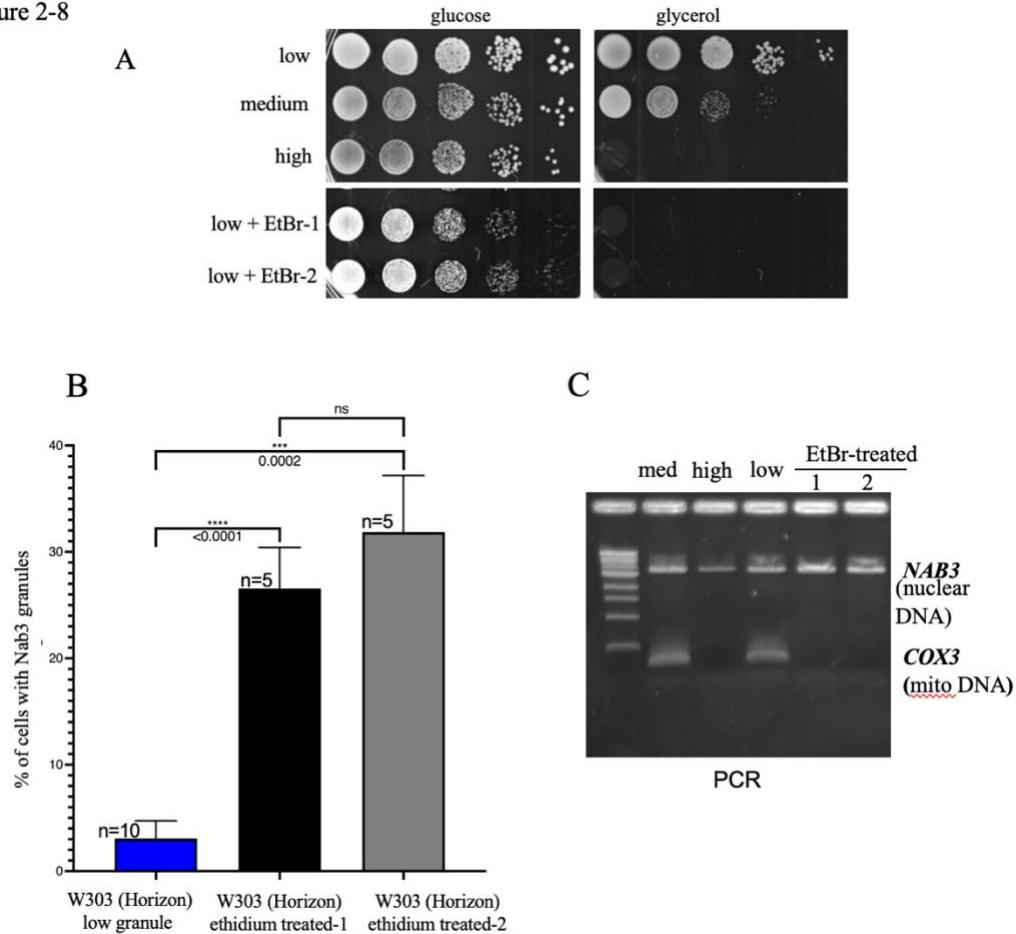


Fig. 2-7 Growth in the absence of glucose varies with the granule accumulation phenotype.

Strains DY4756 (high, green), DY4580 (medium, red), DY4772 (low, blue), were washed free of glucose and incubated at 30°C for 2hrs before reseeded at OD₆₀₀ = 0.1 in fresh glucose-containing, or glucose free media. Cells were grown in 96-well plates at 30°C in a BioTek plate reader and light scattering (600 nm) recorded at intervals. Averages and standard deviations from three technical replicates of each biological triplicate, were plotted.

Figure 2-8

**Fig. 2-8 Granule formation and mitochondrial function.**

(A) *Growth on glycerol/ethanol as a carbon source.* Cultures of strains DY4756 (high), DY4580 (medium), DY4772 (low), DY4849 (ethidium bromide-1), and DY4850 (ethidium bromide-2) were grown to saturation and diluted with sterile water to a concentration of 10^7 cells/ml. They were diluted serially 10-fold and spots of 10 μ l of each dilution were applied to SC-glucose or SC-glycerol/ethanol, as indicated and incubated at 30°C.

(B) *Nab3 granule content for ethidium bromide petite strains.* Strains DY4772, DY4849 (ethidium treated-1), and DY4850 (ethidium treated-2) were glucose-starved and the population

was analyzed by fluorescence microscopy for Nab3 granules. The fraction of cells containing granules was calculated using the computational tool for the indicated number of biological replicates.

(C)*Nuclear and mitochondrial chromosome detection for yeast strains.* DNA was prepared from the strains DY4756 (high), DY4580 (medium), DY4772 (low), DY4849 (ethidium bromide-1), and DY4850 (ethidium bromide-2) and subjected to PCR using primers that detect nuclear gene *NAB3* and mitochondrial gene *COX3* and samples run on an agarose gel and stained with ethidium bromide.

Figure 2-9

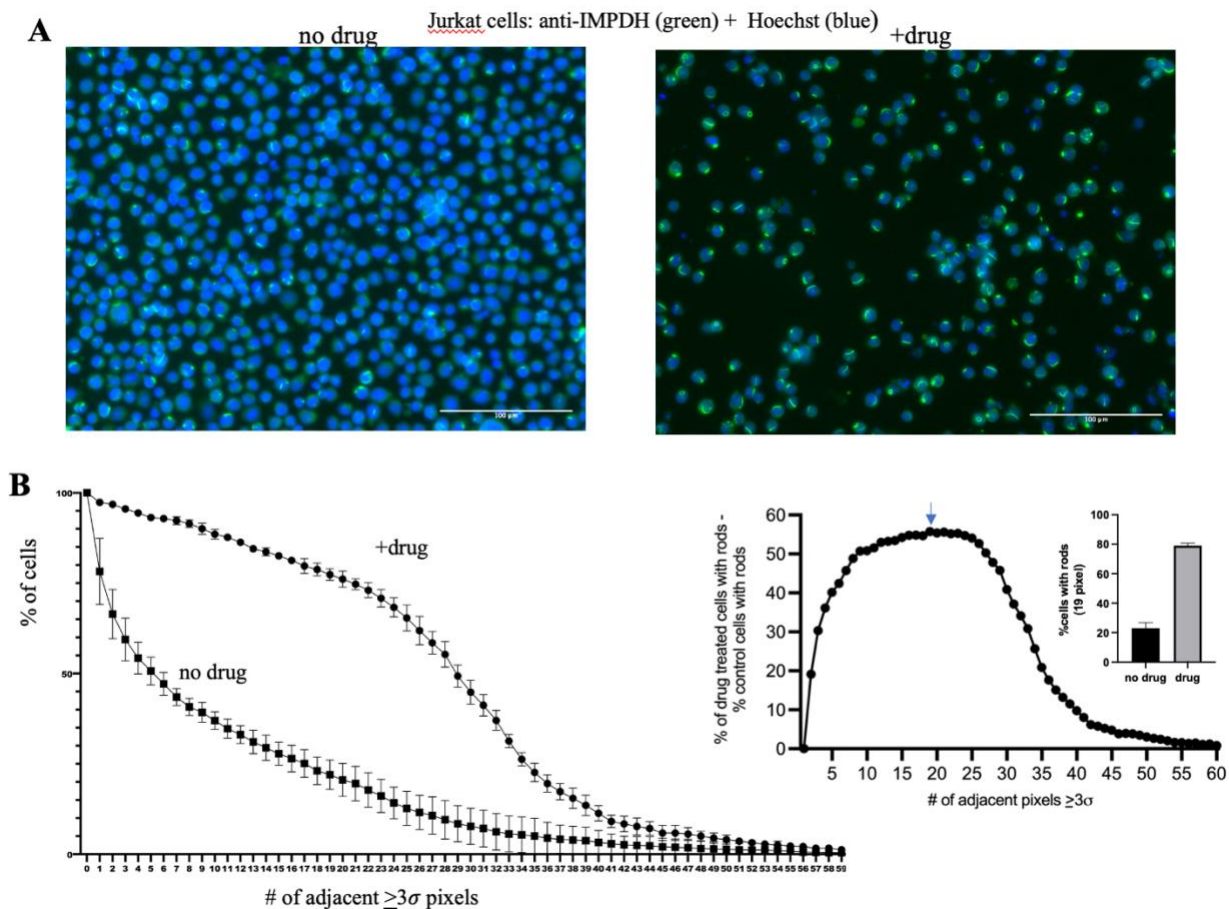


Fig. 2-9 Quantification of drug-induced “rod and ring” formation by IMP dehydrogenase in human Jurkat cells

(A) *Anti-IMP2H immunofluorescence.* Cultured Jurkat cells were treated with mycophenolic acid (right) or vehicle (left) and processed for immunofluorescence using an anti-IMP2H antibody. Nuclei were counterstained with Hoechst dye. Micrographs at 20x magnification are shown in panel A.

(B) *Quantification of drug-induced formation of IMP2H filaments.* Four fields with an average of 179 (vehicle) or 426 (drug treated) Jurkat cells, were stained with anti-IMP2H and processed

using the MATLAB script and Hoechst fluorescence as a nuclear mask. The mean fraction of nuclei from these fields containing 0-59 adjacent 3s pixels was calculated for drug- or vehicle-treated Jurkat cells, as indicated, and plotted (left panel). Error bars represent standard deviations. The difference between drug-treated and control cells was calculated for each number of contiguous 3s pixels and plotted (center). The peak value (19 pixels) is indicated by the arrow. The average fraction of cells possessing 19 contiguous 3s pixels (\pm standard deviation) was extracted from the graph on the left for drug-treated and control cells and is presented as a bar graph on the far right.

Figure S2-1

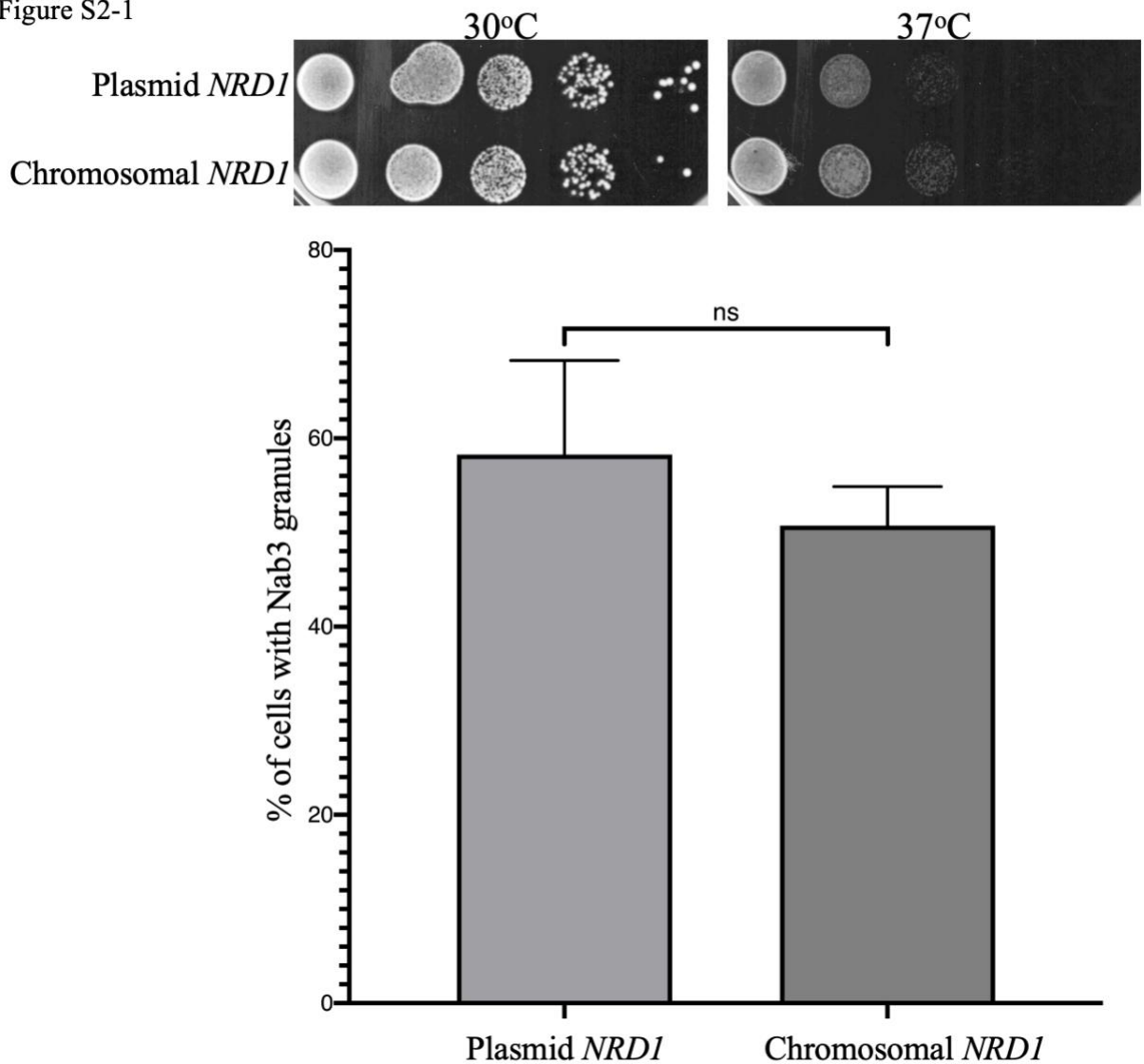


Fig. S2-1 The difference between chromosomal and episomal *NRD1* does not account for the magnitude of granule formation

Using *cas9* editing, the strain DY4826 (“plasmid *NRD1*”) had the *NAT1::nrd1* disruption cassette replaced by *NRD1* donor sequences to restore the endogenous gene in its native location. The strain was then screened for loss of the *NRD1*-containing plasmid yielding DY4834 (“chromosomal *NRD1*”). Both strains were glucose-starved and imaged for GFP-Nab3 granule formation. Strains were also grown at the indicated temperatures to test thermosensitivity. Both

thermosensitivity and granule formation are comparable regardless of whether *NRD1* is episomal or chromosomal.

CHAPTER 3.0: Nab3 nuclear granule accumulation is driven by respiratory capacity

K. Hutchinson was responsible for Fig. 3-2, 3-3, 3-4, S3-2, S3-3 and contributed to Fig. 3-1.

Hutchinson, Katherine et al. “Nab3 nuclear granule accumulation is driven by respiratory capacity”. *bioRxiv*, 10.1101/2022.05.23.492460. 24 May. 2022, doi: 10.1101/2022.05.23.492460

*These findings were posted to the *bioRxiv* preprint server on May 24th, 2022. Supplemental information can be found online at:

<https://www.biorxiv.org/content/10.1101/2022.05.23.492460v1.full.pdf+html>

3.1 Abstract

Numerous biological processes involve proteins capable of transiently assembling into subcellular compartments necessary for cellular functions. One process is the RNA polymerase II transcription cycle which involves initiation, elongation, co-transcriptional modification of nascent RNA, and termination. The essential yeast transcription termination factor Nab3 is required for termination of small non-coding RNAs and accumulates into a compact nuclear granule upon glucose removal. Nab3 nuclear granule accumulation varies in penetrance across yeast strains and a higher Nab3 granule accumulation phenotype is associated with petite strains, suggesting a possible ATP-dependent mechanism for granule disassembly. Here, we demonstrate the uncoupling of mitochondrial oxidative phosphorylation by drug treatment or deletions of nuclear-encoded ATP synthase subunit genes, were sufficient to increase Nab3 granule accumulation and led to an inability to proliferate during prolonged glucose deprivation, which requires respiration. Additionally, by enriching for respiration competent cells from a petite-prone strain, we generated a low granule-accumulating strain from a relatively high one, providing another link between respiratory competency and Nab3 granules. Consistent with the resulting idea that ATP is involved in granule accumulation, the addition of extracellular ATP to semi-permeabilized cells was sufficient to reduce Nab3 granule accumulation. Deleting the *SKY1* gene, which encodes a kinase that phosphorylates nuclear SR repeat-containing proteins and is involved in efficient stress granule disassembly, also resulted in increased granule accumulation. This observation implicates Sky1 in Nab3 granule biogenesis. Taken together, these findings suggest there is normally an equilibrium between termination factor granule assembly and disassembly mediated by ATP-requiring nuclear machinery.

Keywords: Nab3, granule, yeast, mitochondria, low complexity domain

3.2 Introduction

The RNA polymerase II transcription cycle involves RNA-binding proteins that can condense into nuclear foci to perform their functions^{29, 92-96}. Proteins capable of self-assembly often contain a low complexity domain (LCD), a domain lacking stable secondary structure, that becomes structured and organized when assembling into a subcellular compartment. The LCD is often necessary for assembly and localization into a subcellular compartment.

Nab3 is an essential RNA-binding, transcription termination factor that is part of the Nrd1-Nab3-Sen1 RNA polymerase II termination complex in *Saccharomyces cerevisiae*³. This termination complex is responsible for the biogenesis of snoRNAs, snRNAs, and other small non-coding RNAs such as cryptic unstable transcripts (CUTs), and serves to regulate gene expression through attenuation^{3, 63-65, 97, 98}. Nab3 contains a well-characterized LCD that is necessary for its self-assembly into amyloid *in vitro* and its accumulation, with its dimerization partner Nrd1, into a nuclear granule *in vivo*^{24, 29, 58, 62, 99}. The Nab3 nuclear granule shares features with cytoplasmic stress granules; both are composed of RNA-binding proteins with LCDs that can self-assemble, and both accumulate during glucose restriction and dissolve upon refeeding^{29, 49, 100}.

While the mechanisms responsible for the disassembly of the Nab3 nuclear granule are unknown, cytoplasmic stress granules can be disassembled by chaperone ATPases or DEAD-box helicases in an ATP-dependent manner^{73, 101}, as well as by the addition of extracellular ATP to permeabilized cells⁷³. Taken together, sufficient respiratory capacity and proficient production of ATP are necessary for the disassembly of stress granules and by extension, may play a role in Nab3 granule disassembly as well.

The kinase Sky1 is also involved in efficient stress granule disassembly¹⁰². Sky1 is the only known conserved serine-arginine protein kinase (SRPK) expressed in *Saccharomyces cerevisiae*

and has been shown to target RNA-binding proteins, aid in the disassembly of stress granules, localize to the nucleus and cytoplasm, and display a genetic interaction with Nab3, thus making it of interest as a potential protein candidate implicated in Nab3 granule disassembly¹⁰²⁻¹⁰⁵.

We previously developed a computational tool that facilitated the robust quantification of Nab3 granule accumulation across various commonly used laboratory strains of yeast and determined that they displayed a wide variation in the levels of granules¹⁰⁶. We considered the possibility that the variation was due, in part, to differences in respiratory capacity across strains as determined by their relative abilities to grow using ethanol/glycerol as a carbon source, a commonly used method to test respiratory function in yeast. In particular, this was seen in an isolate that was a so-called *petite* strain, a common type of mutant whose mitochondrial genome is partially or completely missing. Another strain with an elevated level of granules was an S288C-based laboratory strain that is known to display mitochondrial genomic instability¹⁰⁷.

Here, to dissect the mechanism of Nab3 granule formation and disassembly, and explicitly test the notion that defects in respiratory capacity contribute to a high Nab3 granule accumulation phenotype, we incapacitated oxidative phosphorylation in a respiratory competent, low granule-accumulating strain through drug treatment or deletion of nuclear-encoded ATP synthase genes. Similarly, we exploited a strain with a relatively high frequency of generating *petite* mutants to enrich for respiratory competence and tracked changes in Nab3 granule accumulation associated therewith. We also reveal that deletion of the gene encoding the conserved serine-arginine protein kinase, *SKY1*, leads to an increase in Nab3 granule accumulation. Taken together, these data suggest a model in which Nab3 and Nrd1, presumably in concert with other factors, self-assemble into a nuclear compartment important for their function, and that ATP production supports normal

levels of granule disassembly providing a mechanism to maintain an equilibrium between soluble and granule-associated transcription termination factors.

3.3 Materials and methods

Yeast Strain Construction

Yeast strains used in this paper are presented in Table 3-1. DY4730 was generated using high efficiency lithium acetate transformation¹⁰⁸ to transform DY4580 with a PCR product encoding *SKY1::kanMX4* amplified from plasmid pFA6a-KanMX4¹⁰⁹ using primers 5'-ACACCCCCTTTTGAGGTTGAAGAGATAGAGTAAAGAAGAAGTGTAGACATTAATGC GTACGCTGCAGGTCGAC-3' and 5'-GAGGTTAAACAGAAAAAAAAAGTAAAAGGCAAGGGCAAATAAAGGTATAAAGGTA ATCATCGACTGAATTCGAGCTCG-3'. Transformants were isolated by growth on G418 and verified by PCR.

DY4851 was generated by lithium acetate transformation of DY4772 with a PCR product encoding *ATP1::kanMX4* amplified from plasmid pFA6a-KanMX4¹⁰⁹ using primers 5'-CGCGAACCATTAGTATAACAGATTGATCGTTCAGCTCTCATAACGTACGCTGCAGGTC GAC-3' and 5'-GAGTCAGTGCTAAGAATGGAATAAACTAGAGGCTATTGTGGTCGACTGAATTCGAG CTCG. Transformants were isolated by growth on G418 and verified by PCR.

DY4856 was made as described above for DY4851. DY4772 was transformed with a PCR product encoding *ATP3::kanMX4* that was amplified using primers 5'-TACGCGAGGAACCCGGACCGCAATAACGATTAAAGAAGGCCCGTACGCTGCAGGT CGAC-3' and 5'-TGTTCTACAAAAACAACGTCAAATAAAGAGGCAATGCAGGGTCGACTGAATTCGAG CTCG-3'.

DY4863 was generated by lithium acetate transformation of DY4772 with a PCR product encoding *SKY1::kanMX4* that was amplified from genomic DNA of DY4730 using primer pair 5'-GTCGGGAACCGAAGCCATTG-3' and 5'-GCAAAGTCAGCTTCCACATC-3'.

Confocal Microscopy and Image Analysis

Confocal microscopy and image analysis was performed as described¹⁰⁶. Briefly, strains containing GFP-tagged Nab3 and fluorescently tagged histone H2B, were grown to mid-logarithmic phase, split, and washed three times into the appropriate media with or without glucose and grown at 30°C for 2 hrs. After 2 hrs, cells were pelleted and placed onto single cavity microscope slides containing 1.5% agar pads in the appropriate media. Z-stacks were captured and images were processed using FIJI⁷⁹ and quantified using the MATLAB software⁸⁰ as described¹⁰⁶. At minimum, five independent biological replicates were used for each condition and passed tests for normality. An unpaired t test with Welch's correction was used to test for statistical significance.

For FCCP treatment, cells were grown to mid-logarithmic phase, split, and washed three times into the appropriate media with or without glucose and grown at 30°C for 2 hours. After 2 hrs, cells were treated with 20 μ M FCCP for 30 min. Cells were imaged as described above. For ATP treatment, cells were grown as described above for 2 hrs in the absence of glucose and treated with 0.5% DMSO for 30 minutes with or without 200 mM ATP. Cells were prepared and imaged as described above.

Yeast Growth Assays

Yeast strains were grown to saturation at 30°C in the appropriate selection media and serially diluted for solid medium growth assays as described¹⁰⁶. Liquid growth assays were performed as described¹⁰⁶. Briefly, cultures were inoculated and grown to saturation at 30°C in the appropriate selection media. A fresh culture was inoculated using the saturated culture and grown to mid-logarithmic phase in the appropriate glucose-containing selection media. The culture was split and washed three times into the appropriate media without glucose (starvation media) or with glucose and incubated at 30°C for 2 hours. Optical densities (600 nm) were measured, and cultures were diluted into the appropriate media to a final value of 0.05. Three 100 µL biological replicates were plated in triplicate in a 96-well plate and placed onto a BioTek Synergy H1 microplate reader at 30°C. Optical densities were recorded every 20 minutes until growth plateaued.

Yeast Growth Assays: Selection for respiration competency

Solid medium growth assays were performed in tandem with liquid medium growth assays. First, yeast strains were grown to saturation at 30°C in the appropriate selection media. A fresh culture was inoculated using the saturated culture and grown to mid-logarithmic phase in the indicated, glucose-containing selection media. An aliquot of culture was taken, serially diluted 10-fold, and five spots of 10 µL of each dilution were applied to the appropriate solid media. Plates were grown at 30°C. An additional aliquot was taken, placed onto an agar pad, and imaged for Nab3 granule accumulation. Images were processed and analyzed as described above. The remaining culture was split, pelleted, and washed three times into the appropriate glucose-depleted media and incubated at 30°C for 2 hrs. An aliquot was taken, placed on an agar pad, and imaged for Nab3 granule accumulation. Images were processed and analyzed as described above.

For growth assays in a plate reader, optical densities were measured at 600 nm and cultures were diluted into the appropriate glucose-depleted media to a final optical density of 0.08. Three 100 μ L biological replicates were plated in triplicate in a 96-well plate and placed onto a BioTek Synergy H1 microplate reader at 30°C. Optical densities were recorded every 20 min. Aliquots were taken at mid-logarithmic growth and serially diluted onto solid medium (YPD or YPEG) or placed on an agar pad and imaged for Nab3 granule accumulation. Images were processed and analyzed as described above.

Whole Genome Sequencing Analysis

Genomic DNA for yeast strains DY4736 and DY4746 was prepared for processing at the Emory Integrated Genomics Core. A library for each strain was constructed and 150 bp paired end reads were generated on a NovaSeq 6000 S4 300 cycle flow cell to achieve 50-fold coverage. The resulting FASTQ files were uploaded to UseGalaxy.org and were mapped to the W303 RefSeq LYZE00000000¹¹⁰ using the sequence alignment program Minimap2¹¹¹. The resulting mappings were visualized with the NCBI Genome Workbench, version 3.7.1 (Fig. S3-1).

3.4 Results

3.4.1 Mitochondrial manipulations in a low granule accumulating yeast strain increase granule accumulation

Prior development of a computational tool enabled quantification of Nab3 granules which showed that accumulation of the granules in response to glucose restriction varied between yeast strains¹⁰⁶. One W303-based strain was an isolate that was extremely effective at forming Nab3 granules with ~80% [‘high’¹⁰⁶] of cells displaying granules. Its inability to grow when

glycerol/ethanol was a carbon source suggested it was defective in respiration in contrast to its parental strain or a W303 strain (“low”) from a repository. This was further confirmed here by whole genome sequencing which revealed the high granule-forming isolate had lost a substantial portion of its mitochondrial genome rendering it an authentic ρ^- petite, while the parental strain presented an intact genome (Fig. S3-1). Hunn *et al.* also observed that a low granule forming strain (~3%) treated with ethidium bromide to induce mitochondrial DNA loss, resulted in a significant increase in the fraction of cells containing granules¹⁰⁶. Since ethidium bromide treatment is a crude tool with which to manipulate mitochondrial function, and is known to result in heterogenous effects such as an elevated frequency of nuclear DNA mutations¹¹², we tested the role of oxidative phosphorylation on granule accumulation with a set of more specific interventions. First, we treated a low granule accumulating strain with the mitochondrial inhibitor, carbonyl cyanide 4-(trifluoromethoxy) phenylhydrazone (FCCP) which is an ionophore that uncouples respiration from ATP synthesis by disrupting the proton gradient¹¹³. FCCP treatment led to a statistically significant increase in Nab3 granule accumulation in DY4772, which is an otherwise low granule accumulating strain (Figs. 3-1A and S3-2). These data strongly suggest that oxidative phosphorylation deficiencies cause an increase in Nab3 granule accumulation.

Turning to a genetic approach, we independently deleted *ATP1* and *ATP3* in the low accumulating strain; these are both nuclear genes encoding subunits of the F₁-ATPase. Either deletion resulted in the inability of the strain to grow on ethanol/ glycerol as a carbon source (Fig. S3-3A) and an inability to grow upon prolonged glucose restriction (Fig. 3-1B), confirming that they were defective in respiration. Both strains also showed a clear increase in Nab3 granule accumulation upon glucose restriction (Fig. 3-1A). Taken together, these results corroborate the

notion that the loss of respiratory capacity leads to an increase in the extent of Nab3 granule accumulation.

3.4.2 Enrichment for a respiratory competent cell population results in a reduction of Nab3 granule accumulation

We previously discovered that the population of a commonly used laboratory strain, S288C, accumulated an intermediate amount of Nab3 granules (~50% of cells, “medium”) compared to the two strains with a low (~3%) and a high (~80%) penetrance of this phenotype¹⁰⁶. This Nab3 granule accumulating phenotype correlated with an intermediate growth phenotype on ethanol/glycerol and an intermediate ability to grow during prolonged glucose deprivation, compared to the low and high accumulating strains¹⁰⁶. The S288C lineage is known to contain mitochondrial defects and to display a high level of mitochondrial genome instability^{90, 91, 114}. These preexisting allelic differences in the S288C background contribute to a high frequency of spontaneous generation of petites with partial mitochondrial genomes (ρ^- cells)¹⁰⁷. Such cultures are mixed, containing cells with both intact and deleted mitochondrial DNA, a condition known as heteroplasmy. Since respiration is necessary for growth during prolonged glucose starvation⁸⁴, we subjected this S288C-derived, intermediate Nab3 granule-accumulating strain to prolonged glucose starvation to enrich for a respiratory competent cell population in which petite derivatives could not survive. Cells were cultured with glucose or for an extended period (~45 hrs) of glucose deprivation, sampled at mid-logarithmic phase, and tested for their ability to grow on glycerol/ethanol (Fig. 3-2A). The cells from the intermediate S288C-based strain that emerged from prolonged glucose deprivation showed improved growth on glycerol (Fig. 3-2A, right bottom panel) as compared to the non-selected population grown in

glucose medium and spotted to glycerol (Fig. 3-2A right top panel). Cells from both culture conditions, as well as those given the standard 2hr glucose starvation, were imaged and Nab3 granules were quantified. The relatively high level of granule accumulation observed for the 2hr starved culture was completely reversed in the prolonged starvation culture (Figs. 3-2B and 3-2C), as predicted if prolonged starvation's selective pressure for respiratory competence reverses granule accumulation. In exploiting this "natural" variation in respiratory function found in a single culture, we obtained independent evidence again supporting the concept that Nab3 granule accumulation is driven by a loss of respiratory competence of the cell. This observation underscores the finding that heterogeneity in cell populations influences granule biology and likely other processes that are sensitive to mitochondrial function such as energy output.

3.4.3 Nab3 granule accumulation is lost upon addition of extracellular ATP

Stress granule assembly, remodeling, and disassembly are modulated by ATP and ATP is implicated in the solubilization of aggregated cellular proteins¹¹⁵⁻¹¹⁸. ATP levels drop rapidly when cells are deprived of glucose and this drop can lead to protein aggregation^{47, 116, 119, 120}. We exploited the finding that ATP added to permeabilized cells can reduce the accumulation of cytoplasmic stress granules⁷³. Upon the addition of extracellular ATP in the presence of DMSO, the fraction of cells with a Nab3 granule were statistically significantly reduced (Figs. 3-3A and 3-3B), suggesting that ATP levels modulate Nab3 granule disassembly in a similar manner to stress granules.

3.4.4 SKY1 knockout results in mitochondrial defects and increased Nab3 granule accumulation

Sky1 is the sole conserved serine-arginine protein kinase (SRPK) expressed in *S. cerevisiae*. Sky1 phosphorylates RNA-binding proteins, aids in the disassembly of stress granules, localizes to both the nucleus and cytoplasm, and displays a genetic interaction with Nab3¹⁰²⁻¹⁰⁵. We deleted *SKY1* in the medium granule accumulating strain and found it led to a statistically significant increase in Nab3 granule accumulation (Fig. 3-4A). Deleting *SKY1* in our low granule accumulating strain also increased the fraction of cells with Nab3 granules (Fig. 3-1A). Taken together, these data implicate Sky1 in Nab3 granule biology.

Since respiration defects lead to an increase in granule accumulation (Figs. 3-1, 3-2, 3-3), we tested if these strains also had a respiration defect. Both Sky1 deletion strains displayed impaired respiration compared to their parental strains (Figs. 3-4B, S3-3) with the S288C-based strain suffering a severe, and perhaps complete, inability to grow on glycerol/ethanol. Regardless of strain background, the loss of *SKY1* clearly resulted in a mitochondrial defect. In a further test of respiratory competence, prolonged growth in the absence of glucose was completely impaired when the S288C strain's *SKY1* gene was deleted, effectively converting the growth pattern of a lower granule-accumulating strain into the growth pattern of a petite strain that accumulates high levels of granules (Fig. 3-4C). Thus, the Sky1 role in Nab3 granule biology appears to be mediated by its mitochondrial function.

3.5 Discussion

Here we provide multiple lines of evidence that strongly implicate mitochondria and respiration in the biogenesis of Nab3 granules. This establishes the first documentation for the underlying regulatory mechanism of Nab3 granules, which resemble stress granules. Nab3 and Nrd1 are, to our knowledge, the only transcription termination factors for which conditional

assembly into a granule has been reported. Whether the granule is a complex ribonucleoprotein structure that is an active termination factor, or simply an aggregate formed from the Nab3 and Nrd1 proteins that both harbor prion-like domains, remains to be elucidated.

The relationship between Nab3 granules and respiration can be understood through a model (Fig. 3-5) in which there is normally an equilibrium between pan-nuclear (soluble) Nab3 and granule-associated Nab3 due to the action of an ATP-requiring granule dissociation machinery. In the presence of glucose (Fig. 3-5, condition 1), Nab3 generally localizes throughout the nucleus when ATP generation using glycolysis is unencumbered and Nab3 condensation is checked by disassembly-ATPases. If respiration is compromised (Fig. 3-5, condition 2), the removal of glucose leads to reduced ATP levels, the disassembly machinery cannot keep Nab3 soluble, and it accumulates into a nuclear granule. In periods of prolonged glucose deprivation (Fig. 3-5, condition 3), cells capable of respiration generate ATP and proliferate, resulting in the disassembly of the Nab3 granule and a return to a pan-nuclear distribution. Note that a small but statistically significant subset of cells display granules even when cells are fully respiration competent (Fig. 3-1, leftmost two bars), contributing to the idea that there is a constant equilibrium that shifts toward assembly when ATP levels become limiting¹⁰⁶.

Precedent for this model can be found from yeast stress granules, which are dispersed by the ATP-dependent dissociation activity of the Hsp104 chaperone ATPase⁷³. Other ATP-dependent mechanisms that regulate protein condensation and stress granule abundance have been identified including DEAD box ATPases¹²¹ and AAA ATPases¹²². Alternatively, high concentrations of ATP may act as a hydrotrope in which it is not hydrolyzed but acts as an amphiphile to directly solubilize phase separated protein condensates¹¹⁵. In either case, it follows that treatments, challenges, or genetic variations that compromise ATP production limit the dissociation ability of

this machinery and lead to granule accumulation because they cannot be efficiently dissolved. The extent to which cells in the population accumulate granules would be a function of the severity of the loss in energy generation. As would be expected, abrupt reversibility of Nab3 granules becomes obvious when cells are refed glucose²⁹.

Variation in the extent to which different strains spawn daughter cells that have a partial or complete absence of the mitochondrial genome (ρ^- or ρ^0 petites), and as a result, manifest a reduced respiratory capacity, yields strain to strain differences in granule count. For some genetic polymorphisms, such as that seen for mitochondrial DNA polymerase gamma *MIP1*, it is easy to grasp how a sequence variant can increase the frequency of mitochondrial genome loss⁹¹. Indeed, variants in the sequence of the conserved *MIP1* human ortholog are linked to mitochondrial disease^{123, 124}. For others, such as the experimentally generated $\Delta sky1$ mutation reported here, the mechanistic relationship between the gene product's function and loss of respiratory capacity needs to be studied further.

A high throughput screen of a collection of yeast gene deletion strains showed the *SKY1* deletion has reduced ability to grow on ethanol as a carbon source, implicating Sky1 in mitochondrial function¹²⁵. Our findings confirm and extend the relationship between Sky1 and mitochondria and suggests its role in influencing the assembly state of both cytoplasmic stress granules¹⁰² and nuclear Nab3 granules could be in providing ATP for the dissociation machinery of each compartment. This explanation is supported by a genetic interaction between *SKY1* and *HSP104*¹⁰². Interestingly, a global genetic interaction survey also picked up a *NAB3-SKY1* synthetic genetic effect which deserves more investigation¹⁰³. Alternatively, the Sky1 kinase could act more directly in each compartment, perhaps by phosphorylating a granule component, as it is known to shuttle between the nucleus and cytoplasm¹⁰⁴. Mutation of enzymes involved in

biosynthesis of the adenine ring or phosphorylation of the nucleotide to the triphosphate level, also modify the ATP energy charge of cells in a manner that can lead to protein aggregation in yeast¹¹⁶.

This report extends to a nuclear transcription termination complex known to undergo regulated compaction, the principles of compartment assembly observed for stress granules. These findings provide important clues to guide the elucidation of the mechanism of assembly and disassembly of this essential complex and the consequence of its compartmentalization on RNA metabolism.

3.6 Acknowledgments

This work was funded by National Institutes of Health (R01 GM120271 to D.R.), the Emory University School of Medicine, and the Emory University Research Committee, and the Emory Integrated Cellular Imaging Core. The content is solely the responsibility of the authors and does not necessarily reflect the official views of the National Institute of Health. The authors acknowledge Drs. Jennifer Kwong, Homa Galei, Gerald Shadel, Joanna Goldberg and Judy Fridovich-Keil for helpful discussions, plate reader usage, or a critical reading of the manuscript. The technical expertise of Laura Fox-Goharioon is also appreciated. Additionally, the authors acknowledge Emory University's Integrated Cellular Imaging Core (ICI) and Integrated Genomics Core.

3.7 Figures & Tables

Table 3-1 *S. cerevisiae* strains used in this paper

Strain	Genotype	Reference
DY4580	<i>MATa his3Δ1 leu2Δ0 met15Δ0 ura3Δ0 GFP-NAB3 HTB2-mCherry::HIS5</i>	Hunn et al., 2022
DY4730	<i>MATa his3Δ1 leu2Δ0 met15Δ0 ura3Δ0 GFP-NAB3 HTB2-mCherry::HIS5 SKY1::kanMX4</i>	This Study
DY4736	<i>MATα can1-100 his3-11,15 leu2-3,112 trp1-1 ura3-1 NRD1::natMX4 [pRS315-HA-Nrd1]</i>	Hunn et al., 2022
DY4746	<i>MATα can1-100 his3-11,15 leu2-3,112 trp1-1 ura3-1 NRD1::natMX4 GFP-NAB3 [pRS315-HA-Nrd1] ρ⁻</i>	Hunn et al., 2022
DY4756	<i>MATα can1-100 his3-11,15 leu2-3,112 trp1-1 ura3-1 NRD1::natMX4 GFP-NAB3 HTB2-yomCherry::kanMX [pRS315-HA-Nrd1] ρ⁻</i>	Hunn et al., 2022
DY4772	<i>MATα ade2-1 can1-100 his3-11,15 leu2-3,112 trp1-1 ura3-1 GFP-NAB3 HTB2-mCherry::HIS5</i>	Hunn et al., 2022
DY4851	<i>MATα ade2-1 can1-100 his3-11,15 leu2-3,112 trp1-1 ura3-1 GFP-NAB3 HTB2-mCherry::HIS5 ATP1::kanMX4</i>	This Study
DY4856	<i>MATα ade2-1 can1-100 his3-11,15 leu2-3,112 trp1-1 ura3-1 GFP-NAB3 HTB2-mCherry::HIS5 ATP3::kanMX4</i>	This Study
DY4863	<i>MATα ade2-1 can1-100 his3-11,15 leu2-3,112 trp1-1 ura3-1 GFP-NAB3 HTB2-mCherry::HIS5 SKY1::kanMX4</i>	This Study

Figure 3-1

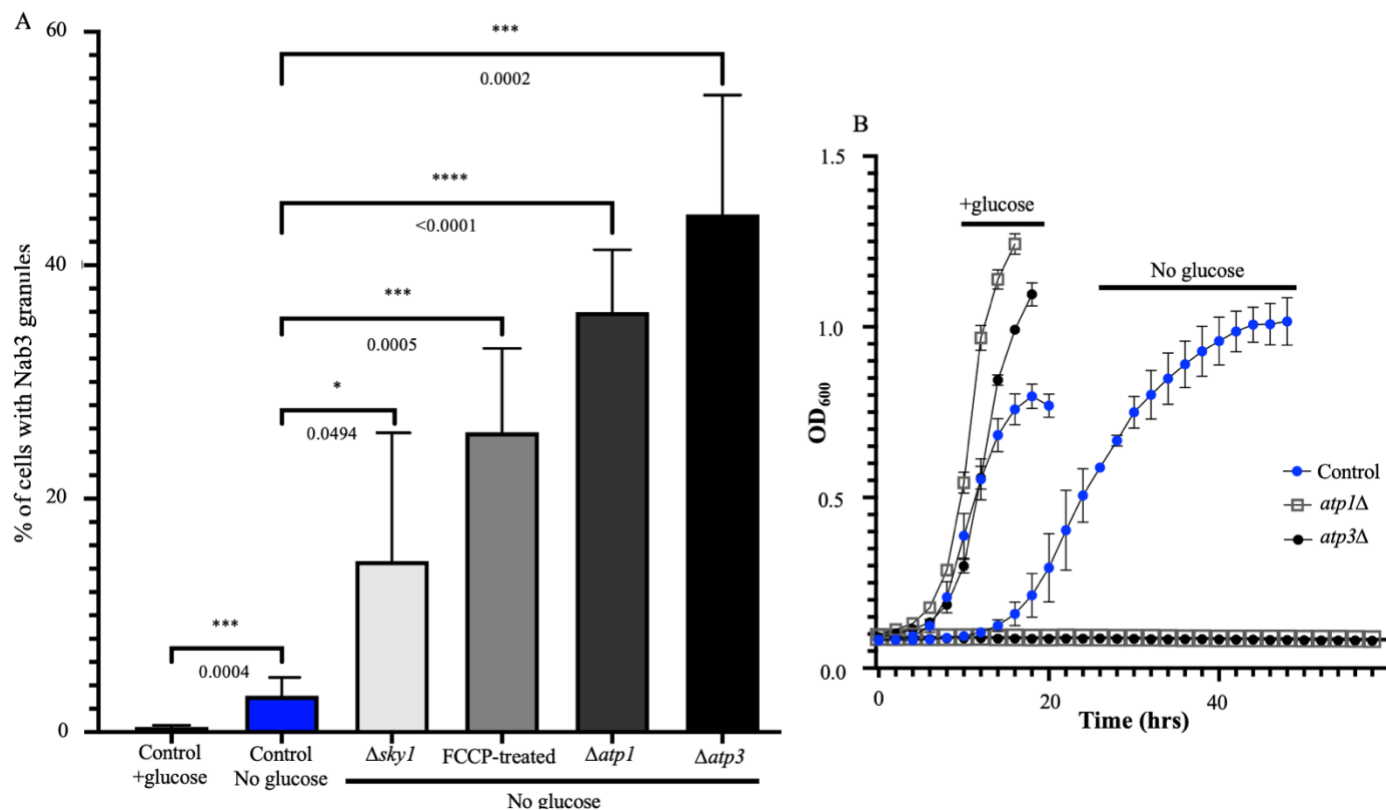


Fig. 3-1 Mitochondrial manipulations in a low granule accumulating yeast strain

(A) Four yeast strains (DY4772, control; DY4851, $\Delta atp1$; DY4856, $\Delta atp3$; DY4863, $\Delta sky1$) were grown to mid-logarithmic phase, washed into starvation media, starved for 2 hours, imaged, and analyzed. Additionally, DY4772 was treated with 20 μ M FCCP, a mitochondrial inhibitor, for 30 minutes prior to imaging and analysis. Averages and standard deviations are plotted, and p-values are presented. [n values for the bar graph (left to right) were, 5, 10, 6, 6, 9, 6, respectively.]

(B) Yeast strains [DY4772 (control, solid blue circle); DY4851 ($\Delta atp1$, open square); DY4856 ($\Delta atp3$, solid black circle)] were grown to mid-logarithmic phase, washed into glucose-containing media or starvation media for 2 hours at 30°C before reseeded at OD₆₀₀= 0.08 in appropriate media. Cell growth OD₆₀₀ was monitored at 30°C in a microplate reader. Averages and standard deviations from three technical replicates of each biological triplicate, were plotted.

Figure 3-2

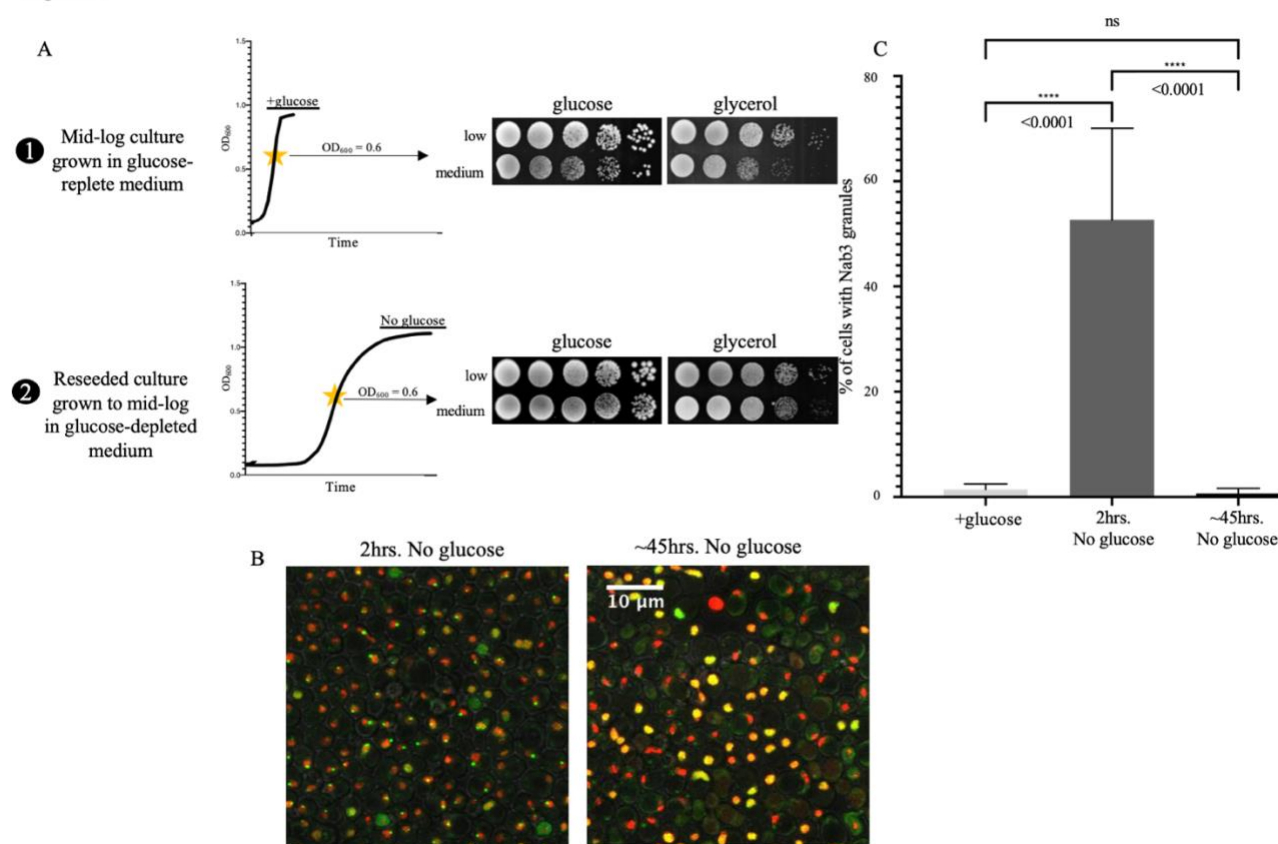


Fig. 3-2 Improved respiration capacity results in a decrease in Nab3 granule accumulation

(A) Low and medium Nab3 granule accumulating yeast strains (DY4772 and DY4580 respectively) were grown to mid-logarithmic phase in glucose, aliquots were serially diluted, and plated onto glucose (YPD) or glycerol (YPEG) solid medium (1). The remaining cells were washed into starvation media for 2 hours at 30°C before reseeded at $OD_{600}=0.08$. Cells were grown to mid-logarithmic phase in prolonged glucose deprivation, aliquots were serially diluted, and plated onto solid YPD or YPEG media (2).

(B) Medium Nab3 granule accumulating yeast strain DY4580 was grown to mid-logarithmic phase, washed into starvation media, starved for 2 hrs., imaged and analyzed. At the conclusion of the 2hr. starvation, cells were reseeded at $OD_{600}=0.08$ and grown to mid-logarithmic phase (~45hrs.) in the absence of glucose for prolonged glucose deprivation, imaged and analyzed.

Representative fields of cells were imaged from independent biological replicates grown on different days.

(C) Medium Nab3 accumulating yeast strain DY4580 was grown to mid-logarithmic phase, washed into media with (+glucose) or without glucose, incubated for 2 hours at 30°C (2 hrs. no glucose), imaged, and analyzed. At the conclusion of the 2-hour starvation, cells were reseeded at $OD_{600} = 0.08$ and grown to mid-logarithmic phase (~45hrs) in the absence of glucose for prolonged glucose deprivation. An aliquot was imaged and analyzed. Averages and standard deviations are plotted, and p-values are presented. [n values for the bar graph (left to right) were, 6, 29, 5, respectively. ns, not significant]

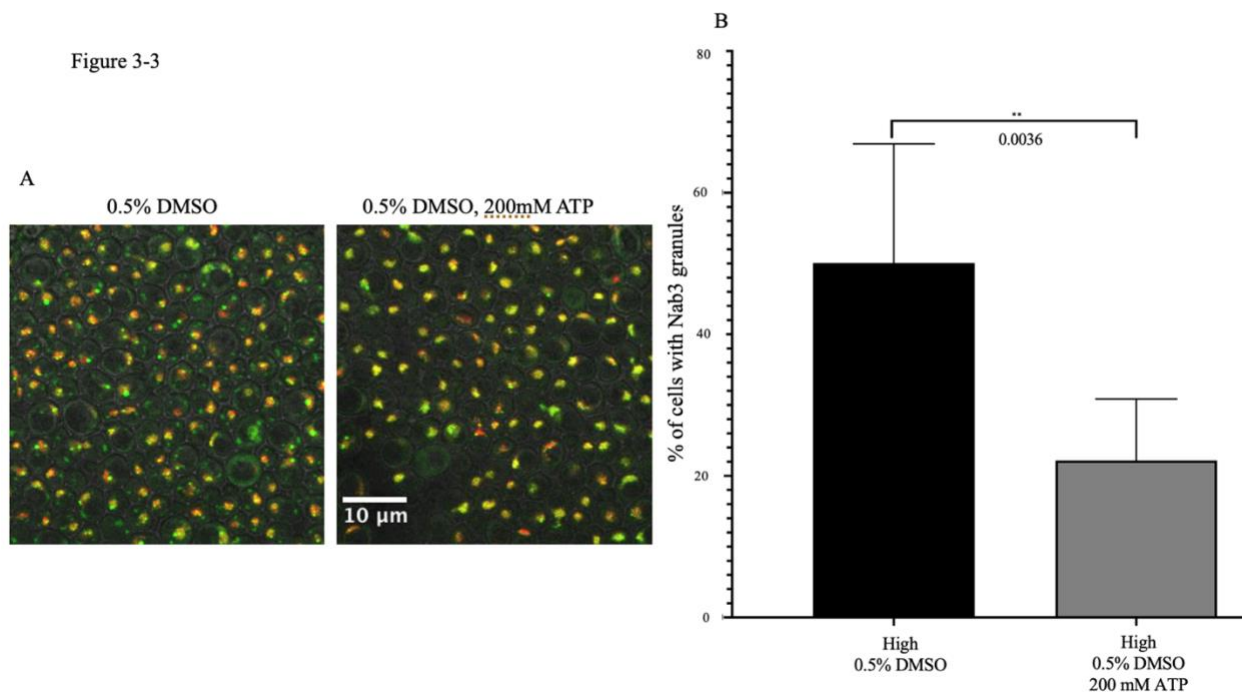


Fig. 3-3 Nab3 granule levels are reduced by the addition of extracellular ATP

(A) High Nab3 granule accumulating yeast strain DY4756 was grown to mid-logarithmic phase, washed into starvation media, starved for 2 hrs., treated with either 0.5% DMSO alone (control) or 0.5% DMSO and 200mM ATP, image and analyzed. Representative fields of cells were imaged from independent biological replicates grown on different days.

(B) Yeast strain DY4756 ('high') was glucose-starved for 2 hours at 30°C and treated with either 0.5% DMSO alone (control) or 0.5% DMSO and 200 mM ATP for 30 min prior to analysis by fluorescent microscopy. Fields of cells were imaged from independent biological replicates grown on different days. The average and standard deviation of the percent of yeast cells containing GFP-Nab3 granules were calculated for each condition and plotted. [n values for the bar graph (left to right) were 7 and 8, respectively.]

Figure 3-4

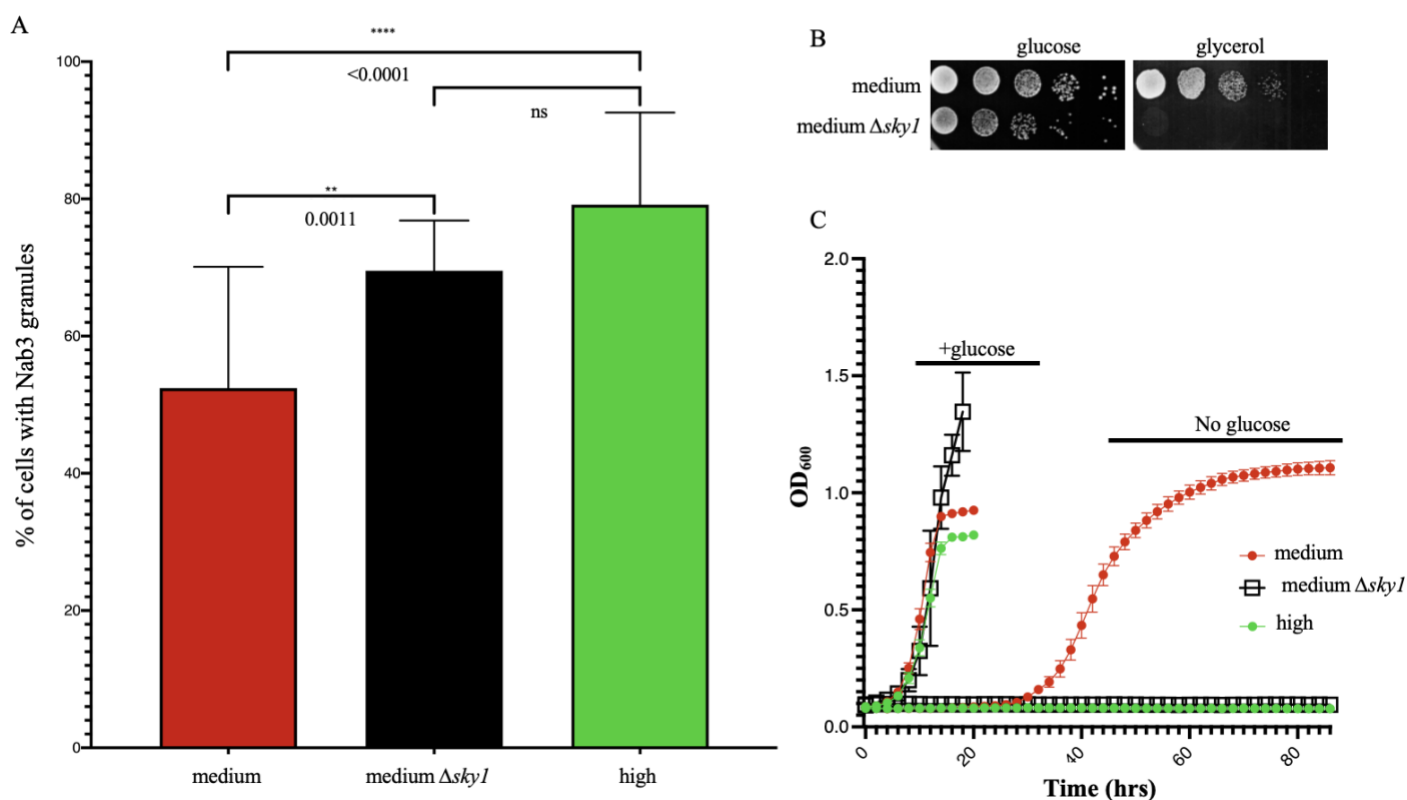


Fig. 3-4 Sky1 knockout results in mitochondrial deficiency and increased Nab3 granule accumulation

(A) Yeast strains DY4580 (medium), DY4730 (medium + $\Delta sky1$) and DY4756 (high) were glucose-starved for 2 hrs at 30°C and analyzed by fluorescent microscopy. Fields of cells were imaged from independent biological replicates grown on different days. The average and standard deviation of the percent of yeast cells containing GFP-Nab3 granules were calculated for each condition and plotted. [n values for the bar graph (left to right) were 28, 6, 10, respectively.]

(B) Yeast strains DY4580 (medium) and DY4730 (medium + $\Delta sky1$) were grown to saturation and diluted with sterile water to a concentration of 10^7 cells/mL. Cells were serially diluted 10-fold and 10 μ L spots of each dilution were spotted on SC-glucose or SC-glycerol/ethanol as indicated and incubated at 30°C.

(C) Three different yeast strains (DY4580 (medium, solid red circle); DY4730 ($\Delta sky1$, open black square), DY4756 (high, solid green circle) were grown to mid-logarithmic phase, washed into glucose-containing media or starvation media for 2 hrs at 30°C and reseeded at $OD_{600} = 0.08$ in appropriate media. Growth of cells was monitored at 30°C in a microplate reader by measuring OD_{600} (600 nm). Averages and standard deviations from three technical replicates of each biological triplicate, were plotted.

Figure 3-5

Equilibrium between pan-nuclear Nab3 and its assembly into a granule

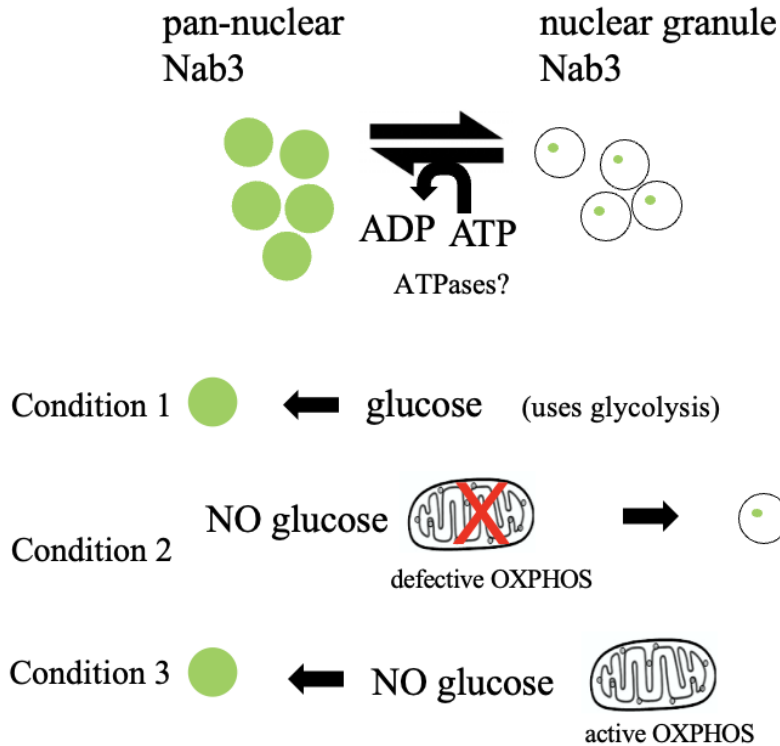
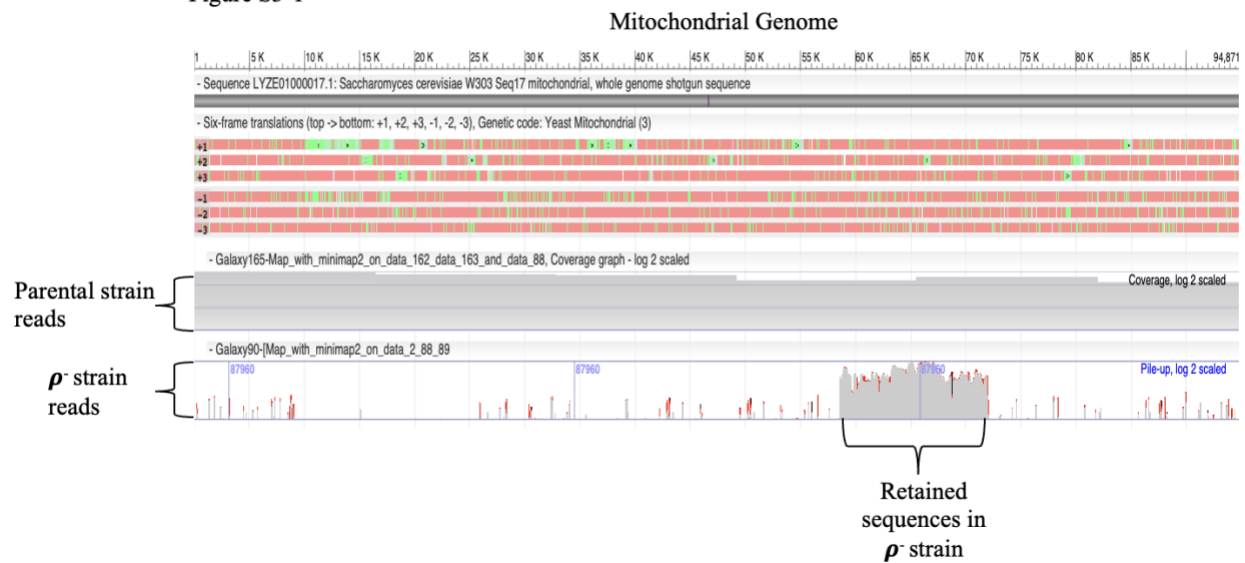


Fig. 3-5 Equilibrium between pan-nuclear Nab3 and its assembly into a nuclear granule: a working model for Nab3 granule disassembly and accumulation.

There is an equilibrium between pan-nuclear and granule-associated Nab3. In the presence of glucose (condition 1), Nab3 generally localizes throughout the nucleus when ATP generation using glycolysis is unencumbered and Nab3 condensation is reversed. If respiration is compromised (“X”, condition 2), the removal of glucose reduces ATP levels, the disassembly machinery cannot keep Nab3 soluble, and the protein accumulates into a nuclear granule. In periods of prolonged glucose deprivation (condition 3), cells capable of respiration can generate ATP and proliferate, resulting in the disassembly of the Nab3 granule and a return to a pan-nuclear distribution.

Figure S3-1

**Fig. S3-1 A high granule accumulating yeast strain is ρ^-**

Whole genome sequencing analysis reveals that the high granule accumulating yeast strain DY4746 (parent to DY4756) is ρ^- as it possesses only a small portion of its mitochondrial genome compared to its parental strain (DY4736). Sequencing reads in the lower two panels of the NCBI viewer are piled in horizontal lines with gray representing identities to the reference sequence and mismatches shown in red. All but ~15 kbp of mitochondrial DNA are lost from this petite strain.

Figure S3-2

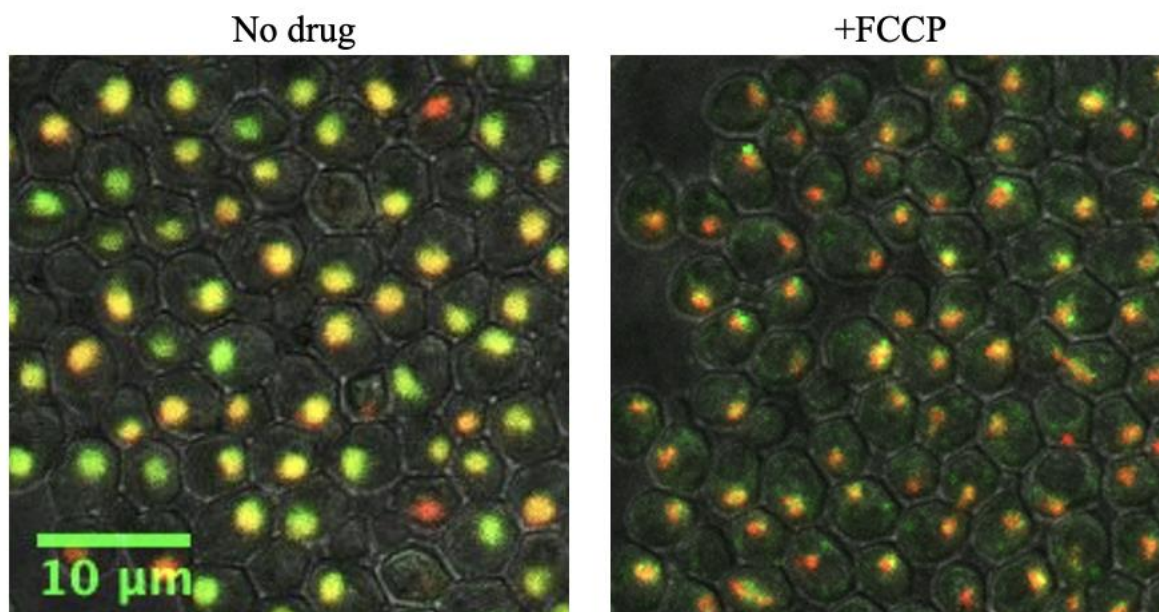


Fig. S2 Confocal microscopy of a glucose starved low granule accumulating strain treated with and without the electron transport uncoupler, FCCP.

Yeast strain DY4772, which is low Nab3 granule accumulating, was grown to mid-logarithmic phase, washed into starvation media, starved for 2 hrs, treated with mock or 20μM FCCP for 30 min, imaged, and analyzed.

Figure S3-3

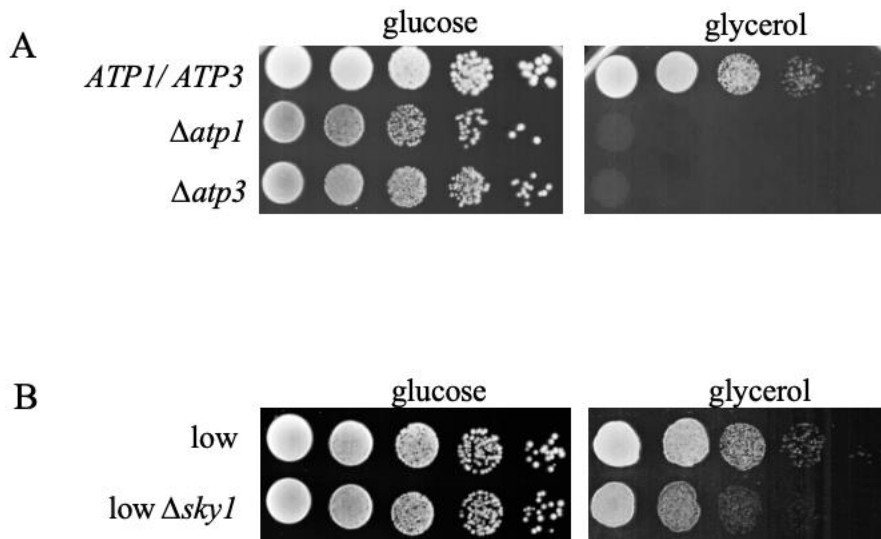


Fig. S3-3 Deletions of nuclear encoded genes result in a mitochondrial defect.

(A) Yeast strains DY4772 (control), DY4851 ($\Delta atp1$) and DY4856 ($\Delta atp3$) were grown to saturation and diluted with sterile water to a concentration of 10^7 cells/mL. Cells were serially diluted 10-fold and 10 μ l of each dilution were spotted onto SC-glucose or SC-glycerol/ethanol as indicated and incubated at 30°C.

(B) Yeast strains DY4772 (control) and DY4863 (low $\Delta sky1$) were grown to saturation and diluted with sterile water to a concentration of 10^7 cells/mL. Cells were serially diluted 10-fold and spotted on SC-glucose or SC-glycerol/ethanol as indicated and incubated at 30°C.

Chapter 4.0: Discussion and Future Directions

4.1 Summary

The goal of this thesis was to explore the underlying mechanism(s) that drives Nab3 nuclear granule accumulation, thus expanding upon the lab's prior research on the fundamentals of gene expression with a focus on the NNS transcription termination complex. The work presented in this thesis provides foundational evidence for oxidative phosphorylation and mitochondrial function as a driving factor of Nab3 granule accumulation using a natural genetic variant. This is a new finding in the context of NNG research; however, it is in agreement with well-established research for other inducible subcellular compartments such as stress granules. This work also presents the development of a computational tool that enables rapid and robust quantification of Nab3 granule accumulation across yeast strains. The key findings in this thesis are as follows:

- (1) Nab3 granule accumulation varies in penetrance across yeast strains (Chapter 2.0).
- (2) The variation in penetrance is, in part, due to mitochondrial/ respiratory deficiencies (Chapters 2.0 & 3.0).
- (3) Cells with intact mitochondria and a robust respiratory capacity have low Nab3 granule accumulation, can grow on ethanol/ glycerol as a carbon source and are able to grow and proliferate during extended glucose deprivation. Further, the opposite holds true for cells with mitochondrial deficiencies and impaired respiratory capacity (Chapters 2.0 & 3.0).
- (4) The addition of extracellular ATP is sufficient to drive down Nab3 granule accumulation, further supporting oxidative phosphorylation (OXPHOS) function as an important driver of Nab3 granule accumulation (Chapter 3.0).

- (5) Sky1 is a serine-arginine kinase implicated in splicing and yeast stress granule disassembly and influences Nab3 granule accumulation through its impact on mitochondrial function (Chapter 3.0).

4.2 The importance of a computational tool to quantify Nab3 granule accumulation in various yeast strains

Prior to this thesis, foundational work was done that paved the way for the Nab3 investigation presented in this thesis. First, it was discovered that mutations in the Nab3 protein led to transcription termination defects and that a removal of only three amino acids from Nab3's C-terminus resulted in compromised Nab3 transcription termination function²¹. This fundamental finding led to further work that demonstrated that this region of Nab3, specifically a stretch of glutamines and the final 18 amino acids found in this region, was able to assemble into a tetrameric form like the human hnRNP-C protein²⁵. Additional experiments showed that the last 134 amino acids of Nab3's C-terminus is of low-complexity nature and can assemble into a hydrogel *in vitro*²⁴. These findings set the stage for work that would further investigate Nab3's ability to polymerize on target transcripts.

Work done by Darby *et al.* showed that Nrd1 and Nab3 condensed into a novel nuclear speckle in response to glucose deprivation *in vivo*⁵⁸. This led to work demonstrating that Nab3's C-terminus was predicted to be prion-like based upon its sequence bias and that this region was able to form amyloid filaments *in vitro*²⁶. It was also found that Nab3's prion-like, C-terminal domain is required for Nab3's assembly into a nuclear granule upon glucose deprivation²⁹. These findings supported other work at the time that showed RNA binding proteins with low complexity domains could form subcellular compartments in which RNA metabolism takes place²⁶.

It is well-established that the formation of subcellular compartments in response to cell stress is important for RNA metabolism^{48, 49}. Thus, given the expansive work done on Nab3's ability to assemble into amyloid filaments *in vitro* and a subcellular nuclear granule *in vivo*, we pursued granule formation to gain a better understanding of the function of the Nab3 granule as well as the mechanisms that govern its assembly and dissociation. Prior to this thesis work, Nab3 granule accumulation was manually quantified. Manual quantification is time consuming and can be subjective. Thus, our lab sought to create a computational tool to enable the rapid and robust quantification of Nab3 granule accumulation. We accomplished this goal by acquiring numerous confocal microscopy images, utilizing these images to build a tool in MATLAB and manually counting to compare manual human and our computational tool's quantification. The algorithm is publicly accessible, only requiring access to MATLAB, and it can be adjusted to meet specific needs. The advent of computer-based quantification enabled us to build more robust datasets that included more independent replicates and quantification of thousands of live cells. The objective calling of granules, and the resulting statistical tests that could be applied, led to our finding that there was substantial strain to strain variation in granule penetrance. The development of this tool will continue to aid in Nab3 granule research as well as research on other subcellular compartments such as nuclear speckles or the mammalian structures known as rods and rings.

4.3 The importance of mitochondrial function on Nab3 granule accumulation

With the development of the computational tool, we analyzed three different yeast strains and quantified each strain for Nab3 granule formation¹⁰⁶. We discovered that Nab3 granule accumulation varies in penetrance across yeast strains and exploited this phenomenon to gain insight into the mechanistic basis for variation.¹⁰⁶ The inability to grow during extended glucose

deprivation positively correlated with the high Nab3 granule accumulation phenotype.¹⁰⁶ Weber *et al.* noted that respiration is crucial for survival and energy maintenance upon glucose deprivation. Taken together these results suggested that respiration is important for Nab3 granule accumulation, providing a possible linkage between metabolism and this nuclear granule. Indeed, the low, medium, and high granule accumulating strains display a continuum of oxidative phosphorylation function consistent with this idea.

Through a series of mitochondrial manipulations, I demonstrated that damage to mitochondrial function and effective oxidative phosphorylation result in a high Nab3 granule accumulation phenotype, thus strengthening the argument that respiration impacts Nab3 granule accumulation. We developed a working model in which there is a natural equilibrium between pan nuclear and granule associated Nab3 (Chapter 3, Fig. 3-5). When ATP is perturbed by a disturbance in mitochondrial function, the equilibrium is shifted in the direction of granule based Nab3. This model was tested by adding extracellular ATP to permeabilized cells rich in Nab3 granules. Providing ATP in this manner substantially decreased Nab3 granule accumulation.

This work contributes to a broader understanding of the factors that influence protein rearrangement in response to changes in environmental conditions. The results of this work and impacts are discussed in the sections below.

4.4 Future directions for this research project

4.4.1 Breaking down the composition of the Nab3 granule

Darby *et al.* first documented the rearrangement of Nrd1 and Nab3 upon glucose starvation into a structure they termed a “perinuclear speckle”⁵⁸. Our lab has since confirmed this finding and documented the colocalization of Nrd1 and Nab3 to a nuclear granule upon glucose starvation. It is not surprising to note the colocalization of Nrd1 and Nab3 considering the two are known to

function as a heterodimer during transcription termination^{2, 3, 11, 14, 16, 17, 21-26}. However, an outstanding question that remains is what the functional purpose of this protein rearrangement is. I suggest the rearrangement of Nrd1 and Nab3 to a granule in response to glucose deprivation is related to its activity as a termination factor. Structures like the Nrd1-Nab3 granule, such as P-bodies and stress granules, are known to form in yeast in response to glucose deprivation^{47, 48}. These are RNP structures, like the Nrd1-Nab3 granule, that have been investigated in depth and for which some functions are known. P-bodies form in response to glucose deprivation to concentrate and house cellular machinery used to degrade mRNA that is no longer needed by the cell^{48, 50}. Stress granules assemble and function as “storage depots” to hold proteins and mRNA until conditions are suitable to resume the translation of mRNA^{48, 50}.

Identifying other components of the Nrd1-Nab3 granule will be a key future direction to begin to understand the functional role of this subcellular structure. One method that can be used to identify proteins in the Nrd1-Nab3 granule is a proximity labeling assay known as APEX2. This assay works by fusing an engineered ascorbate peroxidase biotinylating enzyme to the Nab3 protein¹²⁶⁻¹³⁰. When cell-permeable substrates are added, proteins in proximity (<20 nm) to Nab3 become biotinylated and used as an affinity handle. The purified biotinylated proteins can be detected *via* mass spectrometry¹²⁶⁻¹³¹. Alternatively, granules can be directly purified and the protein contents by mass spectrometry.^{132, 133} Once candidate proteins are identified *via* mass spectrometry, fluorescent versions of these proteins can be made and integrated into yeast strains in order to visualize and confirm the colocalization of the candidate protein and Nab3¹³⁴. A third possible approach would be to , use immunofluorescence to identify candidate proteins for colocalization with the Nab3 granule¹³⁴.

There is the possibility that the granule only contains the Nrd1 and Nab3 proteins or that the granule simply serves as a compartment for misfolded proteins targeted for degradation. Protein misfolding can occur for a variety of reasons including stress-induced denaturation, mutations, or lack of assembly partners¹³⁵. The cellular quality control machinery sorts misfolded proteins based on their ubiquitination state and solubility, and misfolded proteins are sorted into a specific compartment where they are then degraded^{135, 136}. This sorting machinery resides in both the cytoplasm and the nucleus and sorts misfolded proteins into cytosolic juxtannuclear deposits (JUNQ) and intranuclear quality control compartments (INQ) respectively¹³⁶. Btn2 is an INQ-specific aggregase that directs protein deposition into nuclear INQs, thus Btn2 is a good candidate to investigate as a potential component of the NNG¹³⁶. If Btn2 is confirmed as a component, it is possible that the NNG is an INQ or a similar compartment of sorts.

Another key granule component yet to be explored is its RNA content. Jamonnak *et al.* established that the binding targets of Nrd1 and Nab3 change during glucose deprivation²³. Specifically, there is an approximate 100 nucleotide upstream shift in the binding of Nrd1 to snoRNA and this shift places Nrd1 binding within the mature snoRNA²³. They propose that this change could be indicative of earlier termination directed by an altered Nrd1-Nab3 binding specificity or could be attributed to Nrd1-Nab3 binding after snoRNA maturation that may lead to degradation²³. Thus, the Nrd1-Nab3 granule could serve to (1) concentrate factors involved in transcription termination or (2) concentrate factors involved in the degradation of mature snoRNA. One way to identify the RNA components of the granule would be to perform high throughput RNA sequencing on the contents contained within purified material^{132, 133, 137}. Additionally, one could perform fluorescence *in situ* hybridization (FISH) to identify RNA contained within the

NNG¹³². Both methods have successfully been used to identify RNA contained within stress granules¹³².

In addition to the functions mentioned above, there is also the possibility that the granule is a type of “storage depot”, akin to a stress granule. For example, upon glucose starvation, stress granules form and contain the eukaryotic initiation factor (eIF)4E and eIF4G proteins as well as the poly(A) binding protein, Pab1⁴⁹. These proteins are important for translation and are held in the stress granule until conditions favorable for translation lead to the dissolution of the stress granule and translation factors release⁴⁹. Thus, future experiments should aim to identify the types (snRNA, snoRNA, CUTs, mRNA) and states (pre, mature, degraded) of RNA found within the Nrd1-Nab3 granule in order to better understand the granule’s function.

Another possibility is that the granule functions as a site for transcriptional attenuation of a specific subset of transcripts vital to survival during glucose deprivation. van Nues *et al.* used a method known as kinetic CRAC (cross-linking and analysis of cDNAs) to determine roles for Nab3 in gene expression during stress⁷¹. Their work, along with others, revealed that the binding of Nab3 to transcripts changes throughout the time course of glucose deprivation (glucose-replete to 18mins glucose-depleted)^{71, 138}. In the presence of glucose, Nab3 is bound to transcripts such as *NRD1* and *IMD2*, genes that Nrd1 and Nab3 are known to regulate during normal growth conditions^{3, 71}. However, after 4 minutes of glucose deprivation, Nab3 shifts to transcripts such as *ATP1*⁷¹. The binding and attenuation of *ATP1* is intriguing now knowing what we know about the importance of mitochondrial function and Nab3 granule accumulation. The fact that Nab3 binds and attenuates *ATP1* in the first 4 minutes of glucose deprivation but is no longer bound by 18 minutes of glucose deprivation suggests that the granule serves to concentrate the termination of specific transcripts important for cell survival during starvation. Specific transcripts could be

attenuated until the cell senses more favorable growth conditions. Once the cell has transitioned to respiration and survival, genes, such as *ATP1*, are no longer attenuated and the full transcript is transcribed and translated into important machinery needed for respiration and survival during prolonged glucose deprivation (**Fig. 4-1**). Therefore, future experiments should focus on Nab3 binding to RNA transcripts while monitoring (1) ATP levels, (2) cellular transition from fermentation to respiration in response to glucose deprivation and (3) Nab3 granule accumulation and dissociation.

4.4.2 Identifying key players in assembly and disassembly of the Nab3 granule.

While identifying protein and RNA components of the Nrd1-Nab3 granule will help to elucidate the function of the granule, it may or may not aid in identifying key players in assembly and disassembly of the granule. Thus, another important future direction for this work is to design experiments aimed at discovering key players in assembly and disassembly. Looking at work done on other RNP granule structure assembly and disassembly may prove helpful in guiding the design of these experiments. For example, in the absence of ATP hydrolysis or substrate release, DEAD-box proteins remain stably bound to RNA and this serves as a template for recruitment of other proteins to the RNA¹²¹. This initial complex can further trigger the formation of larger RNP granules that then assemble into larger biomolecular condensates that appear as a membraneless subcellular compartment¹²¹. One specific example of this is Sub2, a component of a yeast protein complex important for nuclear mRNA export¹²¹. When Sub2 inhibits mRNA release from the site of transcription, it leads to the formation of nuclear RNP granules¹²¹. Keeping in mind that ATP levels are known to plummet at the onset of glucose deprivation, and that Nrd1-Nab3 granule accumulation is affected by ATP levels, one can imagine a scenario for Nrd1-Nab3 granule

assembly where Nrd1 and Nab3 remain bound to RNA and serve as a template for the recruitment of other proteins to assemble into the membraneless subcellular compartment that is the Nrd1-Nab3 granule.

In addition to protein-RNA serving as templates for granule formation, there are other players that regulate granule formation such as the DEAD-box protein, eukaryotic translation initiation factor 4A (eIF4A)¹²¹. eIF4A was shown to regulate the formation of stress granules that form through the condensation of untranslated mRNPs¹²¹. eIF4A does so by counteracting RNA-RNA multimerization through ATP-dependent RNA-binding, thus inhibiting RNA condensation and stress granule formation. Thus, in the context of Nrd1-Nab3 granule accumulation, one can hypothesize that if ATP levels are low and DEAD-box proteins are unable to counteract Nrd1-Nab3-RNA multimerization, Nrd1-Nab3 granules accumulate. Thus DEAD-box proteins or DEAD-box-like-proteins could be important in the regulation of Nrd1-Nab3 granule assembly.

In the context of disassembly, stress granules may provide insight into factors that drive Nrd1-Nab3 granule disassembly. Stress granule disassembly is known to be modulated by the ATP hydrolase activity of Hsp104 disaggregase as well as cellular ATP levels⁷³. The ATP hydrolase activity of Hsp104 is the critical ATP-consuming step that determines stress granule compartment abundance and size⁷³. Thus, since Nrd1-Nab3 granule accumulation is reduced by the addition of extracellular ATP, it is probable that an ATPase is also involved in the disassembly of the Nrd1-Nab3 granule. Additionally, the serine-arginine protein kinase, Sky1, has been implicated in efficient stress granule disassembly^{102, 104}. Work presented in this thesis demonstrated the relationship between Sky1 and Nrd1-Nab3 granules by showing that a Sky1 deletion resulted in increased Nrd1-Nab3 granule accumulation. We suggest Sky1 is involved in efficient Nrd1-Nab3 granule disassembly by maintaining ATP levels through its influence on

mitochondrial function. We, along with others¹²⁵, show that a gene deletion of *SKY1* results in a reduced ability to grow on ethanol as a carbon source as well as an inability to grow and proliferate during extended glucose deprivation. These data suggest that a gene deletion of *SKY1* results in reduced respiratory capacity.

Thus, while Sky1 may not be directly involved in Nrd1-Nab3 granule disassembly, it does impart an influence on it like stress granule disassembly. Alternatively, Sky1 could act directly on Nrd1-Nab3 granules and stress granules by phosphorylating a granule component as Sky1 is known to shuttle between the cytoplasm and nucleus¹⁰⁴. Regardless of how Sky1 influences Nrd1-Nab3 granule disassembly, it is an example of how (1) stress granules can serve as a paradigm for Nrd1-Nab3 granules and should be used to design future experiments and (2) other key players may have an influential direct or indirect impact on Nrd1-Nab3 granule disassembly.

4.4.3 Discovering other factors that influence Nab3 granule accumulation

The work presented in this thesis identified respiration and mitochondrial function as an important factor in determining Nab3 granule accumulation; however, it is important to think about other cellular aspects that may influence granule accumulation. Yeast regularly experience fluctuations in nutrient availability, temperature, osmolarity and acidity of their environment and they reprogram their gene expression to ensure survival through this ever-changing environment¹³⁹. While it is well-established that glucose starvation induces Nrd1-Nab3 granule accumulation and causes a change in Nrd1-Nab3 binding to transcripts^{23, 29, 58, 71}, it is important to explore other environmental conditions such as heat shock or changes in osmolarity to see if these changes also cause Nrd1-Nab3 granule accumulation and/ or alter the contents of the NNG.

For example, stress granules form in yeast due to a variety of cellular stresses such as glucose deprivation and heat shock. When stress granules form in response to glucose deprivation, they contain the eukaryotic initiation factor (eIF)4E and eIF4G proteins as well as the poly(A) binding protein, Pab1⁴⁹. However, when stress granules form in response to heat shock, they contain 40S ribosomal subunits and eIF3 factors, which are lacking from those formed during glucose deprivation⁴⁹. Additionally, it has been shown that mutations that affect stress granule assembly during glucose starvation have little effect on their assembly under heat shock conditions⁴⁹. These findings demonstrate how different environmental conditions can influence granule formation as well as the contents within them. Thus, it would be worth exploring how different environmental conditions influence NNG assembly and dissociation as well as the contents found within the NNG.

Research aimed at understanding how Nrd1 and Nab3 binding to RNA changes in response to different environmental fluctuations reveals that Nab3 binding profiles can include many genes involved in the heat-shock and oxidative stress responses⁷¹. Additionally, another set of experiments systematically identified Nrd1 and Nab3 in insoluble protein fractions in response to heat shock¹⁴⁰. Using stress granules as a paradigm, I would predict that NNG formation is induced in response to heat shock; however, the contents of the granule may vary between NNG's formed during glucose starvation and those formed during heat shock. This prediction alludes to the idea that NNG formation serves as a compartment to concentrate transcription termination of a specific set of transcripts and while NNG formation would still occur under both conditions, the cellular drivers of formation and dissociation as well as the granule's contents would differ due to the inducing of different stress responses. In a glucose-deprived state, NNG formation is triggered by a drop in ATP levels and is dissociated when ATP levels rise again due to a switch in fermentation

to respiration. The contents of the granule may contain attenuated transcripts of *ATP1*, an important subunit vital to proper oxidative phosphorylation and respiration. However, upon heat shock, NNG formation may be triggered by a cellular signaling response to temperature change and the contents of the NNG may differ to contain heat shock protein gene transcripts instead of transcripts such as *ATP1*. Thus, investigating NNG formation and its contents under different environmental challenges would prove useful in demonstrating both the function of the NNG as well as the dynamic state of the compartment.

4.5 Implications of mitochondrial function in neurodegenerative diseases

Mitochondrial dysfunction is implicated in neurodegenerative diseases such as Alzheimer disease, Parkinson's disease, ALS and Huntington's disease¹⁴¹. This is because mitochondria are regulators of cell death, a key feature of neurodegeneration¹⁴¹. During aging, there is an increased risk of neurodegeneration due, in part, to oxidative stress that leads to the production of reactive oxygen species¹⁴¹ and an accumulation of mutations in mitochondria. In Alzheimer's disease, Parkinson's, ALS and Huntington's disease, there is strong evidence that mitochondrial dysfunction occurs early and acts as a key contributor throughout the progression of the disease¹⁴¹. Additionally, many disease-specific proteins interact with mitochondria and mutations in certain proteins can lead to mitochondrial dysfunction¹⁴¹.

Yeast are an excellent model organism to use for studying mitochondrial function and diseases. More specifically, in the context of our research, the NNS complex is an important topic of study as it is helping to elucidate how players in transcription termination can impact mitochondrial function. For example, it has been shown that deletions in genes involved in cell cycle regulation and mitochondrial maintenance in combination with *nrp1* mutants leads to

synthetic lethality or slow-growing phenotypes⁵⁸. Interestingly, these synthetic interactions correlated with defects in cell size and mitochondrial content in the *nrp1* mutants, suggesting that *NRD1* could help to regulate mitochondrial content and inheritance as well as mitochondria morphology and the stability of mitochondrial DNA⁵⁸.

Another example is Sen1, which is an ATP-dependent 5' to 3' RNA/DNA and DNA helicase that is part of the essential Nrd1-Nab3-Sen1 transcription termination complex^{2, 3, 11, 12, 14, 16, 17, 21-26}. Sen1 plays a role in genome stability through its helicase activity which is responsible for preventing RNA:DNA hybrids that can form from R-loops during transcription¹². Recent studies revealed that an N-terminal truncation of Sen1 causes a slow growth phenotype, loss of mitochondrial DNA, oxidative stress, and downregulation of genes that are required for mitochondrial biogenesis¹². More specifically, data show that *SEN1* mutations results in a significant downregulation of genes that are required for mitochondrial biogenesis and function¹². Because the yeast Sen1 protein has such strong similarity to the human ortholog, senataxin, it has been proposed as a model to study disorders that occur in humans due to mutations in senataxin¹². Mutations in the human *SETX* gene, which encodes senataxin, is associated with progressive neurodegenerative diseases such as ataxia with oculomotor apraxia type 2 (AOA2) and amyotrophic lateral sclerosis type 4 (ALS4)¹². Thus, the loss of mitochondrial DNA, oxidative stress and downregulation of genes required for mitochondrial biogenesis as a result of mutations in Sen1 may provide a link between mitochondrial dysfunction and neurodegenerative disease.

4.6 Final remarks

This body of work established that Nrd1-Nab3 granule formation varies in penetrance across yeast strains and that this variation is influenced, in part, by mitochondrial function and

respiratory capacity. This work identified that ATP homeostasis is an important factor in Nrd1-Nab3 granule disassembly and suggests that some of the machinery involved in Nrd1-Nab3 granule disassembly requires ATP. The serine-arginine protein kinase, Sky1, was discovered to influence Nrd1-Nab3 granule disassembly and, based on the findings of the importance of respiration, led to strong evidence that this is through its role in mitochondrial function. From this work, logical next steps have been established that will aim to identify both protein and RNA components of the granule to further understand the functional role of Nrd1-Nab3 granule formation as well as offering avenues to explore other stress response pathways that have the potential to trigger Nab3 granule assembly and accumulation. These proposed next steps will broaden our understanding of the function and regulation of Nab3 granule assembly and accumulation and will help to broaden and deepen our understanding of other inducible, subcellular compartments found across eukaryotes.

4.7 Figures

Fig.4-1

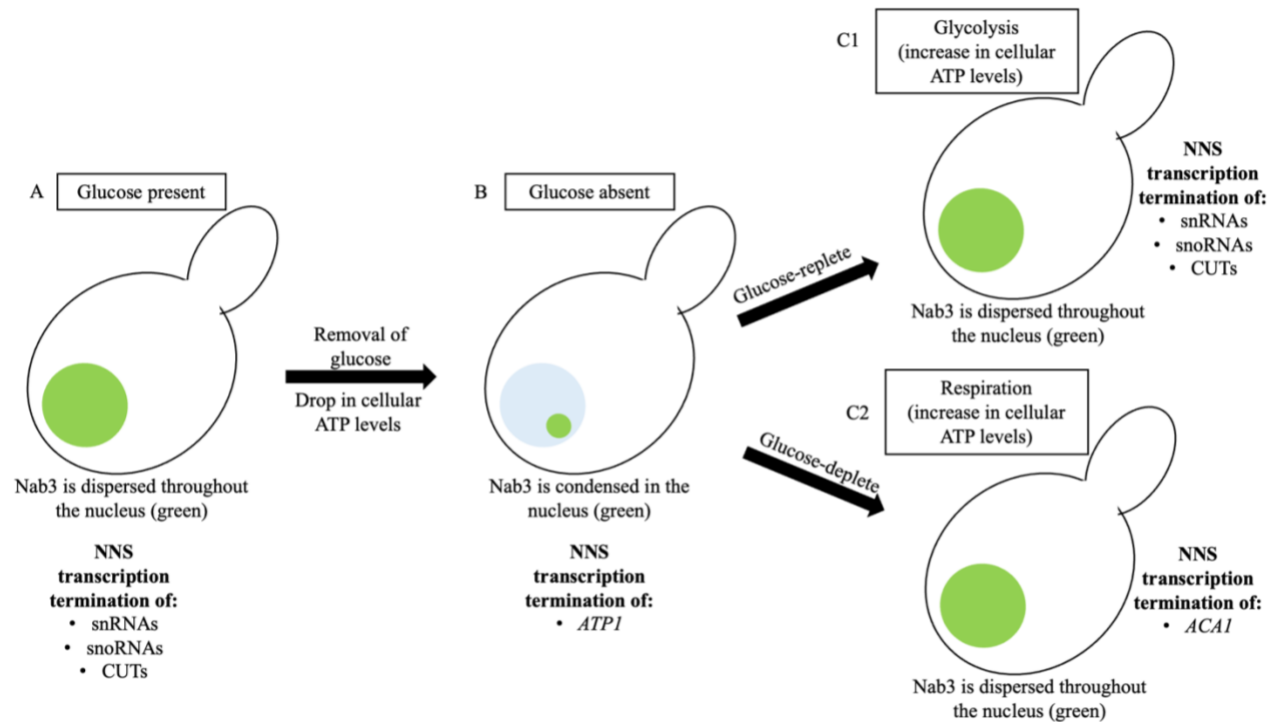


Fig. 4-1 A working model for Nrd1-Nab3 granule function

(A) In the presence of glucose, Nrd1 and Nab3 perform transcription termination of non-coding RNA such as snRNA, snoRNA and CUTs.

(B) Upon the removal of glucose, there is a decrease in cellular ATP levels which results in Nrd1-Nab3 granule accumulation. During this time, the granule serves as a concentrated spot for Nrd1-Nab3 transcription attenuation of specific genes such as *ATP1*, which encodes for a mitochondrial subunit important for oxidative phosphorylation and cellular respiration.

(C) There are two possible outcomes after Nrd1-Nab3 granule accumulation: (C1) glucose is replenished and thus leads to an increase in cellular ATP levels using glycolysis. Cells utilize NNS to terminate the transcription of snRNAs, snoRNAs and CUTs, or (C2) cells remain in a

glucose deplete environment and are forced to use their mitochondria to perform respiration to increase cellular ATP levels. Cells utilize NNS to terminate the transcription of genes such as *ACA1*, which is important for determining carbon source utilization in yeast. The use of glycolysis or respiration dictates the types of transcripts terminated by the Nrd1-Nab3-Sen1 transcription termination complex.

References

1. Koonin, E. V., Does the central dogma still stand? *Biol Direct* **2012**, *7*, 27.
2. Proudfoot, N. J., Transcriptional termination in mammals: Stopping the RNA polymerase II juggernaut. *Science* **2016**, *352* (6291), aad9926.
3. Arndt, K. M.; Reines, D., Termination of Transcription of Short Noncoding RNAs by RNA Polymerase II. *Annu Rev Biochem* **2015**, *84*, 381-404.
4. Haberle, V.; Stark, A., Eukaryotic core promoters and the functional basis of transcription initiation. *Nat Rev Mol Cell Biol* **2018**, *19* (10), 621-637.
5. Jonkers, I.; Lis, J. T., Getting up to speed with transcription elongation by RNA polymerase II. *Nat Rev Mol Cell Biol* **2015**, *16* (3), 167-77.
6. Heym, R. G.; Niessing, D., Principles of mRNA transport in yeast. *Cell Mol Life Sci* **2012**, *69* (11), 1843-53.
7. Morlando, M.; Greco, P.; Dichtl, B.; Fatica, A.; Keller, W.; Bozzoni, I., Functional analysis of yeast snoRNA and snRNA 3'-end formation mediated by uncoupling of cleavage and polyadenylation. *Mol Cell Biol* **2002**, *22* (5), 1379-89.
8. Mitrovich, Q. M.; Guthrie, C., Evolution of small nuclear RNAs in *S. cerevisiae*, *C. albicans*, and other hemiascomycetous yeasts. *RNA* **2007**, *13* (12), 2066-80.
9. Botstein, D.; Fink, G. R., Yeast: an experimental organism for modern biology. *Science* **1988**, *240* (4858), 1439-43.
10. Botstein, D.; Fink, G. R., Yeast: an experimental organism for 21st Century biology. *Genetics* **2011**, *189* (3), 695-704.
11. Porrua, O.; Libri, D., Transcription termination and the control of the transcriptome: why, where and how to stop. *Nat Rev Mol Cell Biol* **2015**, *16* (3), 190-202.
12. Sariki, S. K.; Sahu, P. K.; Golla, U.; Singh, V.; Azad, G. K.; Tomar, R. S., Sen1, the homolog of human Senataxin, is critical for cell survival through regulation of redox homeostasis, mitochondrial function, and the TOR pathway in *Saccharomyces cerevisiae*. *FEBS J* **2016**, *283* (22), 4056-4083.
13. Larochele, M.; Robert, M. A.; Hebert, J. N.; Liu, X.; Matteau, D.; Rodrigue, S.; Tian, B.; Jacques, P. E.; Bachand, F., Common mechanism of transcription termination at coding and noncoding RNA genes in fission yeast. *Nat Commun* **2018**, *9* (1), 4364.
14. Mischo, H. E.; Gomez-Gonzalez, B.; Grzechnik, P.; Rondon, A. G.; Wei, W.; Steinmetz, L.; Aguilera, A.; Proudfoot, N. J., Yeast Sen1 helicase protects the genome from transcription-associated instability. *Mol Cell* **2011**, *41* (1), 21-32.
15. Yuryev, A.; Patturajan, M.; Litingtung, Y.; Joshi, R. V.; Gentile, C.; Gebara, M.; Corden, J. L., The C-terminal domain of the largest subunit of RNA polymerase II interacts with a novel set of serine/arginine-rich proteins. *Proc Natl Acad Sci U S A* **1996**, *93* (14), 6975-80.
16. Heo, D. H.; Yoo, I.; Kong, J.; Lidschreiber, M.; Mayer, A.; Choi, B. Y.; Hahn, Y.; Cramer, P.; Buratowski, S.; Kim, M., The RNA polymerase II C-terminal domain-interacting domain of yeast Nrd1 contributes to the choice of termination pathway and couples to RNA processing by the nuclear exosome. *J Biol Chem* **2013**, *288* (51), 36676-90.
17. Han, Z.; Jasnovidova, O.; Haidara, N.; Tudek, A.; Kubicek, K.; Libri, D.; Stefl, R.; Porrua, O., Termination of non-coding transcription in yeast relies on both an RNA Pol II CTD interaction domain and a CTD-mimicking region in Sen1. *EMBO J* **2020**, *39* (7), e101548.

18. Egloff, S., Role of Ser7 phosphorylation of the CTD during transcription of snRNA genes. *RNA Biol* **2012**, *9* (8), 1033-8.
19. Hsin, J. P.; Sheth, A.; Manley, J. L., RNAP II CTD phosphorylated on threonine-4 is required for histone mRNA 3' end processing. *Science* **2011**, *334* (6056), 683-6.
20. Mayer, A.; Heidemann, M.; Lidschreiber, M.; Schrieck, A.; Sun, M.; Hintermair, C.; Kremmer, E.; Eick, D.; Cramer, P., CTD tyrosine phosphorylation impairs termination factor recruitment to RNA polymerase II. *Science* **2012**, *336* (6089), 1723-5.
21. Loya, T. J.; O'Rourke, T. W.; Reines, D., A genetic screen for terminator function in yeast identifies a role for a new functional domain in termination factor Nab3. *Nucleic Acids Res* **2012**, *40* (15), 7476-91.
22. Grzechnik, P.; Szczepaniak, S. A.; Dhir, S.; Pastucha, A.; Parslow, H.; Matuszek, Z.; Mischo, H. E.; Kufel, J.; Proudfoot, N. J., Nuclear fate of yeast snoRNA is determined by co-transcriptional Rnt1 cleavage. *Nat Commun* **2018**, *9* (1), 1783.
23. Jamonnak, N.; Creamer, T. J.; Darby, M. M.; Schaugency, P.; Wheelan, S. J.; Corden, J. L., Yeast Nrd1, Nab3, and Sen1 transcriptome-wide binding maps suggest multiple roles in post-transcriptional RNA processing. *Rna* **2011**, *17* (11), 2011-25.
24. Loya, T. J.; O'Rourke, T. W.; Degtyareva, N.; Reines, D., A network of interdependent molecular interactions describes a higher order Nrd1-Nab3 complex involved in yeast transcription termination. *J Biol Chem* **2013**, *288* (47), 34158-34167.
25. Loya, T. J.; O'Rourke, T. W.; Reines, D., Yeast Nab3 protein contains a self-assembly domain found in human heterogeneous nuclear ribonucleoprotein-C (hnRNP-C) that is necessary for transcription termination. *J Biol Chem* **2013**, *288* (4), 2111-7.
26. O'Rourke, T. W.; Loya, T. J.; Head, P. E.; Horton, J. R.; Reines, D., Amyloid-like assembly of the low complexity domain of yeast Nab3. *Prion* **2015**, *9* (1), 34-47.
27. Li, W.; Selvam, K.; Rahman, S. A.; Li, S., Sen1, the yeast homolog of human senataxin, plays a more direct role than Rad26 in transcription coupled DNA repair. *Nucleic Acids Res* **2016**, *44* (14), 6794-802.
28. Gregersen, L. H.; Mitter, R.; Ugalde, A. P.; Nojima, T.; Proudfoot, N. J.; Agami, R.; Stewart, A.; Svejstrup, J. Q., SCAF4 and SCAF8, mRNA Anti-Terminator Proteins. *Cell* **2019**, *177* (7), 1797-1813 e18.
29. Loya, T. J.; O'Rourke, T. W.; Simke, W. C.; Kelley, J. B.; Reines, D., Nab3's localization to a nuclear granule in response to nutrient deprivation is determined by its essential prion-like domain. *PLoS One* **2018**, *13* (12), e0209195.
30. Ursic, D.; Himmel, K. L.; Gurley, K. A.; Webb, F.; Culbertson, M. R., The yeast SEN1 gene is required for the processing of diverse RNA classes. *Nucleic Acids Res* **1997**, *25* (23), 4778-85.
31. Hentze, M. W.; Castello, A.; Schwarzl, T.; Preiss, T., A brave new world of RNA-binding proteins. *Nat Rev Mol Cell Biol* **2018**, *19* (5), 327-341.
32. Beckmann, B. M.; Horos, R.; Fischer, B.; Castello, A.; Eichelbaum, K.; Alleaume, A. M.; Schwarzl, T.; Curk, T.; Foehr, S.; Huber, W.; Krijgsveld, J.; Hentze, M. W., The RNA-binding proteomes from yeast to man harbour conserved enigmRBPs. *Nat Commun* **2015**, *6*, 10127.
33. Zhou, W.; Melamed, D.; Banyai, G.; Meyer, C.; Tuschl, T.; Wickens, M.; Cao, J.; Fields, S., Expanding the binding specificity for RNA recognition by a PUF domain. *Nat Commun* **2021**, *12* (1), 5107.
34. Kessler, S. H.; Sachs, A. B., RNA recognition motif 2 of yeast Pab1p is required for its

- functional interaction with eukaryotic translation initiation factor 4G. *Mol Cell Biol* **1998**, *18* (1), 51-7.
35. Sun, C.; Woolford, J. L., Jr., The yeast nucleolar protein Nop4p contains four RNA recognition motifs necessary for ribosome biogenesis. *J Biol Chem* **1997**, *272* (40), 25345-52.
36. Paziewska, A.; Wyrwicz, L. S.; Bujnicki, J. M.; Bomszyk, K.; Ostrowski, J., Cooperative binding of the hnRNP K three KH domains to mRNA targets. *FEBS Lett* **2004**, *577* (1-2), 134-40.
37. Scherrer, T.; Mittal, N.; Janga, S. C.; Gerber, A. P., A screen for RNA-binding proteins in yeast indicates dual functions for many enzymes. *PLoS One* **2010**, *5* (11), e15499.
38. Prusiner, S. B.; Scott, M. R.; DeArmond, S. J.; Cohen, F. E., Prion protein biology. *Cell* **1998**, *93* (3), 337-48.
39. Cascarina, S. M.; Ross, E. D., Yeast prions and human prion-like proteins: sequence features and prediction methods. *Cell Mol Life Sci* **2014**, *71* (11), 2047-63.
40. An, L.; Fitzpatrick, D.; Harrison, P. M., Emergence and evolution of yeast prion and prion-like proteins. *BMC Evol Biol* **2016**, *16*, 24.
41. Fraser, P. E., Prions and prion-like proteins. *J Biol Chem* **2014**, *289* (29), 19839-40.
42. Harbi, D.; Harrison, P. M., Classifying prion and prion-like phenomena. *Prion* **2014**, *8* (2).
43. Alberti, S.; Halfmann, R.; King, O.; Kapila, A.; Lindquist, S., A systematic survey identifies prions and illuminates sequence features of prionogenic proteins. *Cell* **2009**, *137* (1), 146-58.
44. Frost, B.; Diamond, M. I., Prion-like mechanisms in neurodegenerative diseases. *Nat Rev Neurosci* **2010**, *11* (3), 155-9.
45. Li, L.; McGinnis, J. P.; Si, K., Translational Control by Prion-like Proteins. *Trends Cell Biol* **2018**, *28* (6), 494-505.
46. Loya, T. J.; O'Rourke, T. W.; Reines, D., The hnRNP-like Nab3 termination factor can employ heterologous prion-like domains in place of its own essential low complexity domain. *PLoS One* **2017**, *12* (10), e0186187.
47. Ashe, M. P.; De Long, S. K.; Sachs, A. B., Glucose depletion rapidly inhibits translation initiation in yeast. *Mol Biol Cell* **2000**, *11* (3), 833-48.
48. Shah, K. H.; Zhang, B.; Ramachandran, V.; Herman, P. K., Processing body and stress granule assembly occur by independent and differentially regulated pathways in *Saccharomyces cerevisiae*. *Genetics* **2013**, *193* (1), 109-23.
49. Buchan, J. R.; Yoon, J. H.; Parker, R., Stress-specific composition, assembly and kinetics of stress granules in *Saccharomyces cerevisiae*. *J Cell Sci* **2011**, *124* (Pt 2), 228-39.
50. Teixeira, D.; Parker, R., Analysis of P-body assembly in *Saccharomyces cerevisiae*. *Mol Biol Cell* **2007**, *18* (6), 2274-87.
51. Taymaz-Nikerel, H.; Cankorur-Cetinkaya, A.; Kirdar, B., Genome-Wide Transcriptional Response of *Saccharomyces cerevisiae* to Stress-Induced Perturbations. *Front Bioeng Biotechnol* **2016**, *4*, 17.
52. DeRisi, J. L.; Iyer, V. R.; Brown, P. O., Exploring the metabolic and genetic control of gene expression on a genomic scale. *Science* **1997**, *278* (5338), 680-6.
53. Wu, J.; Zhang, N.; Hayes, A.; Panoutsopoulou, K.; Oliver, S. G., Global analysis of nutrient control of gene expression in *Saccharomyces cerevisiae* during growth and starvation. *Proc Natl Acad Sci U S A* **2004**, *101* (9), 3148-53.
54. Boer, V. M.; de Winde, J. H.; Pronk, J. T.; Piper, M. D., The genome-wide transcriptional responses of *Saccharomyces cerevisiae* grown on glucose in aerobic chemostat cultures limited for carbon, nitrogen, phosphorus, or sulfur. *J Biol Chem* **2003**, *278* (5), 3265-74.

55. Hsieh, W. C.; Sutter, B. M.; Ruess, H.; Barnes, S. D.; Malladi, V. S.; Tu, B. P., Glucose starvation induces a switch in the histone acetylome for activation of gluconeogenic and fat metabolism genes. *Mol Cell* **2022**, *82* (1), 60-74 e5.
56. Kresnowati, M. T.; van Winden, W. A.; Almering, M. J.; ten Pierick, A.; Ras, C.; Knijnenburg, T. A.; Daran-Lapujade, P.; Pronk, J. T.; Heijnen, J. J.; Daran, J. M., When transcriptome meets metabolome: fast cellular responses of yeast to sudden relief of glucose limitation. *Mol Syst Biol* **2006**, *2*, 49.
57. van den Brink, J.; Daran-Lapujade, P.; Pronk, J. T.; de Winde, J. H., New insights into the *Saccharomyces cerevisiae* fermentation switch: dynamic transcriptional response to anaerobicity and glucose-excess. *BMC Genomics* **2008**, *9*, 100.
58. Darby, M. M.; Serebreni, L.; Pan, X.; Boeke, J. D.; Corden, J. L., The *Saccharomyces cerevisiae* Nrd1-Nab3 transcription termination pathway acts in opposition to Ras signaling and mediates response to nutrient depletion. *Mol Cell Biol* **2012**, *32* (10), 1762-75.
59. Lin, Y.; Protter, D. S.; Rosen, M. K.; Parker, R., Formation and Maturation of Phase-Separated Liquid Droplets by RNA-Binding Proteins. *Mol Cell* **2015**, *60* (2), 208-19.
60. Harrison, A. F.; Shorter, J., RNA-binding proteins with prion-like domains in health and disease. *Biochem J* **2017**, *474* (8), 1417-1438.
61. Weber, S. C.; Brangwynne, C. P., Getting RNA and protein in phase. *Cell* **2012**, *149* (6), 1188-91.
62. Alberti, S.; Gladfelter, A.; Mittag, T., Considerations and Challenges in Studying Liquid-Liquid Phase Separation and Biomolecular Condensates. *Cell* **2019**, *176* (3), 419-434.
63. Kopcewicz, K. A.; O'Rourke, T. W.; Reines, D., Metabolic regulation of IMD2 transcription and an unusual DNA element that generates short transcripts. *Mol Cell Biol* **2007**, *27* (8), 2821-9.
64. Kuehner, J. N.; Brow, D. A., Regulation of a eukaryotic gene by GTP-dependent start site selection and transcription attenuation. *Mol Cell* **2008**, *31* (2), 201-11.
65. Jenks, M. H.; O'Rourke, T. W.; Reines, D., Properties of an intergenic terminator and start site switch that regulate IMD2 transcription in yeast. *Mol Cell Biol* **2008**, *28* (12), 3883-93.
66. Dichtl, B., Transcriptional ShortCUTs. *Molecular Cell* **2008**, *31* (5), 617-618.
67. Corden, J. L., Yeast Pol II start-site selection: the long and the short of it. *Embo Rep* **2008**, *9* (11), 1084-1086.
68. Wilson, S. M.; Datar, K. V.; Paddy, M. R.; Swedlow, J. R.; Swanson, M. S., Characterization of nuclear polyadenylated RNA-binding proteins in *Saccharomyces cerevisiae*. *J Cell Biol* **1994**, *127* (5), 1173-84.
69. Steinmetz, E. J.; Brow, D. A., Repression of gene expression by an exogenous sequence element acting in concert with a heterogeneous nuclear ribonucleoprotein-like protein, Nrd1, and the putative helicase Sen1. *Molecular and cellular biology* **1996**, *16* (12), 6993-7003.
70. Creamer, T. J.; Darby, M. M.; Jamonnak, N.; Schaugency, P.; Hao, H.; Wheelan, S. J.; Corden, J. L., Transcriptome-wide binding sites for components of the *Saccharomyces cerevisiae* non-poly(A) termination pathway: Nrd1, Nab3, and Sen1. *PLoS Genet* **2011**, *7* (10), e1002329.
71. van Nues, R.; Schweikert, G.; de Leau, E.; Selega, A.; Langford, A.; Franklin, R.; Iosub, I.; Wadsworth, P.; Sanguinetti, G.; Granneman, S., Kinetic CRAC uncovers a role for Nab3 in determining gene expression profiles during stress. *Nat Commun* **2017**, *8* (1), 12.
72. Loya, T. J.; O'Rourke, T. W.; Degtyareva, N.; Reines, D., A network of interdependent molecular interactions describes a higher order Nrd1-Nab3 complex involved in yeast transcription

termination. *J Biol Chem* **2013**, 288 (47), 34158-67.

73. Sathyanarayanan, U.; Musa, M.; Bou Dib, P.; Raimundo, N.; Milosevic, I.; Krisko, A., ATP hydrolysis by yeast Hsp104 determines protein aggregate dissolution and size in vivo. *Nat Commun* **2020**, 11 (1), 5226.

74. Gietz, D.; St Jean, A.; Woods, R. A.; Schiestl, R. H., Improved method for high efficiency transformation of intact yeast cells. *Nucleic acids research* **1992**, 20 (6), 1425.

75. Rothstein, R., Targeting, disruption, replacement, and allele rescue: integrative DNA transformation in yeast. *Methods Enzymol* **1991**, 194, 281-301.

76. Lee, S.; Lim, W. A.; Thorn, K. S., Improved blue, green, and red fluorescent protein tagging vectors for *S. cerevisiae*. *PLoS One* **2013**, 8 (7), e67902.

77. Ryan, O. W.; Skerker, J. M.; Maurer, M. J.; Li, X.; Tsai, J. C.; Poddar, S.; Lee, M. E.; DeLoache, W.; Dueber, J. E.; Arkin, A. P.; Cate, J. H., Selection of chromosomal DNA libraries using a multiplex CRISPR system. *Elife* **2014**, 3.

78. Dirick, L.; Bendris, W.; Loubiere, V.; Gostan, T.; Gueydon, E.; Schwob, E., Metabolic and environmental conditions determine nuclear genomic instability in budding yeast lacking mitochondrial DNA. *G3 (Bethesda)* **2014**, 4 (3), 411-23.

79. Schindelin, J.; Arganda-Carreras, I.; Frise, E.; Kaynig, V.; Longair, M.; Pietzsch, T.; Preibisch, S.; Rueden, C.; Saalfeld, S.; Schmid, B.; Tinevez, J. Y.; White, D. J.; Hartenstein, V.; Eliceiri, K.; Tomancak, P.; Cardona, A., Fiji: an open-source platform for biological-image analysis. *Nat Methods* **2012**, 9 (7), 676-82.

80. MATLAB., Natick, Massachusetts: The MathWorks, Inc. 2020. **R2021a**.

81. Schiavon, C. R.; Griffin, M. E.; Pirozzi, M.; Parashuraman, R.; Zhou, W.; Jinnah, H. A.; Reines, D.; Kahn, R. A., Compositional complexity of rods and rings. *Mol Biol Cell* **2018**, 29 (19), 2303-2316.

82. Brachmann, C. B.; Davies, A.; Cost, G. J.; Caputo, E.; Li, J.; Hieter, P.; Boeke, J. D., Designer deletion strains derived from *Saccharomyces cerevisiae* S288C: a useful set of strains and plasmids for PCR-mediated gene disruption and other applications. *Yeast* **1998**, 14 (2), 115-32.

83. Ilik, I. A.; Aktas, T., Nuclear speckles: dynamic hubs of gene expression regulation. *FEBS J* **2021**.

84. Weber, C. A.; Sekar, K.; Tang, J. H.; Warmer, P.; Sauer, U.; Weis, K., beta-Oxidation and autophagy are critical energy providers during acute glucose depletion in *Saccharomyces cerevisiae*. *Proc Natl Acad Sci U S A* **2020**, 117 (22), 12239-12248.

85. Ephrussi, B.; Jakob, H.; Grandchamp, S., Etudes Sur La Suppressivite Des Mutants a Deficience Respiratoire De La Levure. II. Etapes De La Mutation Grande En Petite Provoquee Par Le Facteur Suppressif. *Genetics* **1966**, 54 (1), 1-29.

86. Fox, T. D.; Folley, L. S.; Mulero, J. J.; McMullin, T. W.; Thorsness, P. E.; Hedin, L. O.; Costanzo, M. C., Analysis and manipulation of yeast mitochondrial genes. *Methods Enzymol* **1991**, 194, 149-65.

87. Ferguson, L. R.; von Borstel, R. C., Induction of the cytoplasmic 'petite' mutation by chemical and physical agents in *Saccharomyces cerevisiae*. *Mutat Res* **1992**, 265 (1), 103-48.

88. Hedstrom, L., IMP dehydrogenase: structure, mechanism, and inhibition. *Chem Rev* **2009**, 109 (7), 2903-28.

89. Carcamo, W. C.; Calise, S. J.; von Muhlen, C. A.; Satoh, M.; Chan, E. K., Molecular cell biology and immunobiology of mammalian rod/ring structures. *Int Rev Cell Mol Biol* **2014**, 308, 35-74.

90. Gaisne, M.; Becam, A. M.; Verdiere, J.; Herbert, C. J., A 'natural' mutation in *Saccharomyces cerevisiae* strains derived from S288c affects the complex regulatory gene HAP1 (CYP1). *Current genetics* **1999**, *36* (4), 195-200.
91. Young, M. J.; Court, D. A., Effects of the S288c genetic background and common auxotrophic markers on mitochondrial DNA function in *Saccharomyces cerevisiae*. *Yeast* **2008**, *25* (12), 903-12.
92. Boehning, M.; Dugast-Darzacq, C.; Rankovic, M.; Hansen, A. S.; Yu, T.; Marie-Nelly, H.; McSwiggen, D. T.; Kokic, G.; Dailey, G. M.; Cramer, P.; Darzacq, X.; Zweckstetter, M., RNA polymerase II clustering through carboxy-terminal domain phase separation. *Nat Struct Mol Biol* **2018**, *25* (9), 833-840.
93. Cho, W. K.; Spille, J. H.; Hecht, M.; Lee, C.; Li, C.; Grube, V.; Cisse, II, Mediator and RNA polymerase II clusters associate in transcription-dependent condensates. *Science* **2018**, *361* (6400), 412-415.
94. Chong, S.; Dugast-Darzacq, C.; Liu, Z.; Dong, P.; Dailey, G. M.; Cattoglio, C.; Heckert, A.; Banala, S.; Lavis, L.; Darzacq, X.; Tjian, R., Imaging dynamic and selective low-complexity domain interactions that control gene transcription. *Science* **2018**, *361* (6400).
95. Lu, H.; Yu, D.; Hansen, A. S.; Ganguly, S.; Liu, R.; Heckert, A.; Darzacq, X.; Zhou, Q., Phase-separation mechanism for C-terminal hyperphosphorylation of RNA polymerase II. *Nature* **2018**, *558* (7709), 318-323.
96. Sabari, B. R.; Dall'Agnese, A.; Boija, A.; Klein, I. A.; Coffey, E. L.; Shrinivas, K.; Abraham, B. J.; Hannett, N. M.; Zamudio, A. V.; Manteiga, J. C.; Li, C. H.; Guo, Y. E.; Day, D. S.; Schuijers, J.; Vasile, E.; Malik, S.; Hnisz, D.; Lee, T. I.; Cisse, II; Roeder, R. G.; Sharp, P. A.; Chakraborty, A. K.; Young, R. A., Coactivator condensation at super-enhancers links phase separation and gene control. *Science* **2018**, *361* (6400).
97. Corden, J. L., Yeast Pol II start-site selection: the long and the short of it. *EMBO Rep* **2008**, *9* (11), 1084-6.
98. Dichtl, B., Transcriptional ShortCUTs. *Mol Cell* **2008**, *31* (5), 617-8.
99. Carroll, K. L.; Ghirlando, R.; Ames, J. M.; Corden, J. L., Interaction of yeast RNA-binding proteins Nrd1 and Nab3 with RNA polymerase II terminator elements. *Rna* **2007**, *13* (3), 361-73.
100. Gilks, N.; Kedersha, N.; Ayodele, M.; Shen, L.; Stoecklin, G.; Dember, L. M.; Anderson, P., Stress granule assembly is mediated by prion-like aggregation of TIA-1. *Mol Biol Cell* **2004**, *15* (12), 5383-98.
101. Tauber, D.; Tauber, G.; Khong, A.; Van Treeck, B.; Pelletier, J.; Parker, R., Modulation of RNA Condensation by the DEAD-Box Protein eIF4A. *Cell* **2020**, *180* (3), 411-426 e16.
102. Shattuck, J. E.; Paul, K. R.; Cascarina, S. M.; Ross, E. D., The prion-like protein kinase Sky1 is required for efficient stress granule disassembly. *Nat Commun* **2019**, *10* (1), 3614.
103. Costanzo, M.; VanderSluis, B.; Koch, E. N.; Baryshnikova, A.; Pons, C.; Tan, G.; Wang, W.; Usaj, M.; Hanchard, J.; Lee, S. D.; Pelechano, V.; Styles, E. B.; Billmann, M.; van Leeuwen, J.; van Dyk, N.; Lin, Z. Y.; Kuzmin, E.; Nelson, J.; Piotrowski, J. S.; Srikumar, T.; Bahr, S.; Chen, Y.; Deshpande, R.; Kurat, C. F.; Li, S. C.; Li, Z.; Usaj, M. M.; Okada, H.; Pascoe, N.; San Luis, B. J.; Sharifpoor, S.; Shuteriqi, E.; Simpkins, S. W.; Snider, J.; Suresh, H. G.; Tan, Y.; Zhu, H.; Malod-Dognin, N.; Janjic, V.; Przulj, N.; Troyanskaya, O. G.; Stagljar, I.; Xia, T.; Ohya, Y.; Gingras, A. C.; Raught, B.; Boutros, M.; Steinmetz, L. M.; Moore, C. L.; Rosebrock, A. P.; Caudy, A. A.; Myers, C. L.; Andrews, B.; Boone, C., A global genetic interaction network maps a wiring diagram of cellular function. *Science* **2016**, *353* (6306).
104. Shattuck, J. E.; Cascarina, S. M.; Paul, K. R.; Ross, E. D., Sky1: at the intersection of

- prion-like proteins and stress granule regulation. *Curr Genet* **2020**, *66* (3), 463-468.
105. Siebel, C. W.; Feng, L.; Guthrie, C.; Fu, X. D., Conservation in budding yeast of a kinase specific for SR splicing factors. *Proc Natl Acad Sci U S A* **1999**, *96* (10), 5440-5.
106. Hunn, J. C.; Hutchinson, K. M.; Kelley, J. B.; Reines, D., Variable penetrance of Nab3 granule accumulation quantified by a new tool for high-throughput single-cell granule analysis. *Curr Genet* **2022**.
107. Dimitrov, L. N.; Brem, R. B.; Kruglyak, L.; Gottschling, D. E., Polymorphisms in multiple genes contribute to the spontaneous mitochondrial genome instability of *Saccharomyces cerevisiae* S288C strains. *Genetics* **2009**, *183* (1), 365-83.
108. Gietz, R. D.; Schiestl, R. H.; Willems, A. R.; Woods, R. A., Studies on the transformation of intact yeast cells by the LiAc/SS-DNA/PEG procedure. *Yeast* **1995**, *11* (4), 355-60.
109. Wach, A.; Brachat, A.; Pohlmann, R.; Philippsen, P., New heterologous modules for classical or PCR-based gene disruptions in *Saccharomyces cerevisiae*. *Yeast* **1994**, *10* (13), 1793-808.
110. Matheson, K.; Parsons, L.; Gammie, A., Whole-Genome Sequence and Variant Analysis of W303, a Widely-Used Strain of *Saccharomyces cerevisiae*. *G3 (Bethesda)* **2017**, *7* (7), 2219-2226.
111. Li, H., Minimap2: pairwise alignment for nucleotide sequences. *Bioinformatics* **2018**, *34* (18), 3094-3100.
112. Rasmussen, A. K.; Chatterjee, A.; Rasmussen, L. J.; Singh, K. K., Mitochondria-mediated nuclear mutator phenotype in *Saccharomyces cerevisiae*. *Nucleic Acids Res* **2003**, *31* (14), 3909-17.
113. Longo, V. D.; Liou, L. L.; Valentine, J. S.; Gralla, E. B., Mitochondrial superoxide decreases yeast survival in stationary phase. *Arch Biochem Biophys* **1999**, *365* (1), 131-42.
114. Shadel, G. S., Yeast as a model for human mtDNA replication. *Am J Hum Genet* **1999**, *65* (5), 1230-7.
115. Patel, A.; Malinowska, L.; Saha, S.; Wang, J.; Alberti, S.; Krishnan, Y.; Hyman, A. A., ATP as a biological hydrotrope. *Science* **2017**, *356* (6339), 753-756.
116. Takaine, M.; Imamura, H.; Yoshida, S., High and stable ATP levels prevent aberrant intracellular protein aggregation in yeast. *Elife* **2022**, *11*.
117. Jain, S.; Wheeler, J. R.; Walters, R. W.; Agrawal, A.; Barsic, A.; Parker, R., ATPase-Modulated Stress Granules Contain a Diverse Proteome and Substructure. *Cell* **2016**, *164* (3), 487-98.
118. Campos-Melo, D.; Hawley, Z. C. E.; Droppelmann, C. A.; Strong, M. J., The Integral Role of RNA in Stress Granule Formation and Function. *Front Cell Dev Biol* **2021**, *9*, 621779.
119. Sridharan, S.; Kurzawa, N.; Werner, T.; Gunthner, I.; Helm, D.; Huber, W.; Bantscheff, M.; Savitski, M. M., Proteome-wide solubility and thermal stability profiling reveals distinct regulatory roles for ATP. *Nat Commun* **2019**, *10* (1), 1155.
120. Wilson, W. A.; Hawley, S. A.; Hardie, D. G., Glucose repression/derepression in budding yeast: SNF1 protein kinase is activated by phosphorylation under derepressing conditions, and this correlates with a high AMP:ATP ratio. *Curr Biol* **1996**, *6* (11), 1426-34.
121. Weis, K.; Hondele, M., The Role of DEAD-Box ATPases in Gene Expression and the Regulation of RNA-Protein Condensates. *Annu Rev Biochem* **2022**.
122. Buchan, J. R.; Kolaitis, R. M.; Taylor, J. P.; Parker, R., Eukaryotic stress granules are cleared by autophagy and Cdc48/VCP function. *Cell* **2013**, *153* (7), 1461-74.
123. Kaliszewska, M.; Kruszewski, J.; Kierdaszuk, B.; Kostera-Pruszczyk, A.; Nojszewska,

- M.; Lusakowska, A.; Vizueta, J.; Sabat, D.; Lutyk, D.; Lower, M.; Piekutowska-Abramczuk, D.; Kaniak-Golik, A.; Pronicka, E.; Kaminska, A.; Bartnik, E.; Golik, P.; Tonska, K., Yeast model analysis of novel polymerase gamma variants found in patients with autosomal recessive mitochondrial disease. *Hum Genet* **2015**, *134* (9), 951-66.
124. Baruffini, E.; Lodi, T.; Dallabona, C.; Puglisi, A.; Zeviani, M.; Ferrero, I., Genetic and chemical rescue of the *Saccharomyces cerevisiae* phenotype induced by mitochondrial DNA polymerase mutations associated with progressive external ophthalmoplegia in humans. *Hum Mol Genet* **2006**, *15* (19), 2846-55.
125. Tigano, M.; Ruotolo, R.; Dallabona, C.; Fontanesi, F.; Barrientos, A.; Donnini, C.; Ottonello, S., Elongator-dependent modification of cytoplasmic tRNA^{Lys}UUU is required for mitochondrial function under stress conditions. *Nucleic Acids Res* **2015**, *43* (17), 8368-80.
126. Hwang, J.; Espenshade, P. J., Proximity-dependent biotin labelling in yeast using the engineered ascorbate peroxidase APEX2. *Biochem J* **2016**, *473* (16), 2463-9.
127. Kaewsapsak, P.; Shechner, D. M.; Mallard, W.; Rinn, J. L.; Ting, A. Y., Live-cell mapping of organelle-associated RNAs via proximity biotinylation combined with protein-RNA crosslinking. *Elife* **2017**, *6*.
128. Lee, S. Y.; Kang, M. G.; Park, J. S.; Lee, G.; Ting, A. Y.; Rhee, H. W., APEX Fingerprinting Reveals the Subcellular Localization of Proteins of Interest. *Cell Rep* **2016**, *15* (8), 1837-47.
129. Padron, A.; Iwasaki, S.; Ingolia, N. T., Proximity RNA Labeling by APEX-Seq Reveals the Organization of Translation Initiation Complexes and Repressive RNA Granules. *Mol Cell* **2019**, *75* (4), 875-887 e5.
130. Zhou, Y.; Wang, G.; Wang, P.; Li, Z.; Yue, T.; Wang, J.; Zou, P., Expanding APEX2 Substrates for Proximity-Dependent Labeling of Nucleic Acids and Proteins in Living Cells. *Angew Chem Int Ed Engl* **2019**, *58* (34), 11763-11767.
131. Rhee, H. W.; Zou, P.; Udeshi, N. D.; Martell, J. D.; Mootha, V. K.; Carr, S. A.; Ting, A. Y., Proteomic mapping of mitochondria in living cells via spatially restricted enzymatic tagging. *Science* **2013**, *339* (6125), 1328-1331.
132. Van Treeck, B.; Parker, R., Principles of Stress Granules Revealed by Imaging Approaches. *Cold Spring Harb Perspect Biol* **2019**, *11* (2).
133. Wheeler, J. R.; Jain, S.; Khong, A.; Parker, R., Isolation of yeast and mammalian stress granule cores. *Methods* **2017**, *126*, 12-17.
134. Buchan, J. R.; Parker, R., Eukaryotic stress granules: the ins and outs of translation. *Mol Cell* **2009**, *36* (6), 932-41.
135. Kaganovich, D.; Kopito, R.; Frydman, J., Misfolded proteins partition between two distinct quality control compartments. *Nature* **2008**, *454* (7208), 1088-95.
136. Miller, S. B.; Ho, C. T.; Winkler, J.; Khokhrina, M.; Neuner, A.; Mohamed, M. Y.; Guilbride, D. L.; Richter, K.; Lisby, M.; Schiebel, E.; Mogk, A.; Bukau, B., Compartment-specific aggregases direct distinct nuclear and cytoplasmic aggregate deposition. *EMBO J* **2015**, *34* (6), 778-97.
137. Khong, A.; Matheny, T.; Jain, S.; Mitchell, S. F.; Wheeler, J. R.; Parker, R., The Stress Granule Transcriptome Reveals Principles of mRNA Accumulation in Stress Granules. *Mol Cell* **2017**, *68* (4), 808-820 e5.
138. Webb, S.; Hector, R. D.; Kudla, G.; Granneman, S., PAR-CLIP data indicate that Nrd1-Nab3-dependent transcription termination regulates expression of hundreds of protein coding genes in yeast. *Genome Biol* **2014**, *15* (1), R8.

139. Gasch, A. P.; Spellman, P. T.; Kao, C. M.; Carmel-Harel, O.; Eisen, M. B.; Storz, G.; Botstein, D.; Brown, P. O., Genomic expression programs in the response of yeast cells to environmental changes. *Mol Biol Cell* **2000**, *11* (12), 4241-57.
140. Cherkasov, V.; Grousl, T.; Theer, P.; Vainshtein, Y.; Glasser, C.; Mongis, C.; Kramer, G.; Stoecklin, G.; Knop, M.; Mogk, A.; Bukau, B., Systemic control of protein synthesis through sequestration of translation and ribosome biogenesis factors during severe heat stress. *FEBS Lett* **2015**, *589* (23), 3654-64.
141. Lin, M. T.; Beal, M. F., Mitochondrial dysfunction and oxidative stress in neurodegenerative diseases. *Nature* **2006**, *443* (7113), 787-95.